N71 - 18680

NATIONAL AERONAUTICS AND SPACE ADMINISTRATION

NASA CR116800

Technical Report 32-1510

Heat Transfer From Partially Ionized Argon Flowing in a Conducting Channel With An Applied, Transverse Magnetic Field

E. J. Roschke

JET PROPULSION LABORATORY
CALIFORNIA INSTITUTE OF TECHNOLOGY
PASADENA, CALIFORNIA

December 15, 1970

Technical Report 32-1510

Heat Transfer From Partially Ionized Argon Flowing in a Conducting Channel With An Applied, Transverse Magnetic Field

E. J. Roschke

Preface

The work described in this report was performed by the Propulsion Division of the Jet Propulsion Laboratory.

Acknowledgments

Contents

Contents (contd)

Tables

Figures

Contents (contd)

Figures (contd)

Contents (contd)

Figures (contd)

Abstract

Wall heat transfer measurements were obtained for laminar flow of partially ionized argon flowing in a square channel with and without an applied, transverse magnetic field. Tests were conducted for subsonic flows and for flows that were supersonic before a magnetic field was applied. Principal results are presented in terms of the Stanton number. The Stanton number increased by a factor of as much as six at the highest magnetic field strengths available (nearly 10 kG) over results observed at zero field. Heat transfer and flow data were used to estimate the effective values of the Joule heating parameter, the Hall coefficient, the Hartmann number, and the current density; these values appeared to be physically realistic. It is believed that the large increases in heat transfer observed with an applied magnetic field were due to (1) a small but sufficient amount of Joule heating, which caused significant changes in the temperature distribution, augmented or accompanied by (2) magnetically induced nonequilibrium ionization. These results represent the only known experimental measurements obtained thus far for heat transfer from a partially ionized gas in steady internal flow with an applied, transverse magnetic field.

Heat Transfer From Partially Ionized Argon Flowing in a Conducting Channel With An Applied, Transverse Magnetic Field

I. Introduction

Heat transfer phenomena as produced by the interaction of electric and magnetic fields with subsonic and supersonic ionized gas-flows provide a rich area of experimental endeavor that remains relatively unexplored. The practical design of steady-state, magnetogasdynamic devices such as generators and accelerators depends to a large extent on cooling requirements, especially in regard to electrodes. However, very few experimental results for convective heat transfer distributions in channel flows of partially ionized gases with applied fields are available.

The purpose of this investigation was to acquire experimental heat transfer distributions and increase the understanding of steady, partially ionized gas flows in channels under the influence of an applied, transverse magnetic field. The flow cross section of the channel was square; the channel was segmented axially, but each of the four walls contained separate coolant passages so that the channel formed a continuous, hollow metallic conductor (Figs. 1 and 2). Since no electric field was applied, the investigated case corresponded to a short-circuit condition of the walls with a load factor $K = 0$. Relatively strong magnetic fields were attainable, covering a range

from zero to nearly 10 kG in the test section. Argon was heated and pre-ionized by means of a conventional electric-arc heater, but measurements were made in a region 4.5 to 6.5 channel-heights downstream of the arc-heater outlet. Flows were laminar and, in most cases, subsonic, although in some tests the flow entering the test section was supersonic before the magnetic field was applied.

Many theoretical analyses for heat transfer in flows with applied electric and magnetic fields are available. Romig (Ref. 1) has summarized the work before 1962; however, the channel flow problem dealt with in that summary applies only to fully developed flow. Since then, flow between parallel plates with applied fields has been studied by various authors (Refs. 2–6) for laminar, incompressible steady flows with constant properties. These analyses vary according to the assumptions made and should be considered and compared on their own merits; however, none of them account for the effects of finite wall conductance, Hall currents, or axial conduction within the fluid. Walls that are electrically conducting have been considered by Yen (Ref. 7) and Snyder (Ref. 8) for fully developed flow between parallel
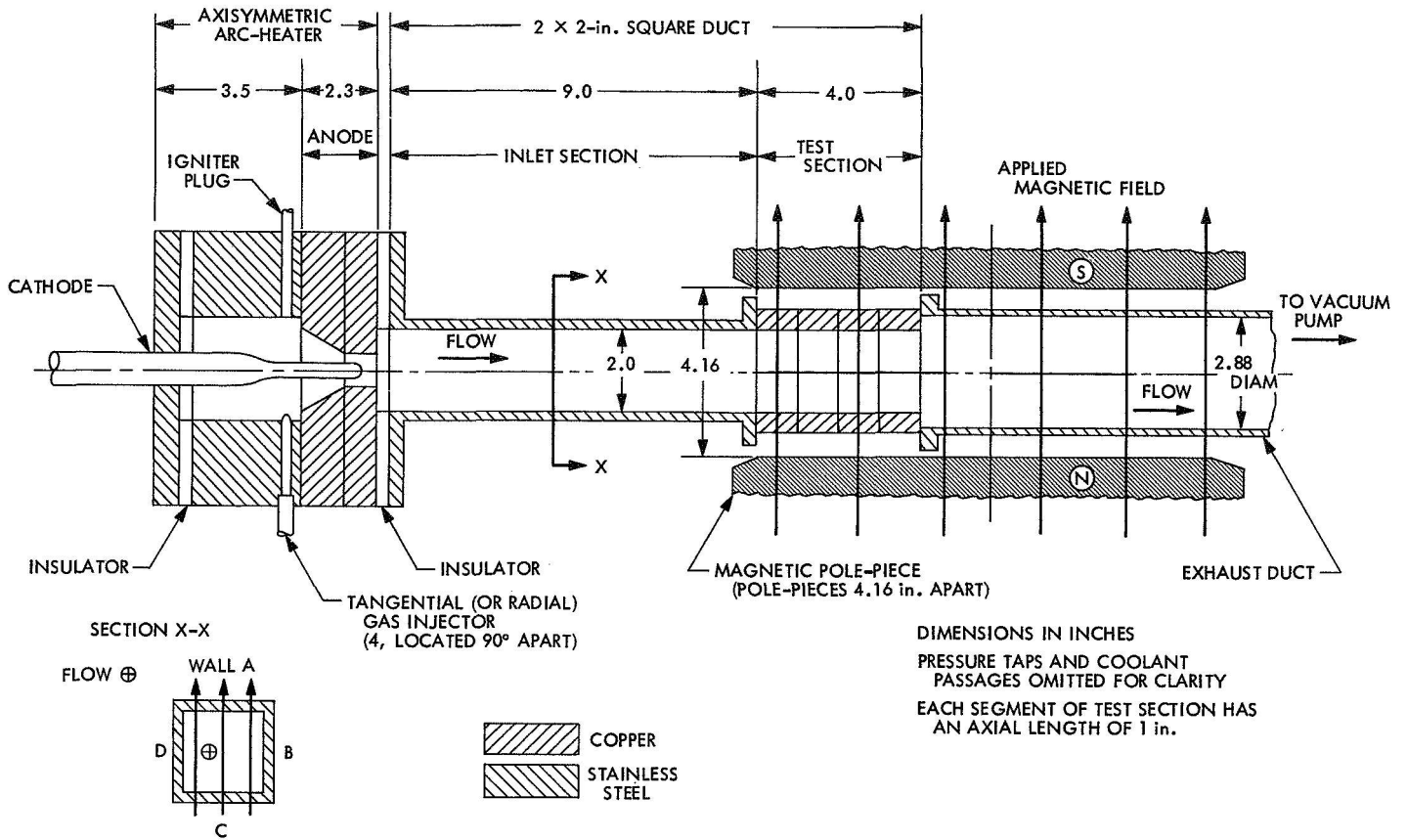
Fig. 1. Side view of in-line arc configuration for heat transfer experiments

THREE PRESSURE TAPS DISTRIBUTED ALONG BOTH
SIDEWALLS ARE NOT SHOWN. COOLANT TUBES
ARE LARGE DIAMETER FLATTENED TO SMALL
DIMENSION SHOWN.
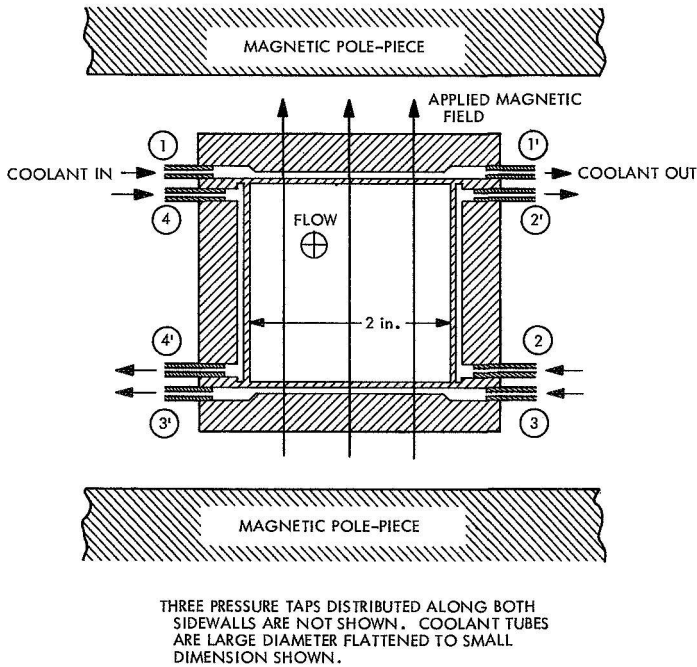
Fig. 2. Cross section of a 2-in.-square copper test section
showing manner of cooling walls

plates, but current flow was restricted to a direction parallel to the walls, and sidewalls were not considered. However, these authors have shown that electrically conducting walls perpendicular to an applied, magnetic field can have significant effects on heat transfer compared with the effects from insulated walls. A simplified analysis including compressibility effects has been treated by Hwang, Fan, and Hwang (Ref. 9) and includes a numerical example for a Mach number of 0.8 with Prandtl number of 0.01; but the effects of compressibility are not clearly demonstrated.

More recently, Back (Ref. 10) has obtained new results for the case of constant property incompressible slug flow, which include axial conduction (slug flow is considered to be a good assumption at high Hartmann number). His results are valuable in that numerical calculations are displayed graphically for a wide range of parameters. The effects of the Joule heating parameter on heat transfer from laminar flows indicate that large increases in heat transfer occur for large Joule heating. Both axial conduction and Hall effects have been con-

sidered by Eraslan and Eraslan (Ref. 11); interesting results were found for strong Hall effects, particularly in the short circuit case. However, the practical significance of Ref. 11 is diminished because the Hall coefficient was varied at constant Hartmann number, a case that is physically unrealistic for thermally ionized gases.

When the flow of a partially ionized gas in a channel of finite dimensions, i.e., finite width, is considered, the shortcomings of the various analyses (Refs. 1–11) become apparent. The flow cannot always be considered incompressible, and the assumption of constant properties may be misleading for highly cooled walls. Although Back (Ref. 12) has shown that consideration of variable properties does not contribute significantly to heat transfer despite large changes in the velocity and temperature distributions, his analysis does not consider this interaction with ionization effects in the presence of applied fields. The assumption of constant electrical conductivity across a channel may be especially poor even if no Hall effects are present (Refs. 13, 14). Thus, the distributions of electrical current may become greatly modified if large temperature gradients exist near the wall. Hall effects further complicate this picture because axial currents require a return route, a condition which may occur in the boundary layers. Reilly and Oates (Ref. 15) have shown that axial current loops can take place when the walls are electric insulators. Such a return path could also occur in the case of conducting walls if the electrical conductivity of the gas were low in the direction perpendicular to the walls. Therefore, simple analyses for Joule heating in channel flows that neglect these considerations are not likely to yield accurate predictions.

In addition to the effects just mentioned, other considerations arise in dealing with real channel flows that detract from the value of simplified theoretical models because they are difficult to incorporate in analyses but may influence real flows considerably. Since channel dimensions are finite in experiments, and Hall effects may be present, secondary flows of both current and gas may exist transverse to the axial flow (Refs. 16–18). In addition, magnetic fields in experiments do not begin or end sharply because of fringe effects; hence, flow development may be modified in the thermal entrance region of the channel (Ref. 19). Finally, the possibility of non-equilibrium ionization in strong magnetic fields exists (Refs. 20–24) but the anisotropic effects of a strong magnetic field on gas transport properties have not yet been well formulated (Refs. 25, 26), especially for routine engineering application.

A survey of the literature disclosed that very little experimental work had been done on convective heat transfer in channels with an applied, transverse magnetic field. From simple theory (e.g., Ref. 10) it is known that large Joule heating should produce increases of convective heat transfer for laminar flow. Thus, the application of a magnetic field alone should produce an increase in heat transfer over a zero-field condition, because of the electric field induced in the moving fluid provided, of course, that the fluid possesses sufficient electrical conductivity. Interestingly, experiments with liquid metals and electrolytes show the opposite effect; that is, application of a magnetic field reduces the convective heat transfer. The important difference, however, is that experiments with liquids have been performed in the turbulent flow regime under conditions when Joule heating was small or negligible. Reduction of heat transfer with an applied magnetic field has been observed for mercury in pipe-flow by Lykoudis (Ref. 27) and in a channel-flow of an electrolyte by Blum (Ref. 28). Similar results were found for channel-flow of liquid gallium by Kovner, et al. (Ref. 29) and verify the empirical analysis made earlier by Krasilnikov (Ref. 30). In general, the decrease in heat transfer found experimentally for turbulent flow of liquids has been ascribed to the suppression of turbulence by the magnetic field. Olin and Kruger (Ref. 31) have demonstrated turbulence suppression in seeded gas-flows with a transverse magnetic field for flow in a square channel having insulated walls.

Only one set of experimental heat transfer data for a partially ionized gas was found in the literature, the work of Dukowicz (Ref. 32) for argon flow in a shock-tube. Dukowicz classifies his results by two categories: (1) weak interaction in which large magnetic fields do not affect heat transfer significantly, apparently because Hall effects are unimpeded, and (2) strong interaction in which large increases in heat transfer occur with large, applied fields, and Hall effects are thought to be suppressed. In the case of strong interaction, Dukowicz measured increases in wall heat flux of 50 to 80% above the zero-field condition for applied magnetic fields of the order of 12 kG. Other experiments have been performed on Joule heating in air by Selamoglu (Ref. 33), but these concern effects between electrodes in the absence of an applied magnetic field; and no direct heat transfer results were given.

Thus, at the present time, the data given in this report appear to be the only experimental heat transfer results available for laminar, steady, channel flow of a partially

ionized gas in the presence of a transverse magnetic field (see Appendix).

II. Description of Apparatus and Instrumentation

A. Heat Transfer Apparatus

The heat transfer apparatus is shown schematically in Fig. 1. It consisted of a conventional, annular, electric-arc heater, an inlet section, a test section, and an exhaust duct. The inlet section and the test section together formed a 2 × 2-in. square channel having a constant cross-sectional area, whereas the arc-heater and exhaust duct were axisymmetric. Thoriated tungsten was used for the cathode, which had an elongated tip approximately 0.375 in. in diameter. Parts forming the anode and the test section were fabricated from high-purity, oxygen-free copper; with the exception of insulators, all other parts were fabricated from stainless steel. The anode throat was 0.75 in. in diameter and formed an outlet-orifice for the arc heater. Argon was injected tangentially, or radially, upstream of the electric arc at subatmospheric pressures, became heated by the arc, and entered the square channel through the anode orifice. Gas temperatures at the outlet of the arc-heater were typically of the order of 10,000°K. Individual walls in the square channel were designated A, B, C, and D (inset, Fig. 1).

The length of the inlet section was selected so that an attached and moderately hot gas flow would be available at the entrance to the test section. As will be discussed later, these ideal conditions were probably not always attained. The exhaust duct was approximately 19.3 in. long and emptied into a small, cylindrical vacuum tank having a diameter of 2 ft and a length of approximately 6 ft. Several large view ports in the vacuum tank allowed visual observation of the exhaust plume at an axial location approximately 2 ft downstream of the end of the test section. The entire apparatus was connected to a vacuum system so that, within limits, the mass rate of flow and pressure in the test section could be varied independently. Insulators were placed between the arc-heater and inlet section, and also between the exhaust duct and vacuum tank. Hence, the test section was electrically isolated from the ground and acquired its own floating potential with respect to the plasma. No external electric fields were applied to the test section.

All parts were cooled with distilled water. Each wall of the inlet section was cooled in a single axial pass (coolant water flowing in a downstream direction) so that the distribution of heat transfer along the inlet sec-

tion was not determined. Pressure taps were provided at the center of each of the four walls of the inlet section and at three axial locations; these locations were approximately 1.0, 2.22, and 3.5 channel-heights downstream from the entrance of the inlet section. The test section was composed of four individual segments, each 1.0 in. long in the axial direction (Fig. 1). The walls of each segment were cooled individually as shown in Fig. 2. Each segment was provided with six pressure taps, three on each sidewall (walls B and D), that were located in a central plane perpendicular to the direction of flow and midway between the upstream and downstream ends of each segment. No pressure taps were located on the upper or lower walls of the test section because of the proximity of the magnet pole-pieces. Several additional pressure taps were placed in the exhaust duct and the vacuum tank.

Originally, view-port window-slots were provided in the second and fourth segments of the test section, but these were never used and were covered with copper strips. However, because of the port construction, cavities remained that were transverse to the flow on the upper and lower walls of the channel but not on the sidewalls. These cavities are shown in detail in Fig. 3; their effect on heat transfer is discussed later. The exhaust duct was cooled externally (Fig. 3) with water flowing in a helically wound, copper tube.

B. Magnet and Distribution of Magnetic Field

A direct current electromagnet was used that was capable of generating approximately 10 kG in an empty air-gap of approximately 4 in. The location of the magnet pole-pieces with respect to the test section is given in Fig. 1; the direction of the field indicated in Fig. 1 is designated as *forward* field. The magnet could also be operated with reverse polarity giving a field opposite in sense to that shown; this is designated as *reverse* field.

Variation of magnet field strength with current supplied to the magnet is shown in Fig. 4; a reduction in field strength was noted when the apparatus occupied the air gap between the pole pieces. Field distributions with an empty air gap are shown in Fig. 5 for directions aligned with the flow and transverse to the flow; measurements were made with a Hall type of probe. Magnetic field distribution with respect to the heat transfer apparatus is shown in Fig. 6, where B_c refers to the value of the field at the center of the pole-pieces. When the apparatus was positioned in the air gap, as shown in Fig. 6, the maximum field value occurred just down-
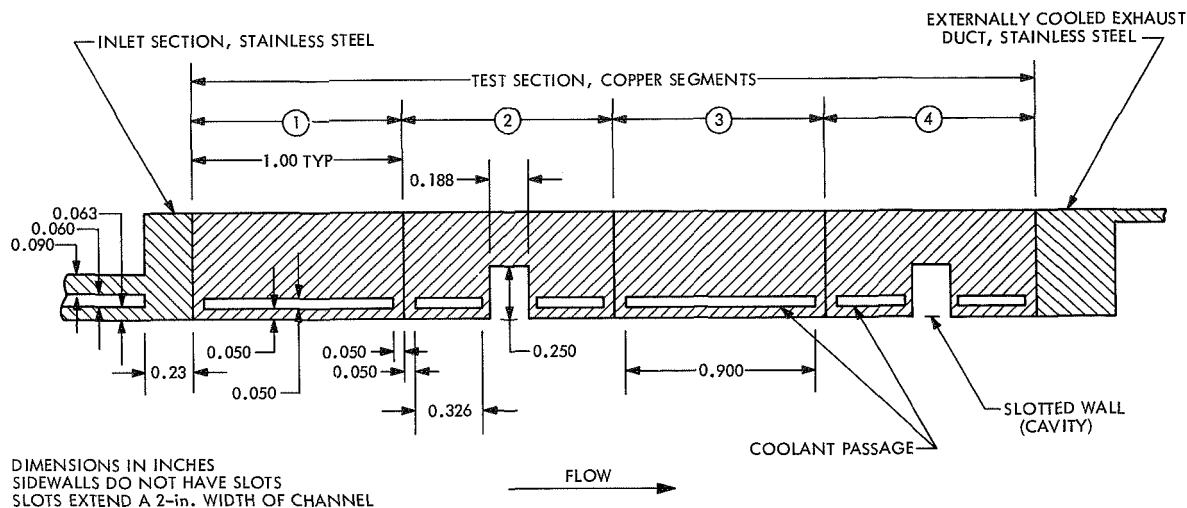
Fig. 3. Axial cross section of channel wall showing cavities formed by slots transverse to flow on upper and lower wall

DIMENSIONS IN INCHES
SIDEWALLS DO NOT HAVE SLOTS
SLOTS EXTEND A 2-in. WIDTH OF CHANNEL
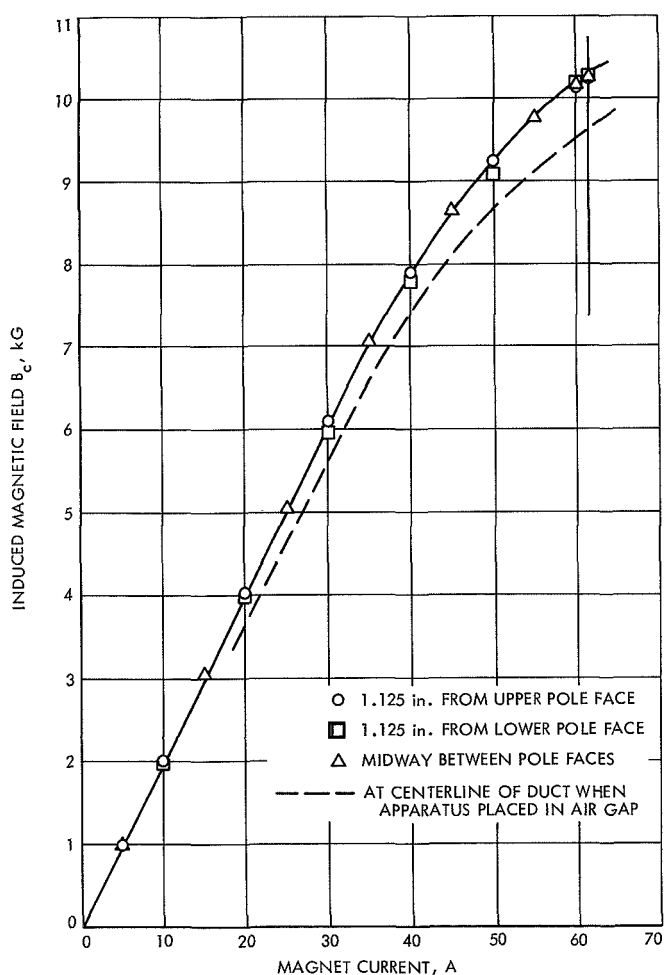
Fig. 4. Induced field at center of pole-pieces, Y-axis, 4.16-in. air gap

stream of the test section. In the vicinity of the electric-arc, the field had a value of roughly 4% of the maximum value. Although arc voltage sometimes varied as the magnetic field was applied downstream, it is believed that this was an accommodation to changing flow conditions rather than a direct influence of the magnetic field itself. The field increased exponentially in the direction of flow and achieved near-maximum value in the second segment of the test section. Attempts to tailor the field to obtain a delayed, but much steeper, rise were not successful.

C. Instrumentation

Argon mass rate of flow was measured by means of calibrated rotometers located far upstream of the apparatus. At that location, the gas was at approximately room temperature; this was measured by a total-temperature thermocouple. Since the flow-control valves operated at choked conditions, the pre-set mass rate of flow remained constant within very narrow limits throughout a given experimental test. Pressure level within the test section was controlled independently by other valves located in the vacuum system.

Direct current power supplied to the electric-arc heater was taken from a regulated, AC-rectified system. Arc voltage and current were monitored continuously. The majority of the tests were conducted at a nominal arc current of 2000 A but the power supplied to the arc heater varied from approximately 30 kW to 60 kW, depending on the flow conditions of the particular test.
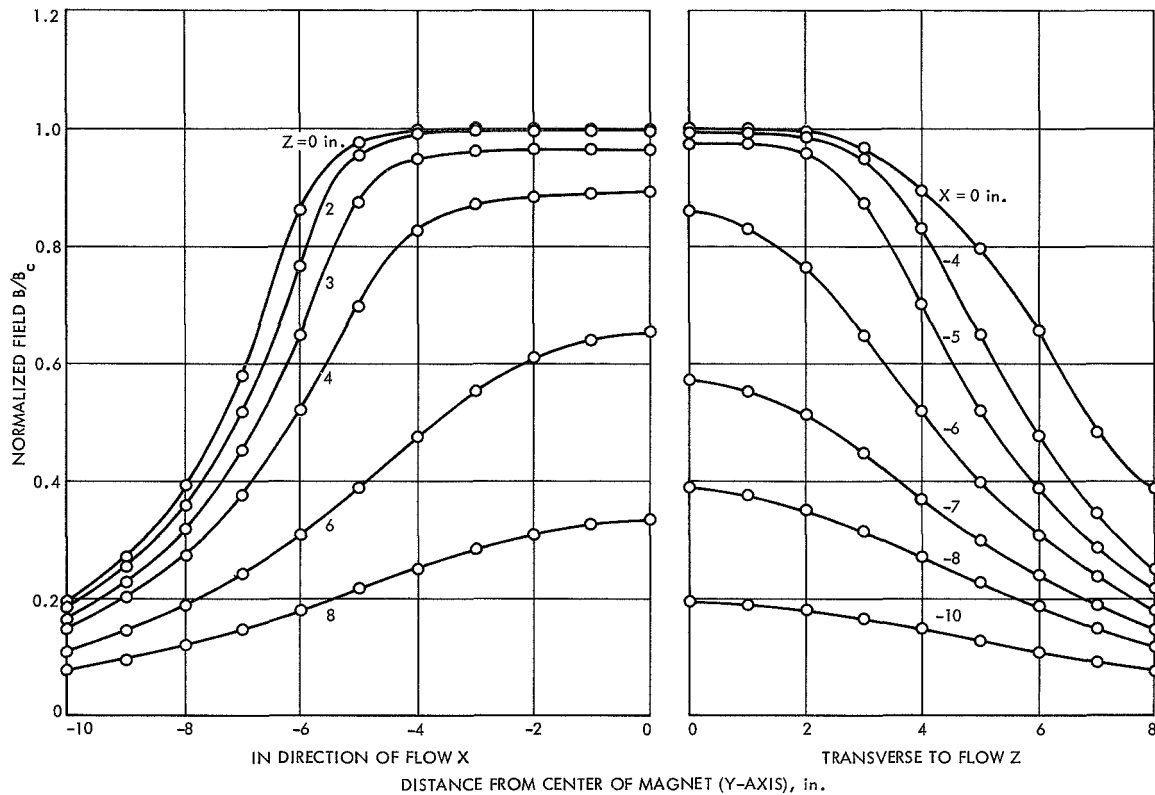
Fig. 5. Survey of induced field in the center plane between magnet pole-pieces, at a magnet current of 50 A, $B_c \simeq 9100$ G

Coolant water flow-rates were measured individually for each coolant passage in the apparatus by means of calibrated rotometers; readings were recorded simultaneously with direct printout readings of the water temperature rise across each coolant passage. Delta thermocouples were used to measure the changes in water temperature. Semi-local, gas-side wall temperatures were estimated from the thickness and composition of the wall material and water-side heat transfer coefficients; typical values ranged from 500°F to as high as 1100°F in the stainless steel inlet section and from 300 to 700°F in the segments of the copper test section.

Static pressures along the walls of the duct were measured with oil manometers. Locations of the pressure taps have been discussed previously. The strength of the applied magnetic field was controlled by varying magnet supply current and correlating these values with cold-flow calibrations similar to those shown in Figs. 4 and 6. Many of the delta thermocouples mentioned were located near the magnet. Cold-flow tests with distilled water circulating through the coolant system indicated that strong magnetic fields had no influence on these thermocouple readings.

No internal or spectroscopic measurements were made. Overall energy balances on the system indicated that the electric power applied to the arc was usually accounted for to within 3 or 4%.

III. Experimental Procedure and Data Analysis

Coolant flow rates were adjusted to yield approximately the same water temperature rise in adjacent passages proceeding downstream in the axial direction (Fig. 3). This precaution was taken to minimize axial heat conduction between the walls of adjacent segments of the test section. Calculations have shown that axial heat conduction was negligible except, perhaps, in the vicinity of the flanges located upstream and downstream of the test section.

The apparatus was operated until steady-state flow conditions and stable arc conditions prevailed; this was accomplished in the absence of a magnetic field. After the preliminary conditions were recorded, the magnetic field was applied and changed in selected increments. An entire set of data was recorded at steady-state conditions for each value of magnetic field selected, without
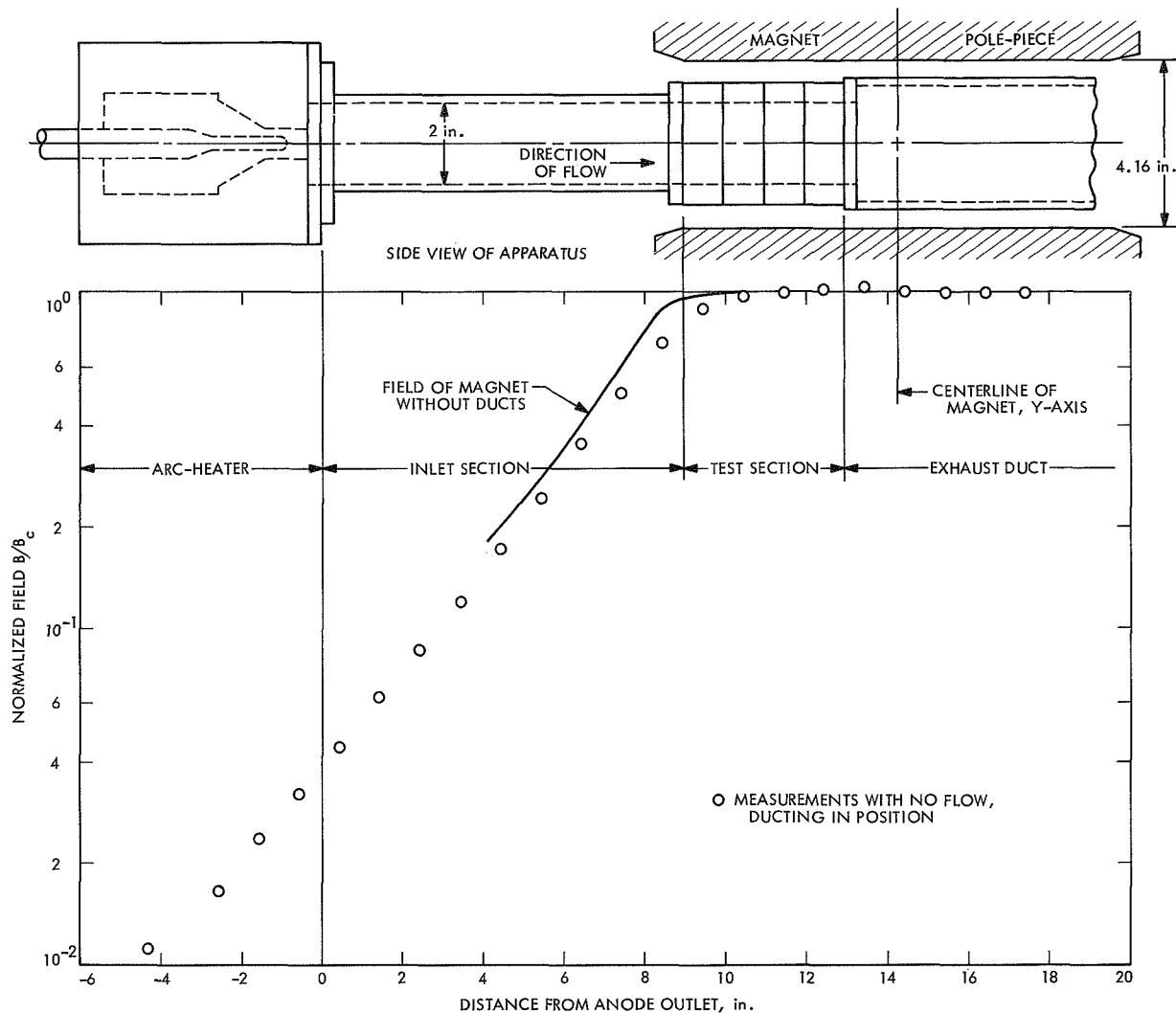
Fig. 6. Survey of induced field along duct centerline at magnet current of 57.5 A

altering any pre-set flow conditions or arc conditions. Such a set of data shall be referred to as a *test series*. The mass rate of flow remained essentially constant throughout a given test series. However, arc voltage sometimes changed or became unsteady even when no magnetic field was applied. These arc voltage changes probably occurred as a result of accommodation to new flow conditions brought about by the magnetic field far downstream. Data were never recorded except during quiescent, near-steady conditions.

The applied magnetic field was varied in two different procedural steps. In one method, maximum forward field was applied, reduced in steps to zero, and then increased in steps to maximum reverse field. Sometimes, the order of forward-to-reverse field was inverted. In another method, the field was increased in steps from zero to

maximum, and returned to zero, and then the cycle was completed by repeating the procedure for the field direction of opposite polarity. Visual observation of the exhaust plume was maintained throughout a test series and unusual conditions were recorded.

A chart indicating the range of parameters covered in the experiments for zero applied magnetic field is shown in Fig. 7. Note that the total enthalpy at the entrance to the test section, not the enthalpy at arc-heater outlet, is plotted against pressure for various mass rates of flow. Enthalpy of the gas varied strongly with pressure, but the variation with mass rate of flow was less evident. Tangential gas injection (flow with swirl) produced a gas of higher energy content than did radial injection for the same test-section pressure and arc current, because the power input to the arc was substantially
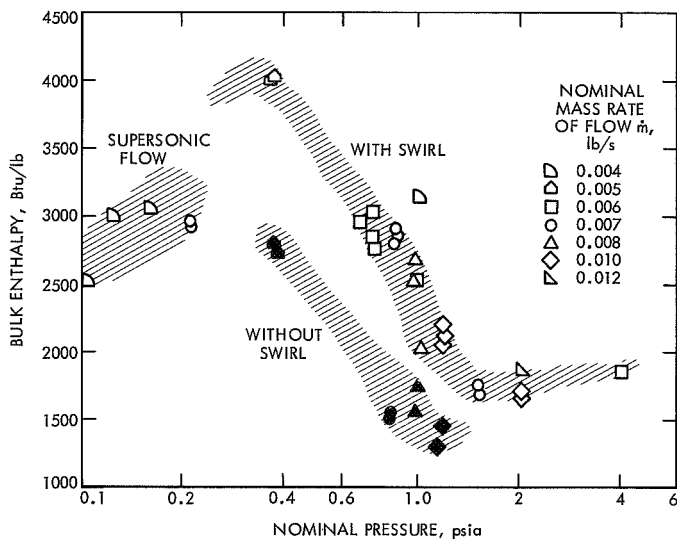
Fig. 7. Range of test conditions — total enthalpy and nominal pressure; both at entrance of test section at zero magnetic field

higher. For this reason, most tests were conducted by using tangential injection. Note that a reduction in enthalpy occurred at the lowest pressures for which the flow was supersonic (Fig. 7). This reduction could have occurred because of flow attachment to the walls of the inlet section in a much shorter axial distance than for the subsonic-flow tests. More energy would then be lost to cooling for supersonic flow than for subsonic flow, and the gas would therefore retain less energy at the test section inlet.

In the absence of an electric field, a magnetic field alone has no influence on the total enthalpy in an ionized gas flow (Ref. 34). Average values of the total enthalpy along the duct were established by an energy balance. Since the duct was of constant cross-sectional area, the average or bulk value of the mass flux $\overline{\rho u}$ remained constant along the channel. Static pressure along the duct was measured. The principal unknown quantities were static temperature and density, bulk velocity, and ionization fraction. Assuming conditions of equilibrium, the unknown quantities were computed by iterating the following equations:

Energy (definition of enthalpy):

$$H = H_t - \frac{u^2}{2g} = \frac{5}{2} R (1 + \alpha) T + I\alpha \qquad (1)$$

State:

$$\rho = p/(1 + \alpha) RT \qquad (2)$$

Conservation of species (Saha equation, Ref. 35):

$$\frac{\alpha^2}{1 - \alpha^2} = \frac{1.308 \times 10^{-6} \, T^{5/2}}{p} e^{-182900/T} \times [2 + e^{-2060/T}] \qquad (3)$$

where p is in atm, and T in °K

Continuity:

$$\overline{\rho u} = (\dot{m}/A) \qquad (4)$$

Other variables, such as acoustic velocity (e.g., Ref. 35), Mach number, and Reynolds number were then obtained easily. Values of the variables at stagnation conditions were computed by introducing the entropy relation and assuming that the process between the static state and the stagnation state was isentropic. This procedure enabled semi-local, bulk values of the flow parameters to be determined along the channel. Calculations were performed by electronic computer and included such items as Hartmann number and magnetic Reynolds number.

A discussion on the consequences of nonequilibrium is given later. Transport properties for argon were obtained from deVoto (Ref. 36); these included viscosity, thermal conductivity, Prandtl number, and electrical conductivity. Revised tables of transport properties from deVoto (Ref. 37) were unavailable during data reduction of the present experiments. Reference 37 indicates some substantial differences in the thermal and electrical conductivities at 1 atm compared with results given in Ref. 36.

Table 1 shows nominal values and ranges covered for several parameters of importance. These values refer to the center of the first segment of the test section and are given for zero magnetic field and maximum forward field. Reynolds numbers were well within the laminar range; transition Reynolds numbers for rectangular channels of low aspect ratio and for square channels are similar to those found for circular pipes (Ref. 38). Magnetic Reynolds numbers were small, based on scalar electrical conductivity, indicating that the induced magnetic fields were small compared with the applied magnetic field; these values are probably an upper limit compared with those that were actually present in the experiments. Theoretical values of Hartmann number based on scalar electrical conductivity ranged up to values exceeding 70 in these experiments; however, these values were also much higher than effective values, as will be discussed later.

Table 1. Nominal values and ranges of parameters computed from energy balance at center of first segment of test section.[a] Equilibrium assumed, transport properties from Ref. 36.

Item	Range of values	
	Zero magnetic field	Maximum forward field
Total enthalpy, Btu/lb	1265 to 3940	940 to 3000
Total bulk temperature, °K	5650 to 9770	4200 to 9250
Static bulk temperature, °K	5590 to 9660	4170 to 9170
Ionization fraction α	2.5×10^{-4} to 8.8×10^{-2}	4×10^{-6} to 5.8×10^{-2}
Reynolds number Re	155 to 455	160 to 530
Peclet number $RePr$	43 to 290	48 to 355
Bulk (av) velocity, ft/s	200 to 5030	160 to 3150
Eckert number Ec	10^{-3} to 0.36	8×10^{-4} to 0.185
Mach number M	0.04 to 1.10	0.033 to 0.7
Magnetic Reynolds number Re_m	—	~0 to 0.14
Hartmann number Ha	—	~0 to 71

[a]High values and low values do not necessarily occur simultaneously by groups.

IV. Factors Affecting Flow and Heat Transfer

Discussion in this section pertains to those factors in the experiments that could be evaluated with comparative ease. Other factors, especially those associated with the magnetic field, will be dealt with in Section VII under Discussion.

A. Thermal Radiation

Thermal radiation can become an important contribution to heat transfer in ionized argon flows at temperatures above 10,000°K; but this value was an upper limit in these experiments for flow near the entrance to the test section (Table 1). Previously, experiments had been conducted with argon in an apparatus similar to the one used here (Ref. 39), for flow conditions not significantly different. Although those experiments were somewhat crude, they were sufficient to establish that thermal radiation was, at most, 2% of the total heat transfer to the walls of the duct.

In Ref. 39, comparison was made with the continuum theory of Barzelay (Ref. 40), which appeared to agree favorably with the experimental data of Tankin and Berry (Ref. 41). The results given by Tankin and Berry were approximately one order of magnitude too low (Ref. 42) because of a numerical error in their presentation. Correcting these data (Ref. 41) brings it into much

better agreement with the results of Emmons (Ref. 43). Applying the corrected results of Tankin and Berry to the conditions of these experiments shows that only in a few tests could the radiant heat flux have approached 10% of the total heat flux to the walls. Therefore, it is believed that thermal radiation was essentially negligible in these experiments. It is conceded that thermal radiation could have been important in the entrance region of the channel, near to the electric arc, but this region was relatively far from the location of the measurements.

B. Effects of Ionization

For the case of highly cooled walls, the effects of free-stream ionization on heat flux to the walls can be estimated by using the results of Back (Ref. 44). In the presence of ionization, the total energy flux to the walls includes a diffusive contribution in addition to the usual conductive contribution. Back has examined this contribution assuming ambipolar diffusion to the walls by ion-electron pairs. The diffusive contribution depends primarily on the fraction of energy in ionization, and on the Lewis number. For constant, low, free-stream velocity with diffusion rate large compared with the net ion production, the solutions are given by Eqs. (21) and (22) of Ref. 44. When the walls are highly cooled ($g_w = z_{Iw} = 0$ in Back's nomenclature), the ratio of the diffusive energy flux to the total heat flux can be expressed simply in

terms of the Lewis number and the ionization energy fraction,

$$\frac{q_{dw}}{q_{Tw}} = \frac{\Phi_a \left(\chi + \Omega\right)}{1 + \Phi_a \chi} \tag{5}$$

where

$$\Phi_a = \frac{\alpha I}{H_t} \tag{6}$$

$$\chi + \Omega = Le^{2/3} \tag{7}$$

$$\chi \simeq \left(Le^{0.63} - 1\right) \tag{8}$$

The result is plotted in Fig. 8; for low Lewis number and low Φ_a, the diffusive contribution is only a few percent of the total heat flux. An appropriate Lewis number for the present experiments is $Le \leq 0.25$ (Ref. 44) and the ionization energy fraction was $\Phi_a < 0.25$ except for the high-enthalpy, high-subsonic tests (Fig. 7). Thus, conservative estimates indicate that ionization effects
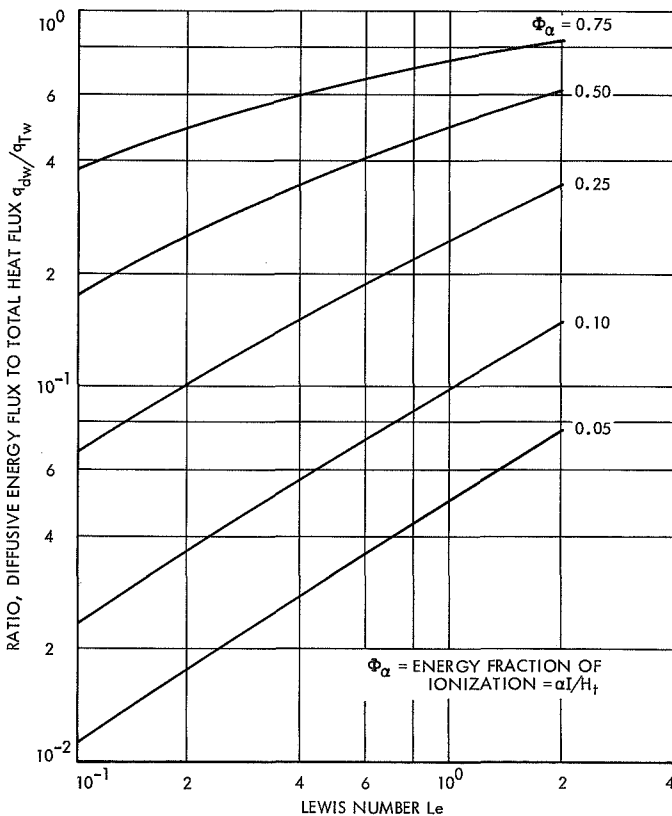
Fig. 8. Effect of ionization on total heat-flux-to-wall. For highly cooled wall and constant free-stream velocity, Ref. 44

contributed less than 10% of the total heat flux in the majority of the experiments. This is less than the experimental scatter, and was not considered significant. Again, it is possible that ionization effects were more significant upstream of the test section and near to the electric arc.

Care must be exercised in applying the results of Fig. 8 to actual experiments because the numerator and denominator of Eq. (5) pertain only to equivalent values of the enthalpy driving potential between the free-stream and the wall. That is, the ratio q_{dw}/q_{Tw} was obtained by cancelling the enthalpy driving potential $(H_{t,b} - H_w)$, which appears in both of the expressions for q_{dw} and q_{Tw}. Thus, the absolute values of q_{dw} could differ greatly in two separate experiments if the enthalpy driving potential (hence q_{Tw}) were different, even though identical values of Le and Φ_a occurred in both experiments.

C. Free Convection

Applying the results of Refs. 45–47 to the present experiments indicates clearly that free convection effects could have had no influence on the heat transfer whatever. The product of Rayleigh number and Reynolds number in the experiments was several orders of magnitude below the threshold at which free-convection effects begin to become important.

D. Effects of Swirl and Other Secondary Flows

For highly cooled walls, Back (Ref. 48) has shown that swirl-to-axial velocity ratios considerably larger than 1.0 are required to produce any significant increases in heat transfer for laminar flow, as compared with flow with no swirl. (Even then, the increases are rather modest compared with the influence of the magnetic field observed in these tests.) This result follows because the enthalpy profiles across the boundary layer are not greatly affected by swirl despite large distortions in the velocity profiles. Wall friction, however, was found to be strongly dependent on swirl, and increases rapidly as swirl ratio increases (Ref. 48).

In these experiments, swirl was present when tangential injection was used. Tangential velocity at injection, upstream of the electric-arc, depended on pressure and mass rate of flow but typically was of the order of 200 ft/s or less. Values of tangential velocity downstream in the test section were probably much less than this value, which already is small compared to values of bulk, axial velocity as listed in Table 1. It is clear that ratios of tangential to axial velocity in these experiments

could never have approached unity. Thus, the influence of swirl on heat transfer is not likely to have been significant in these experiments, at least for zero, applied magnetic field. It is possible that the presence of swirl had some effect on flow attachment in the inlet section which, in turn, would have some effect on the heat transfer measured at a fixed, downstream axial location.

The effect of a transverse magnetic field on the swirl component of flow is rather complicated. Consider an incompressible, inviscid but electrically conducting, fluid-mass rotating uniformly about an axis that is perpendicular to a uniform, transverse magnetic field. The application of Ohm's law and the radial momentum equation indicates, at once, the presence of nonaxisymmetric current flow and Lorentz forces. Radial distribution of pressure could not be axisymmetric. However, if the swirl was very weak compared with an axial flow upon which it was superimposed, the effects of distortion would be correspondingly weak. An experiment performed so that the direction of the magnetic field could be reversed with respect to the direction of rotation of the flow should reveal the relative effects of swirl. The present experiments will be discussed with this point of view in mind.

In addition to swirl, other secondary flows were probably present in these experiments. First, reversed flow must have been present upstream of the flow-attachment point in the inlet section. This has little bearing on the heat transfer measurements further downstream, and is not discussed further. Second, corner flows or eddies were present because of the square channel. Thicker boundary layers in the corners might be expected to inhibit heat transfer in those regions. Montgomery and Wibulswas (Ref. 49) have obtained theoretical solutions for laminar heat transfer with constant properties in rectangular channels for the case in which axial heat conduction is negligible. In terms of Nusselt number, their results indicate that the heat transfer is approximately 15 to 20% less for a square channel than for a circular tube of similar dimension (diameter of tube equal to height of square channel).

Again, the effect of a magnetic field on secondary flows is complex and largely unknown. An interesting series of experiments has been performed by Boedeker and Covert (Ref. 50). They studied the flow of an electrolyte in a helical channel that had an approximately square cross section, and applied a magnetic field transverse to the axis of the helical coil. Because of wall curvature, flow in a helical passage possesses secondary flows similar to those observed in curved pipes (e.g., Ref. 51); this results in a reduction of mass flow rate compared with a straight channel of the same length and having the same pressure gradient. Boedeker and Covert believe these secondary flows were appreciably altered by a transverse magnetic field. They found that the magnetic field caused further reductions in mass flow for constant pressure gradient (owing to axial drag because of Lorentz forces), but this was partially offset by a reduction in secondary flow losses in the helix brought about by the magnetic field.

Finally, the presence of a magnetic field might tend to set up new secondary flows caused by Hall effects (Refs. 16 and 18). The presence of swirl and other secondary flows in these experiments are believed to have been of small consequence compared with Hall effects and related phenomena. It is unlikely that they contributed significantly to the large changes in heat transfer that were measured when the magnetic field was applied.

E. Nonequilibrium Without Magnetic Field

In the literature dealing with experimental, arc-generated plasmas, the possibility of nonequilibrium in subsonic, nonaccelerated flows in the absence of strong fields is considered small when the pressure is above 1 or 2 psia or the electron density is greater than 10^{15} to 10^{16} per cubic centimeter. The concept and various criteria for local thermodynamic equilibrium have been discussed by Griem (Ref. 52), Eckert and Pfender (Ref. 53), and Olsen, et al. (Ref. 54). In the present experiments, average electron densities ranged generally from 10^{14} to 10^{15} per cubic centimeter in the region of heat transfer measurements, when no magnetic field was applied. However, it appears that at least partial local thermodynamic equilibrium existed for most of these experiments (Ref. 54) except, perhaps, in the vicinity of the electric arc and in boundary layers near the cold walls.

Within the framework of local thermodynamic equilibrium (Ref. 53) it is possible to sustain a kinetic temperature difference between electrons and ions, or heavy species, leading to the two-temperature concept (Ref. 53). Large temperature and density gradients can lead to electron–heavy particle nonequilibrium according to Jacobs and Grey (Ref. 55), especially when the flow velocities are large. Applying several criteria (Refs. 53 and 55) to the present experiments, it appears that large departures from $T_e = T_a = T_h$ were not likely in the core

of the flow. However, in the boundary layers, substantial departures from kinetic equilibrium might be expected. In the absence of electric or magnetic fields, it is difficult to imagine any direct influence on heat transfer resulting from $T_e > T_h$ except those effects from a change in transport properties and a change in ionization fraction α. These effects could be significant, provided α increased substantially.

Jacobs and Grey (Ref. 55) have shown that the increase in enthalpy associated with an elevated electron temperature is negligible when the nonequilibrium state is considered as a departure from the equilibrium state corresponding to the heavy particle temperature. Their result was obtained by allowing the electron temperature to increase above the heavy particle temperature in a unit volume of gas, but maintaining constant values of

the heavy particle temperature, electron density, and ionization fraction. Thus, the energy associated with heating the electrons is small compared with the original energy content of the gas if further ionization above the equilibrium state does not occur. However, if this restriction is removed, large changes in enthalpy can occur as the result of thermal nonequilibrium even for moderate values of T_e/T_a. The static enthalpy per unit mass of gas can be written for the nonequilibrium condition as

$$H_{nonequil} = \frac{5}{2} R (T_a + \alpha T_e) + I\alpha \qquad (9)$$

where it is customary to evaluate α from the Saha relation at the electron temperature T_e. This relation is plotted in Fig. 9 for argon at 0.01 atm pressure, which corresponds approximately to the lowest pressure that
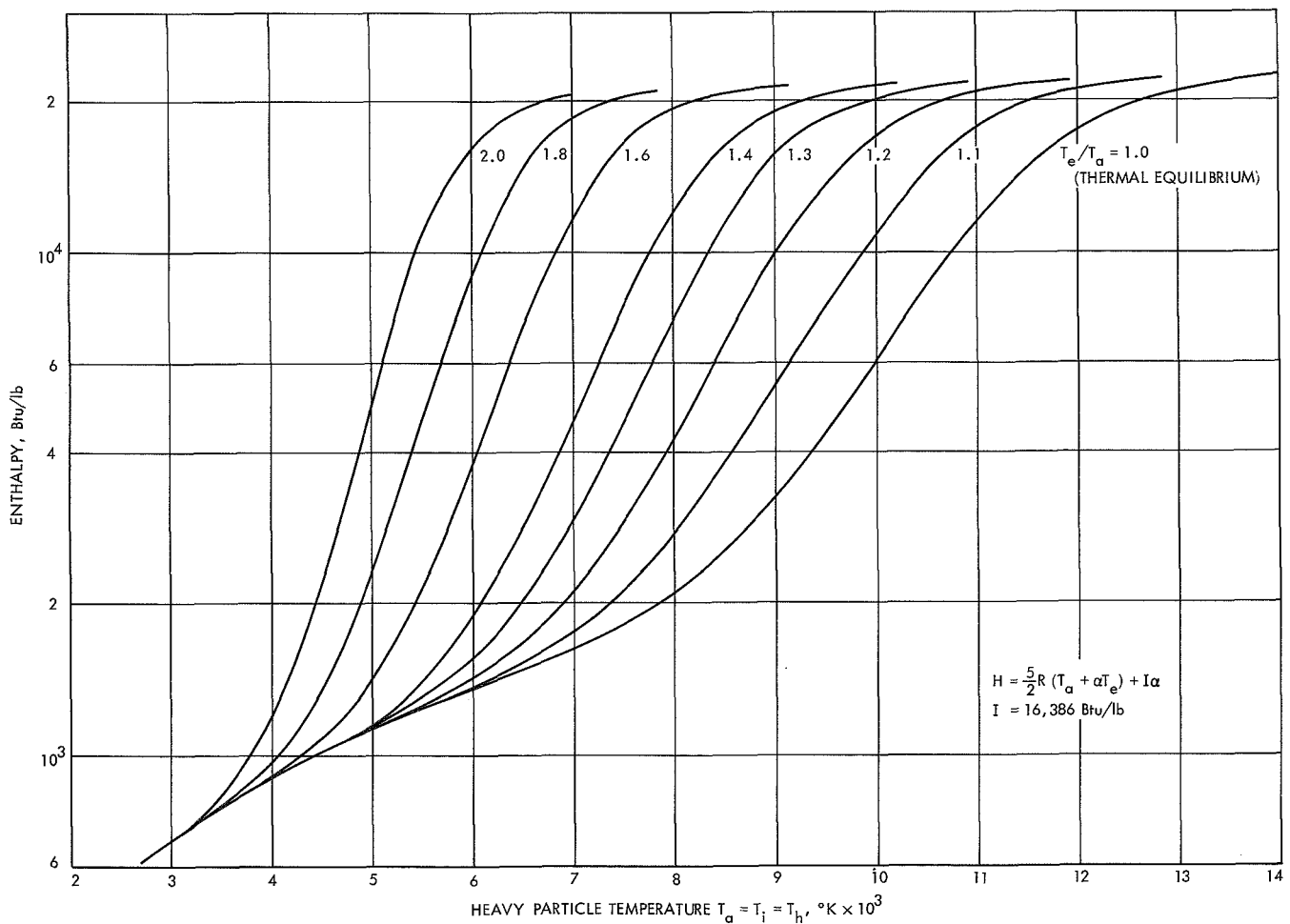
Fig. 9. Effect of thermal nonequilibrium on static enthalpy of singly ionized argon when the ionization fraction is based on electron temperature; for a pressure of 0.01 atm

occurred in the experimental tests. For equilibrium conditions $T_e = T_a$, Eq. (9) reduces to

$$H_{equil} = \frac{5}{2} R (1 + \alpha) T_a + I\alpha \qquad (10)$$

Comparing a nonequilibrium state to an equilibrium state, both at the same heavy particle temperature $T_h = T_a$, it is clear from Fig. 9 that large changes in enthalpy occur as the result of nonequilibrium $T_e > T_a$. In view of Jacobs' and Grey's results (Ref. 55), it is also clear that these large changes are due almost entirely to an increase in ionization fraction α corresponding to the elevated electron temperature, and not heating of the electrons.

In the experimental tests, the total, bulk energy content of the gas was determined along the direction of flow by a direct energy balance that was independent of the presence or absence of thermal nonequilibrium or other phenomena. However, it is useful to examine the consequences of the presence of thermal nonequilibrium and the effects of these consequences on heat transfer. To accomplish this, it is convenient to compare an equilibrium state of the gas with a nonequilibrium state for an equivalent value of enthalpy per unit mass of gas. Assuming that kinetic energy contributions are negligible, and ascribing subscripts 1 and 2 to the equilibrium and nonequilibrium states, respectively, Eqs. (9) and (10) are set equal to one another. The ionization fraction for each state is obtained from the usual Saha relation at the electron temperature. For equilibrium $T_a = T_h = T_e$,

$$H = \frac{5}{2} R (1 + \alpha_1) T_{h1} + I\alpha_1 = \frac{5}{2} R (T_{h2} + \alpha_2 T_{e2}) + I\alpha_2 \qquad (11)$$

Eq. (11) can be arranged in more convenient forms to assess the relation between the heavy particle temperatures $T_{h1} = T_{a1}$ and $T_{h2} = T_{a2}$:

$$(T_{h1} - T_{h2}) = (\alpha_2 - \alpha_1) \frac{2I}{5R} + (\alpha_2 T_{e2} - \alpha_1 T_{h1}) \qquad (12)$$

or

$$\left[1 + \alpha_2 \left(\frac{T_{e2}}{T_{h2}} \right) \right] \frac{T_{h2}}{T_{h1}} = (1 + \alpha_1) - \frac{(\alpha_2 - \alpha_1)}{T_{h1}} \frac{2I}{5R} \qquad (13)$$

It is clear from Eq. (12) or Eq. (13) that, at constant pressure, when $T_{e2} > T_{h2}$ and $\alpha_2 > \alpha_1$, then $T_{h2} < T_{h1}$. That is, if a unit mass of gas passes from an equilibrium state $T_{e1} = T_{h1}$ to a nonequilibrium state $T_{e2} > T_{h2}$ without changing its energy content, the heavy particle temperature must decrease $T_{h2} < T_{h1}$. This result is plotted in Fig. 10 for various values of the static enthalpy; values of T_{h2}/T_{h1} are almost independent of H for $4000 < H < 10{,}000$ Btu/lb. The reduction in T_{h2} relative to T_{h1} is large, and increases with increasing T_{e2}/T_{h2}; for $4000 < H < 10{,}000$ Btu/lb, the temperature T_{h2}/T_{h1} approaches $(T_{e2}/T_{h2})^{-1}$.

Hence, in the present experiments, the result of assuming equilibrium conditions in the presence of thermal nonequilibrium would lead to an over-estimation of the heavy particle temperature. Therefore, the evaluation of heat transfer groups involving both the heavy particle temperature and transport properties based on the heavy particle temperature would be in error. If large departures from thermal nonequilibrium did exist but were not taken into account, it is likely that evidence of this would have appeared in the heat transfer correlations. Values of enthalpy in the present experiments were generally in the range $1300 < H_t < 3000$ Btu/lb (Fig. 7). Without magnetic field, it is believed that departures from thermal nonequilibrium were probably very small in the core of the flow, as judged by the results given in Refs. 53 and 55.
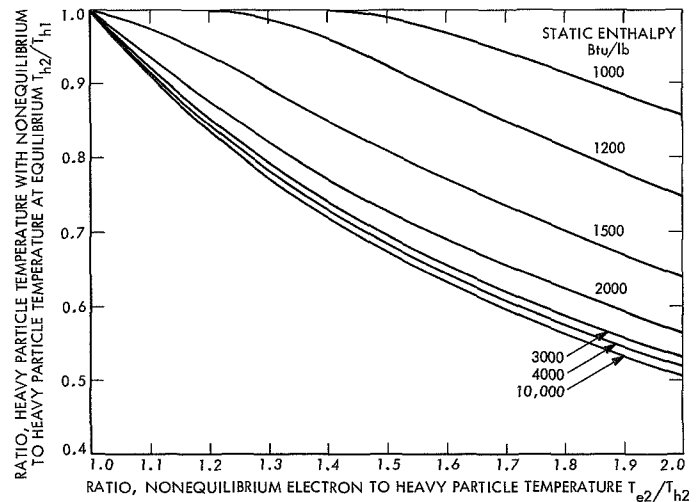
Fig. 10. Relative reduction in heavy-particle temperature due to thermal nonequilibrium when the energy per unit mass is held constant but ionization fraction is based on electron temperature; singly ionized argon at 0.01 atm.

The possibilities of thermal nonequilibrium in the present experiments have been discussed only with reference to flow-induced phenomena. In the presence of strong magnetic fields, magnetically induced nonequilibrium ionization can occur in partially ionized gases. This is discussed in Section VII, Part A.

F. Joule Heating

The analysis of Back (Ref. 10) forms a convenient tool for assessing the effects of Joule heating. The results of that analysis have been extended to include a more refined range of conditions consistent with the present experiments. Back's analysis applies for the laminar, steady, incompressible flow of an electrically conducting fluid having constant properties. The slug flow approximation was introduced, since at high Hartmann numbers the predicted velocity profiles become greatly flattened; experimentally, this effect has been well established for turbulent flow, e.g., Ref. 27. Axial heat conduction was retained in the energy equation. The axial momentum equation reduced to two terms since viscous effects were eliminated; the axial pressure gradient was balanced by the Lorentz force. A transverse magnetic field was applied perpendicular to the flow between two parallel plates that were isothermal and electrically nonconducting. An electric field was applied perpendicular to both the flow and the direction of the magnetic field. Since flow along the perfectly conducting sidewalls was not treated, heat transfer to electrodes was not studied. As a consequence of the assumptions, the electric current was parallel to the plates and uniformly distributed across the plate-spacing or channel-height, which was $2a$. Hall currents, ion-slip, and nonequilibrium were not considered.

The two principal independent variables were taken as the nondimensional axial variable $\bar{x}$ and the Joule heating parameter S. The symbol

$$\bar{x} = \frac{\dfrac{x}{2a}}{RePr} \tag{14}$$

and

$$S = Ha^2 Ec (1 - K)^2 Pr \tag{15}$$

where Ha is the Hartmann number and Ec is the Eckert number. The electric field factor, or load factor K, is $K = E/\bar{u}B$ and is zero when there is no applied electric field (short-circuit case). To first order, Eq. (15) could

be modified allowing for Hall currents and ion-slip by using a more complete form for Ohm's law than was used in Ref. 10.

Results were presented in terms of the Nusselt number Nu and a nondimensional wall heat flux parameter (designated here by the symbol Q^*),

$$Nu = (2a)\frac{h}{k} \tag{16}$$

$$Q^* = 2a\frac{q_w}{k_i(T_i - T_w)} \tag{17}$$

where

$$h = \frac{q_w}{(T_b - T_w)} \tag{18}$$

and a nondimensional temperature-difference ratio θ. The symbol

$$\theta = \frac{T_b - T_w}{T_i - T_w} \tag{19}$$

It is also useful to define a Stanton number, St, as

$$St = \frac{h}{\rho \bar{u} c} \tag{20}$$

To present the effects of Joule heating on heat transfer, the various heat transfer groups have been normalized with respect to their values for Joule heating equal to zero, i.e., $S = 0$. For a constant inlet temperature T_i, constant wall temperature T_w, and constant properties, the following relationships hold for a constant-area channel,

$$\frac{h}{h_0} = \frac{Nu}{Nu_0} = \frac{St}{St_0} = \frac{Q^*}{Q_0^*}\frac{\theta_0}{\theta} \tag{21}$$

where $h_0 = h_{S=0}$, and so on.

Since axial heat conduction is essentially negligible for $RePr > 50$, variations of Q^* and Nu are very weakly dependent on $RePr$ for values larger than 50. Results are plotted in Fig. 11 for $RePr = 100$ with Joule heating parameter S and $\bar{x}$ as independent variables. All dependent variables have been normalized with respect to their values at $S = 0$ to show the effects of Joule heating more clearly. Results for Q^*/Q_0^* are given in the upper graph; large changes in nondimensional heat flux occur
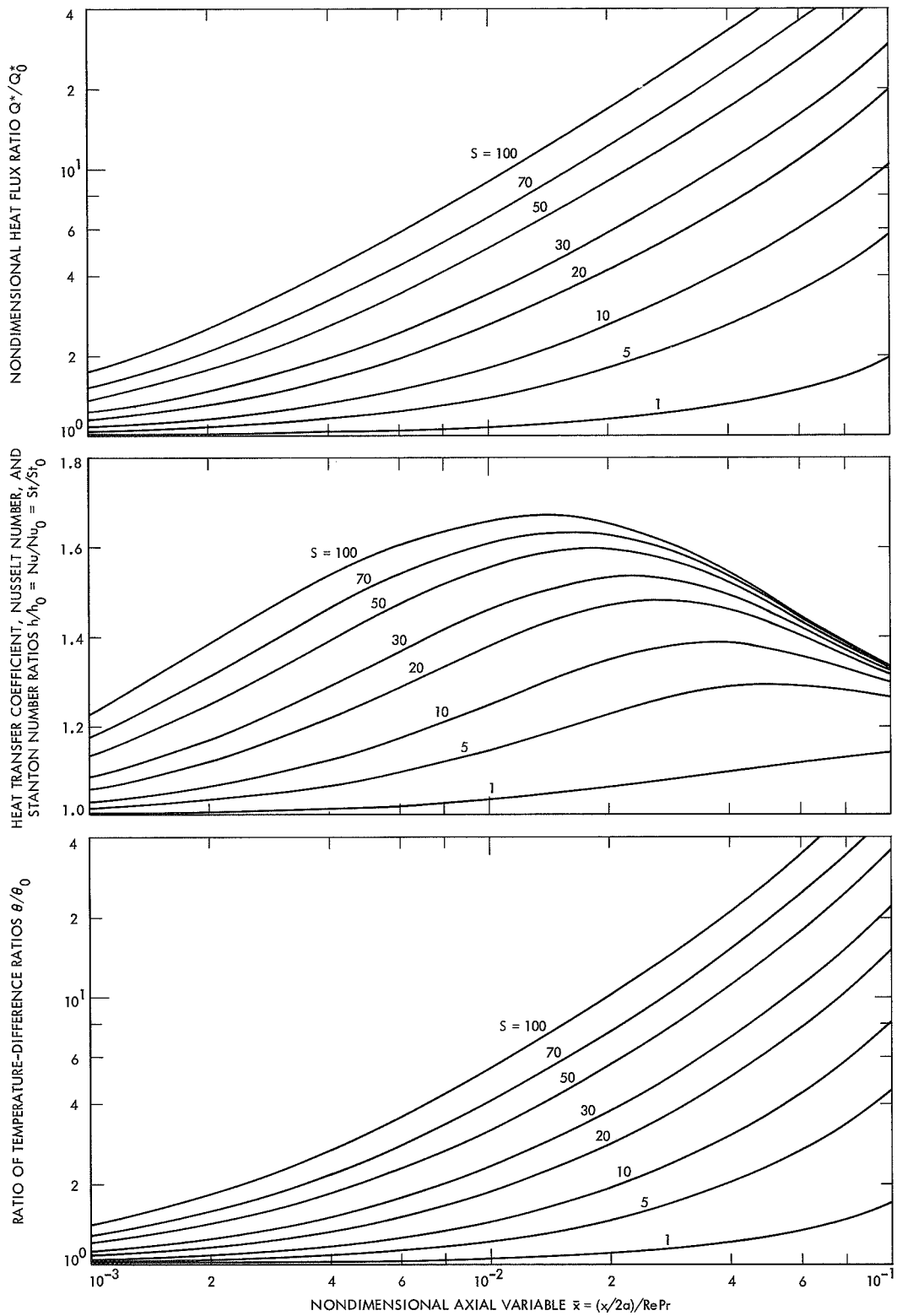
Fig. 11. Effect of Joule heating for laminar, incompressible slug-flow with constant properties (Ref. 10). Effect on non-dimensional heat flux, various heat transfer groups and axial temperature distribution for $RePr = 100$

when S is large, even at low values of $\bar{x}$. The center graph gives results for h/h_0, Nu/Nu_0, and St/St_0, which are related to Q^*/Q_0^* through θ/θ_0 given in Eq. (21). Joule heating has much less influence on these heat transfer groups than on Q^*/Q_0^* because of the large changes in θ/θ_0, lower graph. In fact, the curves for h/h_0, etc., exhibit maxima, which occur at successively lower values of $\bar{x}$ as S increases, because the slopes of θ/θ_0 become steeper at large $\bar{x}$ than do the slopes of Q^*/Q_0^*.

Within the assumptions of Ref. 10, the results given in Fig. 11 apply when an electric field is present, because E is included in the definition of S, Eq. (15). When applied electric and magnetic fields are present, heat transfer from the fluid to the walls can increase owing to two factors: (1) an increased energy content of the gas arising from the electric field, and (2) an increased temperature gradient at the walls. However, with just an applied magnetic field, only item (2) can contribute to an increased heat transfer because a magnetic field alone cannot alter the total energy content of the fluid. This important distinction must be kept in mind when relating theory to experiment. Thus, the term *Joule heating* is somewhat misleading when an applied magnetic field alone is considered.

In Fig. 11, the increase of θ/θ_0 with $\bar{x}$ is an indication of the rise in static temperature, in the axial direction, which the fluid undergoes because of Joule heating. In Ref. 10, $d\theta/dx$ passes from negative to positive for some value of the Joule heating parameter $1 < S < 10$. The theoretical basis for this is easily demonstrated even for the case of the zero electric field. For assumptions consistent with Ref. 10 and the further assumption that $E = 0$, an energy balance is written for a differential element of fluid dx in length, and this is combined with the axial momentum equation to yield

$$T_b - T_i = \frac{1}{c}\left[-\frac{\mathscr{P}}{\dot{m}}\int_0^x q_w\,dx + \frac{1}{\rho}j_z\,Bx \right] \qquad (22)$$

In Eq. (22), $\mathscr{P}$ is the perimeter of the channel, q_w is taken positive out of the control element, and j_z is the uniform current density induced as a consequence of uniform B applied for $x \geq 0$. When the two terms on the right are equal, the flow is isothermal. When the second term exceeds the first term, a rise in static temperature occurs so that $T_b > T_i$. Equation (22) applies only for an incompressible fluid.

In the absence of an applied electric field, however, Eq. (22) does not apply to an actual experiment performed in a constant-area channel. Since the bulk velocity would be constant for an incompressible fluid, Eq. (22) implies an increase in stagnation temperature that could not occur for an electrically conducting liquid in the absence of an applied electric field. Physically, in the case of a liquid, an increase in static temperature could occur only at the expense of a decreased kinetic energy of the fluid. However, if the fluid were an ionized gas, a reduction in the energy of ionization could be converted into a static temperature rise. Even then the maximum rise in static temperature could not exceed the sum of the kinetic energy and the ionization energy.

It has been demonstrated that the effects of Joule heating on heat transfer can be very large, provided values of the Joule heating parameter S are very large. Values of S computed for the experiments but based on theoretical, scalar electrical conductivity were easily of sufficient magnitude to explain the large changes in heat transfer that occurred by applying a magnetic field. However, it remains to be demonstrated whether such large values of S actually occurred in the experiments. This matter is examined further in Section VII in reference to the presence of Hall or ion-slip effects and corrections to scalar electrical conductivity.

G. Summary of Effects

For the conditions of the present experiments, it has been shown that the effects of thermal radiation, ionization, free convection, and secondary flows were all likely to have been small compared with the convective heat transfer. Even if the effects produced by these phenomena were additive, or cumulative, the combined effect on heat transfer was probably small compared with the large effects produced by the applied magnetic field in the experiments.

It is believed that large departures from thermal nonequilibrium were small in the core of the flow at zero, applied magnetic field. However, no direct method of determining thermal nonequilibrium was available. It was conceded that the presence of magnetically induced nonequilibrium ionization, the subject of a later discussion, was a possibility.

Finally, it was shown that, theoretically, Joule heating can have a dominating influence on convective heat transfer if the electrical conductivity is of sufficient magnitude. This, too, will be examined further in the light of the experiments themselves.

V. Experimental Results

A. Heat Transfer for Zero Applied Magnetic Field

The results of laminar heat transfer in a square channel without an applied magnetic field have been presented and discussed (Ref. 56). The results of average heat transfer over the four walls of the square channel were given for the second and third segments of the test section (see Figs. 1 and 3), and were correlated in terms of the nondimensional heat flux Q^* and the axial variable $\bar{x}$. To obtain the correlation, an estimation of the point of flow attachment in the inlet section was taken as the inlet condition or starting-point of the flow. The values of both Q^* and $\bar{x}$ depend on the flow-attachment point. Qualitative flow-attachment results were presented in a companion article (Ref. 57). Later it was discovered that the flow-attachment results used for heat transfer (Ref. 56) were not consistent with those given in Ref. 57; an error was made so that the attachment-length results reported for the square duct (Ref. 57, Introduction, and Fig. 6) were exactly half of the actual values used in obtaining the heat transfer correlation. In terms of channel-heights from the anode outlet, the corrected attachment-lengths for these tests are, approximately:

Nondimensional attachment length	Flow regime
$3.75 < (\Delta x/2a) < 5.0$	Subsonic, with swirl
$1.75 < (\Delta x/2a) < 2.5$	Supersonic, with swirl
$2.75 < (\Delta x/2a) < 4.0$	Subsonic, without swirl

The corrected values are consistent with the heat transfer results (Ref. 56) reproduced here in Fig. 12. The attachment length approached five channel heights in some cases, which was in the vicinity of the entrance to the test section. The corrected results can be verified approximately by comparing the average wall heat-flux in the first segment of the test section to that which occurred in the inlet section for subsonic flow. This was done to yield a rough approximation for location of peak heat flux and hence the location of flow attachment. Such a comparison is shown in Fig. 13; for $RePr < 100$ heat flux in the first segment of the test section exceeded average heat flux in the inlet section. Since a peak in the heat flux usually occurs in close proximity to a point of flow attachment, the results indicate that, for $RePr < 100$, the flow must have attached near to the downstream end of the inlet section or in the first segment of the test section. Flow attachment seems to have been sensitive
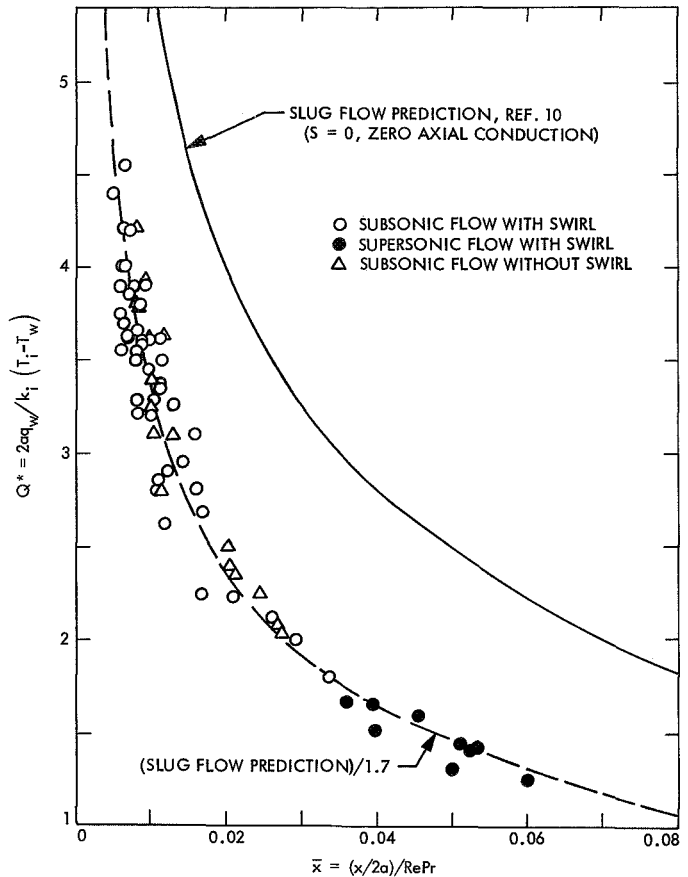
Fig. 12. Laminar heat transfer in a square channel (zero applied magnetic field)

to Reynolds number in the range encountered here. This is now believed to be the underlying reason that the corrected results for the square duct and the circular duct results (Ref. 57, Fig. 6) are no longer in agreement. That is, for the same mass rate of flow and hydraulic diameter, the Reynolds number of a square duct is only $(\pi/4)$ times the value in a circular duct. For this configuration, flow-attachment length appeared to decrease with increasing Reynolds number. Recent unreported flow visualization experiments, which were conducted for the same Reynolds number range by using water in a half-scale model, have tended to confirm this conclusion.

Returning to the zero-field heat transfer correlation in Fig. 12, it is evident that the experimental results cluster about a curve that lies 70% below Back's slug-flow prediction (Ref. 10) for $S = 0$, i.e., no Joule heating. This is not too surprising since it has been pointed out by Back and Witte (Ref. 58) that the actual heat flux for low-speed, constant-property flow over a flat plate is 70% less than a slug-flow prediction for $Pr = 1.0$. The zero-
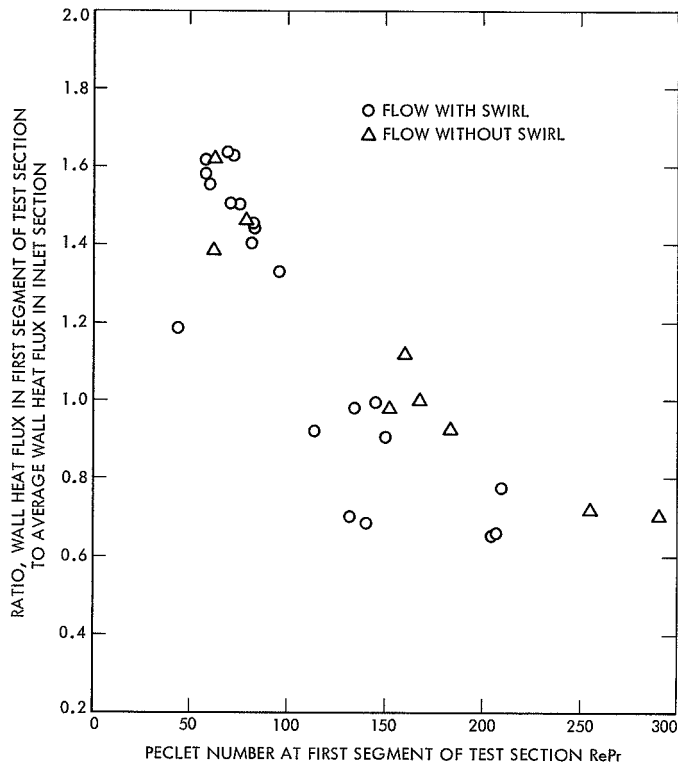
Fig. 13. Heat flux ratio in test apparatus for subsonic flow with zero, applied magnetic field. An approximate indication of region of flow attachment to walls (zero applied magnetic field)

field data is compared with Back's zero-field, slug-flow prediction because the latter was used as the normalizing factor to obtain the relative effects of Joule heating (Fig. 11) and will be referred to later. The experimental results shown in Fig. 12 include tests for both subsonic and supersonic flow with swirl, and subsonic flow without swirl. No significant effects of swirl or free-stream ionization were evident in this representation. Values of T_i and k_i that appear in Q^* were based on the heavy particle temperature determined from an energy balance by assuming thermal equilibrium. Since the experimental results generally were 70% less than slug-flow theory, a result previously predicted (Ref. 58), there is some added confidence given to the assumption of thermal equilibrium in the data analysis for zero magnetic field. If large departures from thermal equilibrium had occurred, the results of Fig. 12 probably would not have been obtained. This was discussed in Section IV, Part E.

In addition to normal experimental error, three factors contribute to the scatter seen in Fig. 12: (1) uncertainty associated with the location of flow attachment, (2) uncertainty in values of transport properties, and (3) uncertainty arising from the fact that the results refer to the average of four separate measurements (for the four walls), which varied sometimes about the average value.

Individual points in Fig. 12 are not designated according to whether they refer to the second or the third segment of the test section. Earlier it was mentioned that the transverse slots or cavities present in the second segment (Fig. 3) had an effect on the local heat transfer to the upper and lower walls of the channel. For zero magnetic field, it was determined that the heat flux to the coolant passage immediately downstream of the cavity was approximately 10 to 40% higher than the heat flux to the coolant passage located upstream of the cavity. However, the surface area associated with the higher (disturbed) heat flux in the segment was only 25% of the total surface area of that segment. Therefore, the error associated with the total averaged heat transfer to the second segment is not expected to exceed 10% of the values shown in Fig. 12 and was probably less than that for most of the tests. The error associated with the third segment would be lower yet. The magnitude of these errors is within the scatter of the data.

A comparison of the heat transfer correlation (Fig. 12) with several theoretical predictions is made in Fig. 14. All of the theoretical predictions apply to laminar flow for the case of constant wall temperature and not constant wall heat-flux. Although neither heat flux nor wall temperature were constant in these experiments, the assumption of constant wall temperature was closest to reality.

The faired experimental heat transfer correlation is well below the predictions for constant-property, slug flow between parallel plates (Ref. 10). Somewhat better agreement is achieved with the variable-property prediction for a flat plate (Ref. 12), especially when the Prandtl number approaches its low-temperature theoretical value of two thirds. Excellent agreement is obtained with the theoretical prediction of Montgomery and Wibulswas for a square duct with $Pr = 0.72$ (Refs. 49 and 59), with constant properties and zero axial heat-conduction. The latter result was obtained by combining the graphical data for Nusselt number (Ref. 49) with the graphical data for temperature distribution (Ref. 59) to yield Q^*; some error in Q^* is expected because the original graphs were small and difficult to read. Interestingly the Nusselt number prediction of Montgomery and Wibulswas for a square duct is below that for a circular duct having the same hydraulic diameter (Ref. 49).

18
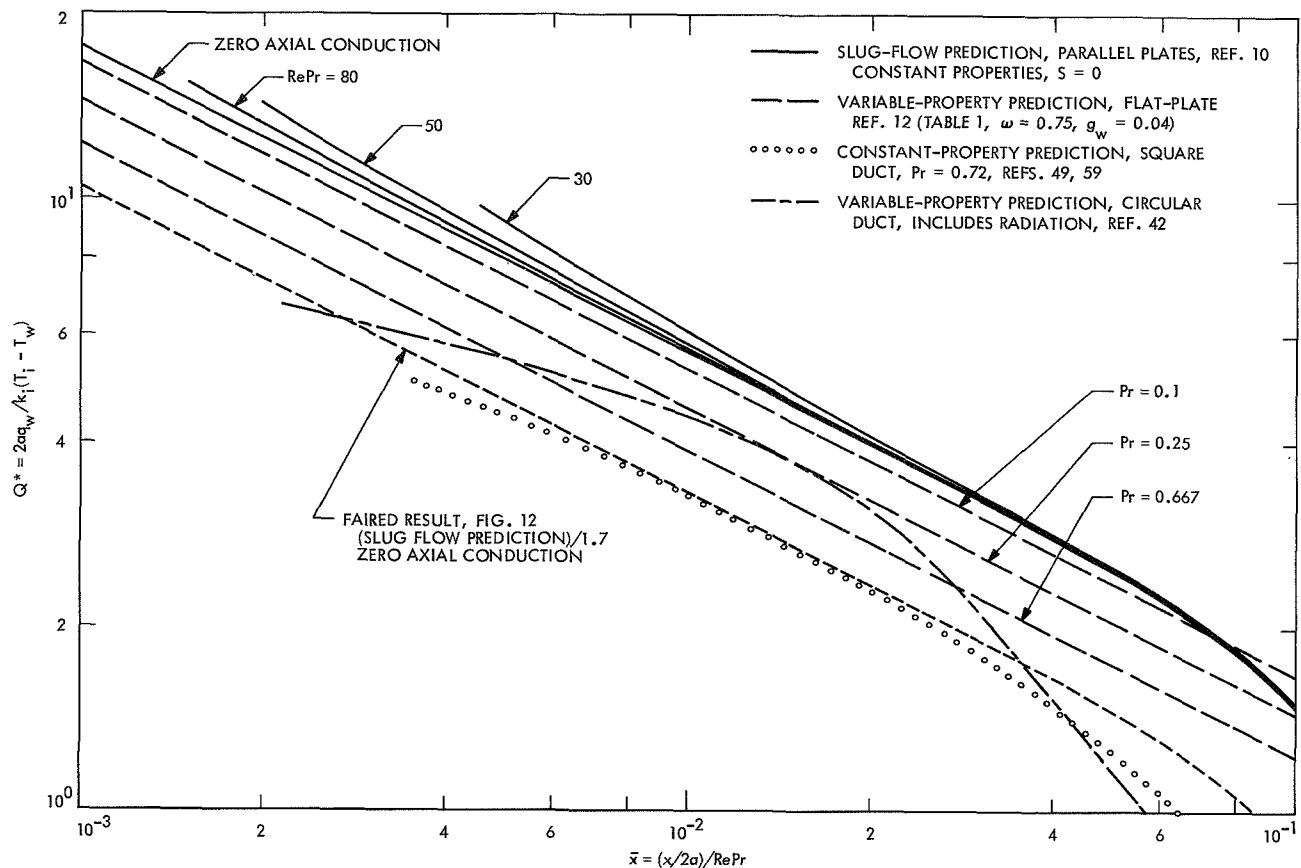
Fig. 14. Laminar heat transfer, comparison of experimental data with several theoretical predictions (zero applied magnetic field)

Also shown in Fig. 14 is the laminar prediction of Incropera and Leppert (Ref. 42) for high-temperature argon plasma-flow in a circular tube. This prediction includes viscous dissipation, thermal radiation, and axial heat conduction, but was solved for an assumed, initial velocity and enthalpy profile. Again, their graphical results were used by the present author to convert from Nusselt number to nondimensional heat-flux Q^*. The peculiar shape of the prediction bears the influence of thermal radiation, which was considered negligible for the present experiments. Incropera and Leppert give four different Nusselt number predictions; the one used here (Fig. 14) is based on enthalpy difference obtained with an energy balance technique.

A comparison of the present experimental results for laminar heat transfer with those of Schmidt (Ref. 60) and Wethern and Brodkey (Ref. 61) is given in Fig. 15. This is done most readily on a Nusselt number basis; values of the independent variable (Refs. 60 and 61) have been adjusted to conform to the use of $\bar{x}$ here.

Additional data for argon is available (Ref. 62) for a configuration remarkably similar to the one used here (approximately half-scale to this configuration, but axisymmetric). Unfortunately, those data were in a form unsuitable for direct comparison with the data of Fig. 15 and no corrections were made for flow-attachment; it is mentioned because plasma heat transfer data is so meager. The data for helium (Fig. 15) do not appear to have the same trend as the data for argon.

Definitions of the Nusselt number used in Fig. 15 are as follows:

Square duct (these data), height $2a$

$$Nu = \frac{2ac_p q_{exp}}{k_b (H_b - H_w)} \tag{23}$$

where total enthalpy is used for the bulk condition and k is based on local bulk temperature. The symbol $c_p = 0.1243$ Btu/lb,°R.
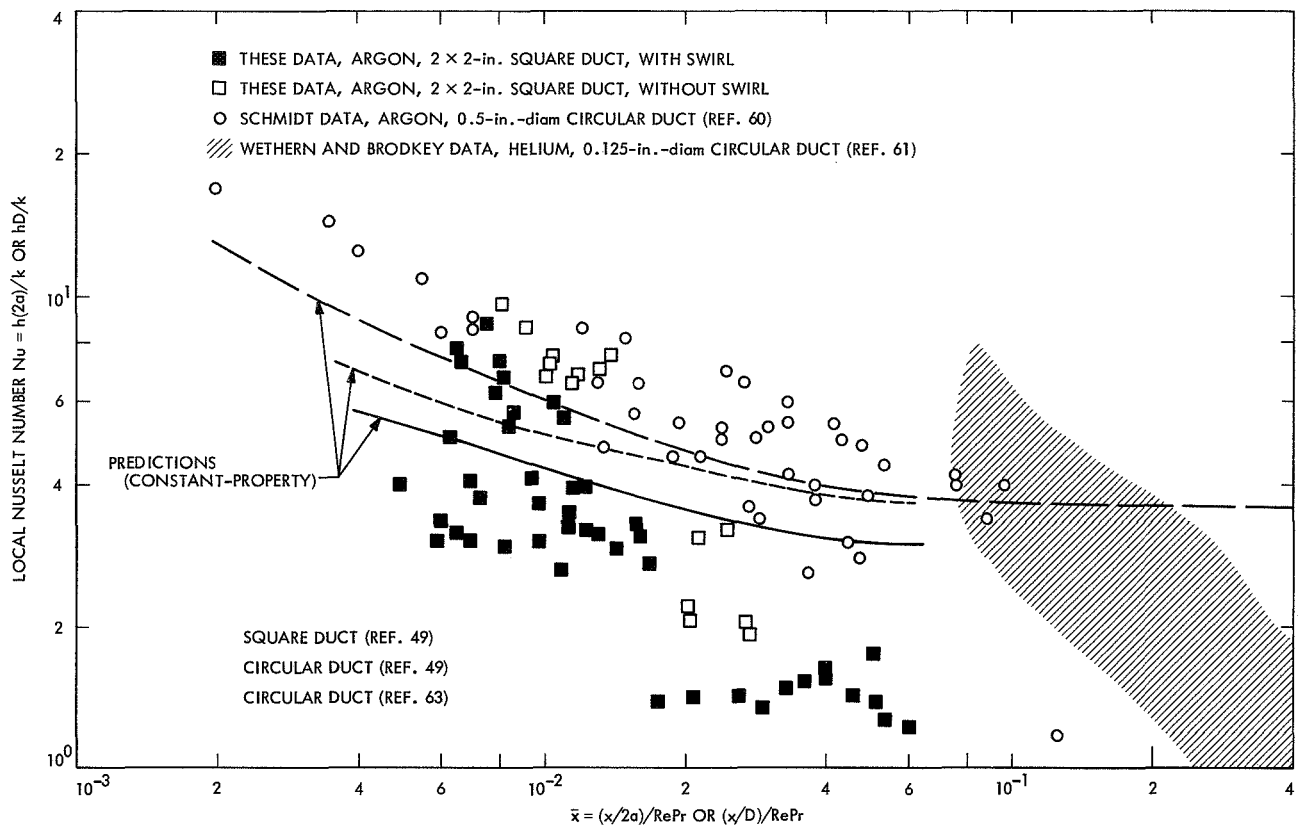
Fig. 15. Experimental laminar heat transfer data for high temperature, arc-generated, internal flows with highly cooled walls (zero applied magnetic field)

Circular duct (Ref. 60), diameter D

$$Nu = \frac{Dc_p q_{exp}}{k_m (H_m - H_w)} \qquad (24)$$

where H_m is a total, mixed-mean enthalpy similar to H_b.

Circular duct (Ref. 61), diameter D

$$Nu = \frac{Dq_{exp}}{k_b (T_b - T_w)} \qquad (25)$$

In these expressions, q_{exp} is the experimental heat flux to the wall taken as an average around the perimeter of the duct.

Schmidt's data for argon were obtained for considerably higher gas-inlet temperatures than were obtained here, and include substantial thermal radiation effects. This may account for the relatively higher Nusselt numbers in his experiment compared with the present data.

The use of the local Nusselt number to correlate the heat transfer data for the square duct (Fig. 15) has given rise to an apparent difference between the results with swirl and the results without swirl. This is probably because the local enthalpy difference was much smaller when no swirl was present in the flow (Fig. 7) and is not considered to be a real effect due to the swirl component of flow itself. This effect, taken with the consequence of assuming constant specific heat, also produced the same type of variation within the data with swirl. The lower group of shaded points for flow with swirl in the range $0.02 < \bar{x} < 0.06$ (Fig. 15) are the data corresponding to high-subsonic and supersonic flow. The relatively greater amount of scatter in the present experimental heat transfer data in Fig. 15 over that in Fig. 12 is due to two factors: (1) the Nusselt number, which is based on local gas conditions, was a less effective parameter than Q^* for correlating the present data, and (2) logarithmic scales were used in Fig. 15, whereas linear scales were used in Fig. 12. The parameter Q^* is based on inlet gas conditions, Eq. (17), and is related to Nu through the temperature-difference ratio θ.

Several theoretical constant-property predictions have been included in Fig. 15 for comparison with the various data; Kays' early result (Ref. 63) was also used by Schmidt in his presentation.

B. General Heat Transfer Results With an Applied Magnetic Field

The simplest way to present the effects of an applied magnetic field on heat transfer would be to display the variation of heat flux with magnetic field strength at a fixed axial location (Ref. 64). Several weaknesses are present in this simple approach. First, the entire flow field, including inlet conditions, changed significantly in the presence of the magnetic field; in general, the energy content, temperature, and velocity of the gas decreased with increasing magnetic field (regardless of its polarity). Hence, it would be desirable to use a method of presentation which includes these changes. In addition, changes in flow parameters produced large changes in transport properties even when the effect of the magnetic field on transport properties was ignored. Second, there was evidence that one effect of the magnetic field was to shift the attachment point of the flow further upstream. This shift would produce a longer flow-development length with a relative reduction in heat transfer at a fixed downstream location. The magnitude of this effect was not determined in these experiments.

The local Stanton number and the local heat transfer coefficient, based on stagnation enthalpy difference, have been selected as the most appropriate groups with which to present the data with an applied magnetic field. Although neither of them account for a shifting flow-development length, they involve no transport properties and include local changes in the enthalpy difference. Since the determination of stagnation enthalpy in these experiments did not depend on an assumption of thermal equilibrium, the use of enthalpy is to be preferred rather than temperature.

$$h' = \frac{q_{exp}}{(H_{t,b} - H_w)} \qquad (26)$$

and

$$St = \frac{h'}{\overline{\rho u}} \qquad (27)$$

A zero subscript attached to these parameters is used to designate values for zero magnetic field. Since the mass

flux $\overline{\rho u}$ was not influenced by the magnetic field in these experiments,

$$\frac{St}{St_0} = \frac{h'}{h'_0} \qquad (28)$$

Zero-field results were presented for the second and third segments of the test section, in Part A, because they were located downstream of the flow-attachment point, whereas the first segment was relatively closer to the flow-attachment point. The effect of the transverse slots (upper and lower walls, second segment) on the heat transfer measurements was small. At high magnetic field values, however, the slots had a substantial effect on heat transfer and their presence could not be ignored. Thus, only heat transfer results for the first segment of the test section will be given in the case of an applied magnetic field. This selection may be better than might have been anticipated with respect to the effect of nearby flow-attachment on the heat transfer results because one effect of the magnetic field was to decrease the flow attachment length. Error associated with axial heat conduction between the flange of the inlet section and the first segment (Fig. 3) was investigated. The maximum likely error associated with this was established at approximately 10%.

Experiments performed by Branover, et al. (Refs. 65 and 66) with a turbulent flow of mercury expanding from an orifice into a channel showed that an applied magnetic field (1) tended to smooth out flow asymmetries, (2) appreciably flattened the velocity profile, and (3) caused the flow to expand more rapidly than was so without a field, i.e., caused earlier flow-attachment. Because transverse velocity gradients are also present in an expanding laminar flow, an accelerated rate of expansion might also be expected in these experiments with applied magnetic field. Indeed, static wall-pressure distributions tended to verify this. The effect of a transverse magnetic field towards enhancing the degree of expansion (divergence) already present in a flow field may also have influenced flow over the slotted walls in these experiments (Fig. 3). Thus, the flow may have penetrated more deeply into the slots with magnetic field than for the case of zero magnetic field, thereby causing an increased heat transfer. Indeed, a theoretical basis for these hypotheses is available in the work of Branover, et al. (Ref. 67), for flow over slots with a transverse magnetic field. There, the magnetic field had the effect of deflecting the flow more deeply into the

slot but also produced increased shear around the pe-
rimeter of the slot walls, which would also result in
increased heat transfer to the walls within the slot.

A summary of the general effects of applied magnetic
field on heat transfer is shown in Fig. 16; some points
have been shifted slightly for clarity. Results are dis-
played in terms of Stanton number ratio, for maximum
field conditions only, and the nominal pressure. Heat
transfer results for only the upper wall A and the lower
wall C are given. Sidewalls will be discussed later.
Although there is considerable scatter in the data, the
trend with pressure is unmistakable. This might be
interpreted in terms of electrical conductivity, since elec-
trical conductivity, hence current flow, would increase
with decreasing pressure.

A detailed examination of the data in Fig. 16 reveals
no obvious or consistent differences arising from the
orientation of the applied field or from the presence of
swirl in the flow. However, wall C consistently under-
went larger changes with applied field than did wall A.
This is clarified further in Table 2, which indicates the
relative frequency with which heat transfer to wall C
exceeded heat transfer to wall A as a result of the mag-
netic field. An entirely satisfactory explanation for this
phenomenon has not been determined. Possibly the
initial flow produced by the arc-heater had a fixed asym-
metry, which was preserved or increased by the mag-
netic field.

The changes in Stanton number resulting from the
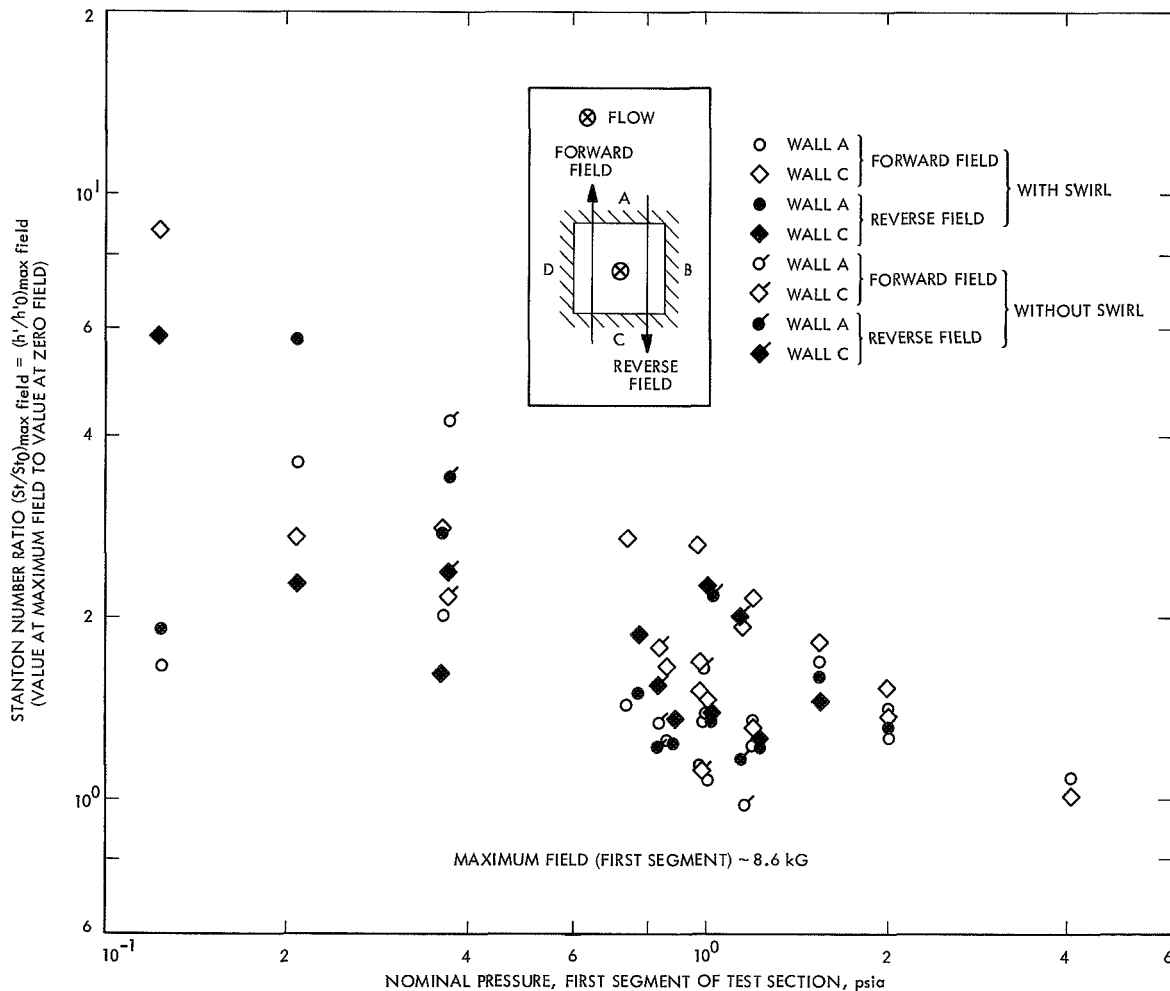applied magnetic field were large, especially at low

Fig. 16. General heat transfer results for first segment of test section at
maximum, applied magnetic field

Table 2. Effect of maximum magnetic field on Stanton number ratios for walls perpendicular to applied magnetic field

Item	Maximum forward field		Maximum reverse field	
	With swirl	Without swirl	With swirl	Without swirl
Total point-pairs	15	4	10	4
Values for wall C exceeding values for wall A	13	2	7	2

pressure. Despite the several uncertainties and errors associated with the data, the effects of the field are clearly significant. A closer examination of several selected tests will be discussed next.

C. Description of Selected Tests With Flow Results

Three test series with swirl and one without swirl have been selected to illustrate the effects of the transverse magnetic field on heat transfer, and flow, in more detail. The conditions and parameters for these test series are given in Table 3, which is presented in two parts. Part A lists the basic input conditions and bulk flow parameters at the center of the first segment of the test section; values at zero magnetic field and at maximum forward field are given for contrast. Part B lists several magnetic parameters for maximum forward field with scalar electrical conductivity; the term *ideal* designates the use of scalar electrical conductivity.

Test Series 18-H was conducted at moderately high pressure but low velocity; the applied magnetic field produced relatively small increases in heat transfer. Test Series 25-H and 26-H were conducted at successively lower pressures and higher gas velocities. Test Series 26-H was initially supersonic in the test section before a magnetic field was applied. Test Series 30-H, without swirl, has been included for comparison with Test Series 25-H because these two test series had a similar flow rate and pressure in the test section.

Magnetic Reynolds numbers for these test series were small (Table 3, Part B). However, values of the Hartmann number, Joule heating parameter, and induced electric current density $j_z = \sigma_0 \bar{u} B$, all based on theoretical scalar

electrical conductivity, were large at maximum magnetic field. Values are given for the center of the first segment of the test section; in general, these parameters reached a peak in the second segment of the test section.

Axial distributions of bulk temperature, pressure, and Mach number for the four test series are displayed in Fig. 17, and include results at zero and at maximum forward magnetic field. For subsonic flow at zero magnetic field, both static temperature and bulk velocity decreased with axial distance, as is typical of high temperature flows of this type with heat transfer. The effect of the magnetic field was to decelerate the flow, to increase the static pressure, and to decrease the static temperature as a consequence of the increase in heat transfer that occurred. In addition, the axial temperature gradient was generally increased by the presence of the magnetic field and was greater when no swirl was present in the flow than it was in cases of flow with swirl.

However, for supersonic flow at zero magnetic field, flow acceleration occurred along the length of the square channel and bulk velocity increased with axial distance. Corresponding to this, flow initially supersonic had a different pressure distribution than did cases of subsonic flow. This is seen in Fig. 17 when Test Series 26-H is compared with the other test series for subsonic flow. Flow initially supersonic responded somewhat differently to an applied magnetic field than did subsonic flow cases. Again, an overall retardation of the flow was produced with a reduction in bulk velocity so that the entire flow became subsonic; however, a positive axial velocity gradient (corresponding to accelerated flow) persisted well into the test section (Fig. 17). Thus, important differences in these channel flows were evident and depended upon the initial conditions of the flow (subsonic or supersonic) before the magnetic field was applied.

Note that Fig. 17 portrays bulk, or average, properties across the duct only. Thus, except for static wall pressure, the bulk values are incorrect in the part of the channel immediately downstream of the anode outlet (Fig. 1) because the flow was not yet attached to the walls in that region. However, values in the test section based on the entire cross-sectional area of the channel are appropriate and correct. It is well known from both theory and experiment that a transverse magnetic field greatly flattens the velocity profile in the y-direction, but less effect is observed in the z-direction. The effect of the magnetic field on the temperature profile, which directly affects heat transfer to the walls, is not well

Table 3. Values of parameters for selected tests computed from energy balance assuming equilibrium. Transport properties from Ref. 36.

	Test Series 18-H		Test Series 25-H		Test Series 26-H		Test Series 30-H	
A. Nonmagnetic parameters								
Item	Zero field	Maximum forward field	Zero field	Maximum forward field	Zero field	Maximum forward field	Zero field	Maximum forward field
Presence of swirl	With swirl		With swirl		With swirl		Without swirl	
Mass rate of flow $\dot{m}$, lb/s	0.007		0.005		0.007		0.005	
Nominal arc current, A	2000		2000		2000		2000	
Electric power to arc, kW	49.55	48.49	43.69	42.12	48.49	45.42	36.02	34.61
Total enthalpy, Btu/lb arc-heater outlet	4530	4390	5145	4790	3985	3620	3670	3165
Total enthalpy, Btu/lb; entrance to test section	2920	2565	4005	3145	2970	2300	2800	1580
Values at center, first segment of test section								
Average static pressure, psia	0.856	0.901	0.363	0.424	0.211	0.320	0.373	0.393
Bulk temperature, °K	9260	8880	9630	9165	8505	8070	8880	6465
Bulk velocity, ft/s	1365	1235	2505	1965	5030	3100	2120	1420
Reynolds number Re	270	260	230	200	260	260	190	200
Peclet number $RePr$	81	87	57	59	93	104	61	115
Eckert number Ec	0.028	0.027	0.066	0.054	0.36	0.18	0.069	0.058
Ionization fraction α	0.037	0.023	0.088	0.047	0.028	0.012	0.035	0.0005
Electron number density n_e, per cm³	1.65×10^{15}	1.10×10^{15}	1.50×10^{15}	1.05×10^{15}	0.34×10^{15}	0.23×10^{15}	0.71×10^{15}	0.015×10^{15}

Item[a]	Test Series 18-H	Test Series 25-H	Test Series 26-H	Test Series 30-H
B. Ideal, magnetic parameters for maximum forward field, first segment of test section				
Magnetic Reynolds number Re_m	0.05	0.09	0.095	0.013
Hartmann number Ha	64	71	56	32
Transverse induced current j_z, A/in.²	435	780	825	115
Joule heating parameter	37	80	230	35

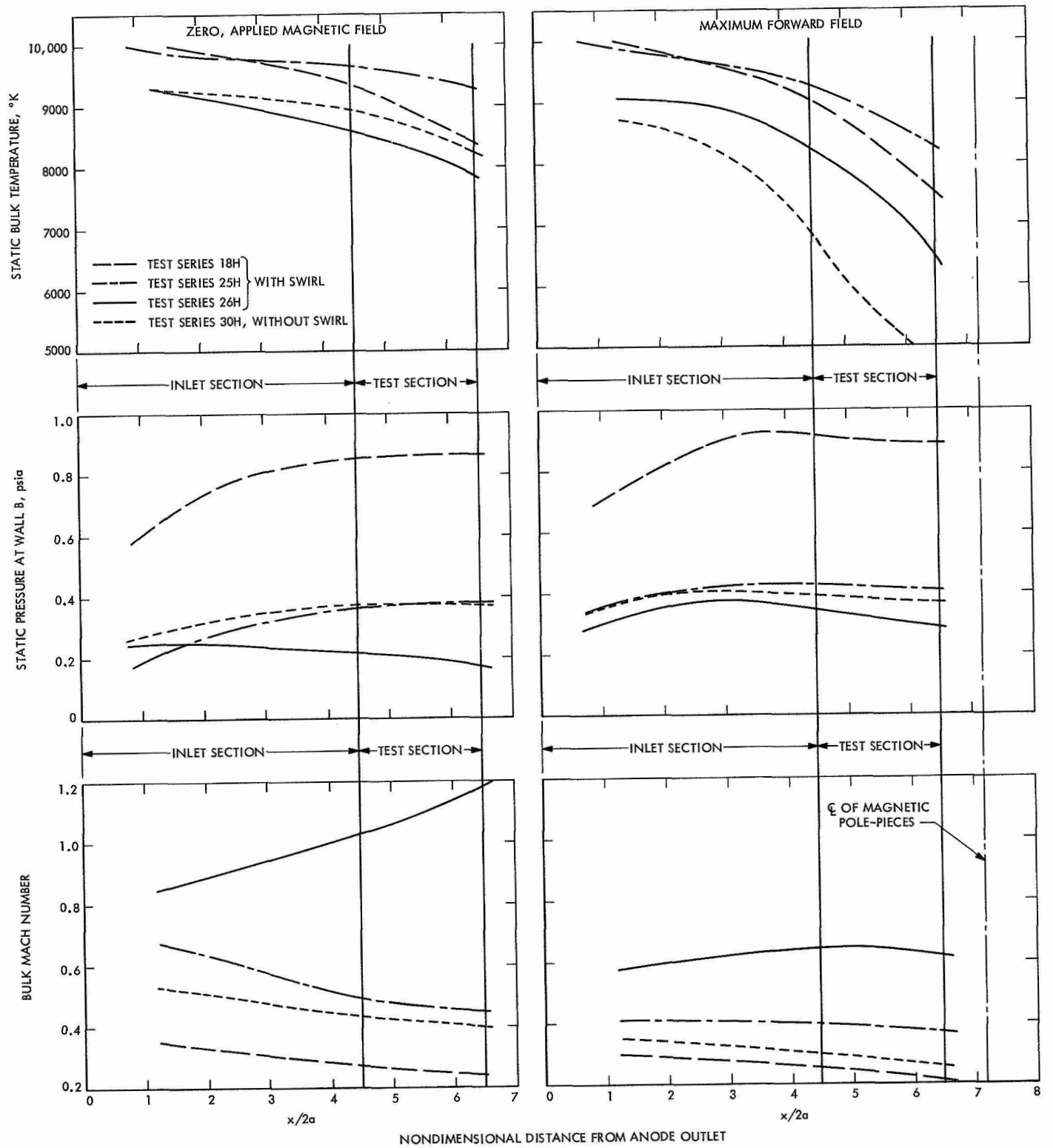[a]All items based on scalar electrical conductivity (Ref. 36).

Fig. 17. Axial distributions of flow parameters for selected test series, based on energy balance assuming equilibrium

known from published experimental results, especially when Hall effects, electrically conducting walls, and highly cooled walls are considered. From the heat transfer measurements, there was evidence in these experiments that the temperature profiles across the channel were not symmetric with respect to the centerline in the presence of a magnetic field.

Throughout the experiments, there was not a single case in which the static temperature increased with axial distance, as might be expected for example, with large Joule heating for low-speed laminar flow (Ref. 10). This was true for subsonic and supersonic flow, with or without swirl, even at the largest magnetic field that could be obtained. However, the analysis is not strictly applicable to a compressible ionized gas in which nonequilibrium effects can occur.

D. Heat Transfer Results With Magnetic Field for Selected Tests

Since differences in heat transfer to individual walls of the channel occurred as a result of the applied magnetic field, it is appropriate to examine the heat transfer results for the walls separately. This will be done for the four test series described in the previous section. Again, the Stanton number will be used as the dependent variable—Eqs. (26) and (27)—and results will be normalized to conditions at zero magnetic field—Eq. (28). The experimental heat flux for each wall was used in Eq. (26) for the local heat transfer coefficient, which is based on enthalpy difference. One disadvantage of this procedure is that the local bulk enthalpy $H_{t,b}$ would not necessarily be appropriate for individual walls if the flow field were asymmetric with respect to the centerline of the channel. In the absence of internal measurements there was no way to check or test this.

The applied magnetic field will be used directly as the independent variable because (1) it was the only parameter varied directly within a given experiment, (2) its value was well known, and (3) actual Joule heating appeared to have been very small, as will be shown later, and was difficult to establish with precision. Consistent with past discussion (and Ref. 10), the Joule heating term in the energy equation, for $E = 0$ and no Hall or ion-slip effects, is written

$$\frac{j^2}{\sigma_0} = \frac{j_z^2}{\sigma_0} = \sigma_0 \bar{u}^2 B^2 \qquad (29)$$

This may be nondimensionalized to yield S as

$$S = \frac{j^2}{\sigma_0} \left[\frac{a^2}{k_i \, (T_i - T_w)} \right] = Ha^2 \, Ec \, Pr \qquad (30)$$

or

$$S = \frac{\sigma_0 \, (\bar{u} \, Ba)^2}{k_i \, (T_i - T_w)} \qquad (31)$$

S is small when σ_0 is small even with large magnetic field B, i.e., σ may decrease more rapidly than B^2 increases if Hall effects are large. Much uncertainty exists regarding σ and k in the presence of an applied magnetic field so that S as defined by Eq. (31) is of limited use as an independent variable.

Heat transfer results for the four tests are presented in Figs. 18 to 21; horizontal walls A and C were perpendicular to the direction of the applied magnetic field, whereas sidewalls B and D were parallel to the direction of the applied field. It is evident that the heat transfer to horizontal walls A and C generally increased as the strength of the applied magnetic field increased, regardless of the direction of the applied field. With the possible exception of Test Series 26-H no evidence is present that any effect of swirl existed, because the trends of the curves do not show any consistent dependence on the direction of the magnetic field. Furthermore, the variation in heat transfer for the case of no swirl, Test Series 30-H, was as large as when swirl was present. In comparing Test Series 25-H and 30-H, it is evident that the relative effects of the magnetic field were larger for walls A and C when no swirl was present in the flow.

Results for sidewalls B and D were not only different from results for walls A and C but varied from test series to test series. In Test Series 18-H (Fig. 18) one of the sidewalls underwent only small increases in heat transfer, whereas the opposite wall experienced a sharp decrease in heat transfer. The effect on the walls became reversed when the magnetic field was reversed; this result was confirmed by seeing lateral (side-to-side) deflection of the exhaust plume. The same phenomenon occurred in Test Series 25-H (Fig. 19) except that increases in heat transfer were evident as well as decreases. However in Test Series 26-H (Fig. 20), the forward magnetic field produced moderate increases in heat transfer on both sidewalls, and a different result when the magnetic field was reversed. Test Series 30-H with no swirl (Fig. 21) was
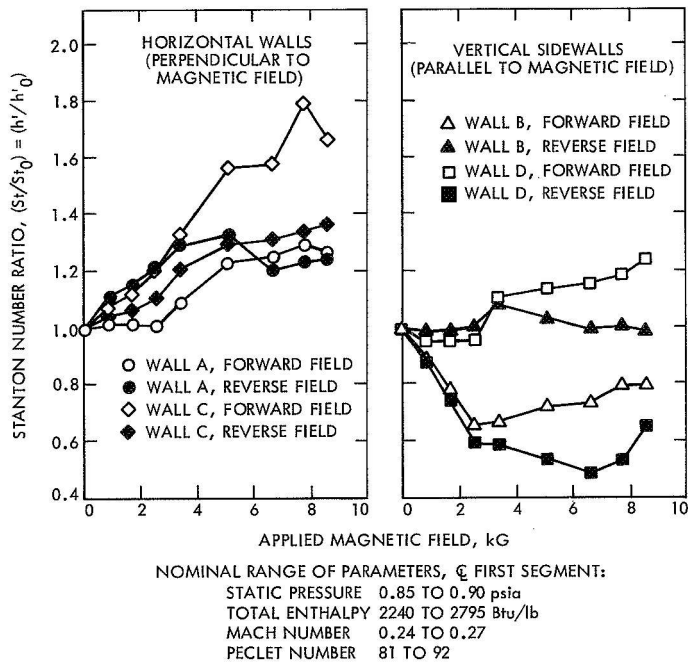
Fig. 18. Effect of magnetic field on heat transfer in first segment of test section, Test Series 18-H, flow with swirl
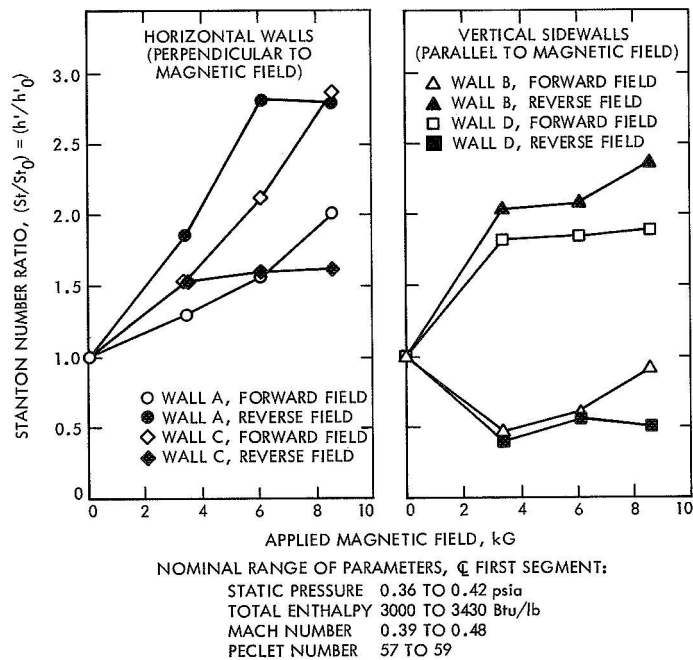
Fig. 19. Effect of magnetic field on heat transfer in first segment of test section, Test Series 25-H, flow with swirl
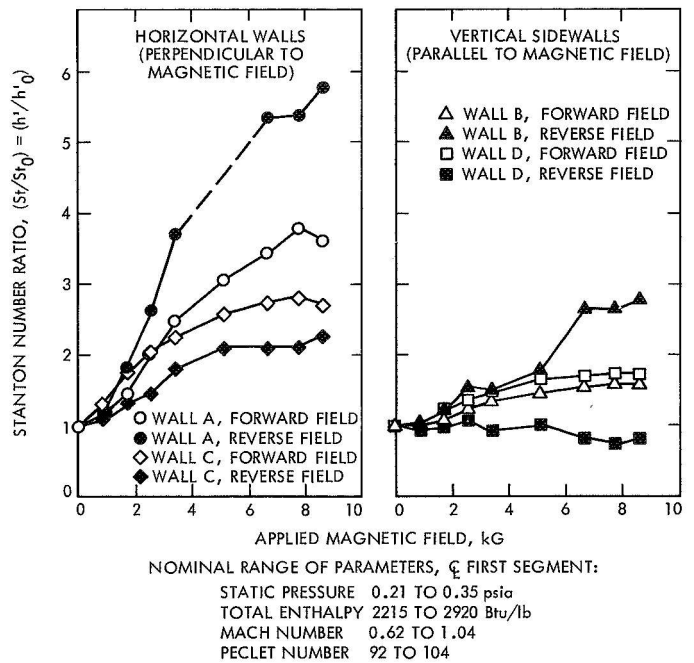
Fig. 20. Effect of magnetic field on heat transfer in first segment of test section, Test Series 26-H, flow with swirl
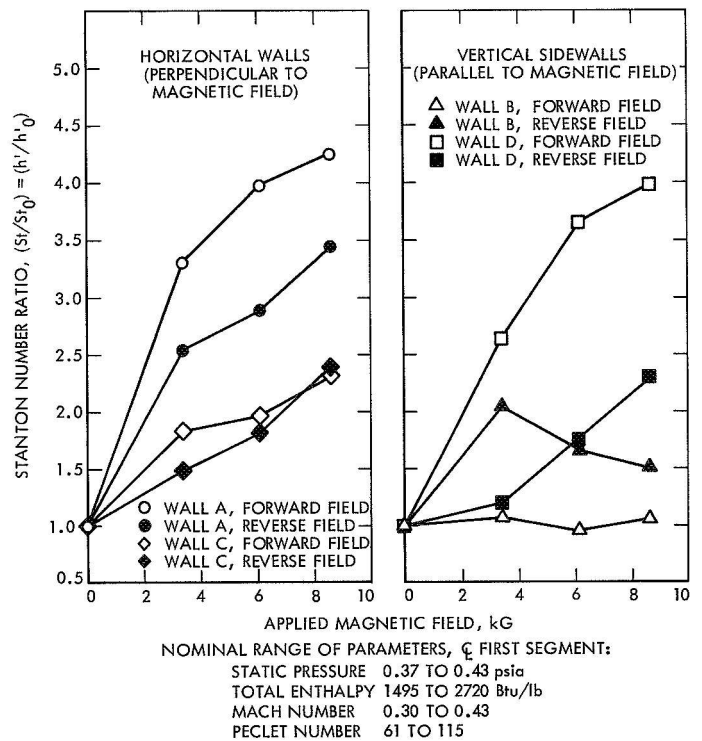
Fig. 21. Effect of magnetic field on heat transfer in first segment of test section, Test Series 30-H, flow without swirl

yet different, and does not compare with Test Series 25-H (Fig. 19).

The large, relative increases in Stanton number produced at walls A and C as a result of the magnetic field (Figs. 19, 20, 21) are clearly significant. To show that these increases more than offset any decreases in heat transfer to the sidewalls, the average Stanton numbers for the four walls is displayed in Fig. 22. The fact that the curves are reasonably symmetric with respect to the zero-field condition indicates that the direction of the applied magnetic field was not very important. The increases in average heat transfer were significant for all tests except Test Series 18-H, a test conducted at relatively high pressure.

E. Effects of Magnetic Field on Static Pressure Distributions

Axial distributions of static pressure along the walls of the square channel were measured by means of oil manometers. On sidewalls B and D pressure taps were located along the entire length of the channel; however, the upper and lower walls A and C were provided with pressure taps only in the inlet section of the channel. Again, it is well to mention that the magnetic field strength increased throughout the inlet section and attained a maximum value in the test section (Fig. 6). In general, the applied magnetic field produced two effects whether the flow was subsonic or initially supersonic, with swirl or without swirl: (1) the entire pressure level became elevated, except just downstream of the anode outlet, and (2) a peak pressure was produced somewhere in the inlet section and upstream of the test section.

Typical results for subsonic flow are shown in Figs. 23 and 24 for Test Series 18-H; only results for forward field are given since reverse field produced the same results qualitatively. The lowest curve in Fig. 23, for zero magnetic field, is typical of an expanding and attaching low-speed flow; the pressure is nearly constant in the test section following flow attachment to the walls of the channel. With increasing magnetic field, the pressure increases and a peak in pressure is produced near the end of the inlet section. Walls perpendicular to the direction of the applied field underwent a larger increase in pressure than did the sidewalls. This difference in pressure increased with increasing magnetic field strength and was correlated in terms of a parameter that contained the square of the theoretical transverse current $j_z = \sigma_0 \bar{u} B$. Extrapolating this correlation, predictions

Fig. 22. Heat transfer in first segment of test section averaged over four walls of channel

Fig. 23. Effect of magnetic field on axial pressure distribution along walls A and C, Test Series 18-H

Fig. 24. Static pressure in inlet section at an axial location one channel-height upstream of test section, Test Series 18-H

In Fig. 24, static pressure for each of the four walls at an axial location $x/2a = 3.5$ is plotted as a function of strength of the magnetic field at that axial location. Increase in pressure with increasing field is evident for both forward and reverse field; upper and lower walls underwent larger pressure than did the sidewalls. Note that with forward field the pressure was generally higher for wall C than for wall A and also higher for wall D than for wall B at the larger field values. For reverse field, opposite trends are evident. It is believed that this observation could result because of Hall effects and the resulting lateral Lorentz force; however, it could also be a consequence of swirl present in the flow. With respect to sidewalls, it was found that the wall undergoing the highest pressure usually underwent the highest heat transfer. Correlations with visual observations of the exhaust plume also indicated that the luminous plume always was deflected transversely in the direction towards the wall having the highest pressure.

Figures 23 and 24 apply for a case of flow with swirl. Similar results were obtained for tests without swirl but several differences were noted. In comparing the two cases for similar pressure in the test section, it was noted that at zero field the case without swirl had a higher initial pressure in the inlet section, a more gradual rise in pressure, and a somewhat flatter pressure distribution in the test section than did the case of flow with swirl. Otherwise, the results compared closely with those shown in Fig. 23. However, the differences between individual walls were not so pronounced as that for the swirl case (Fig. 24), and did not exhibit as clear a difference between horizontal and vertical walls or the small effects produced by reversed field.

Pressure distributions for flow that was initially supersonic within the test section before a magnetic field was applied were distinctly different from pressure distributions for subsonic flow. Results from the effect of the magnetic field are shown in Figs. 25 and 26 for Test Series 26-H. Again, however, the magnetic field was found to produce a peak pressure upstream of the test section. Note that relative changes in static pressure are even larger for the supersonic case than for the subsonic case at comparable field strengths. A comparison of Fig. 26 with 24 shows that the role of individual walls with respect to a reversal in magnetic field are not clearly evident for the supersonic case. Visual observations of the exhaust plume revealed much less lateral deflection of the luminous core for supersonic tests than for subsonic tests.

were made for the pressure on walls A and C in the test section; the results are shown in Fig. 23 by the dashed curves for wall A. The peaking in wall-pressure distributions observed here from the magnetic field was also observed in experiments with mercury flows by Branover, et al. (Ref. 66).

The fact that the magnetic field produced a steeper pressure gradient in the inlet section, which became zero and then changed sign upstream of the test section, is taken as strong evidence that the flow attachment point moved upstream as the magnetic field was applied. This upstream movement would have an important effect on the heat transfer because it would result in a longer flow development length with more heat transfer occurring upstream of the first segment of the test section. Thus the heat transfer results given in Figs. 18–21, which are values relative to the zero field values, are probably too low because the denominators of the normalized heat transfer groups were based on a shorter flow-development length than were the numerators.

Fig. 25. Effect of magnetic field on axial pressure distribution along sidewall B, Test Series 26-H

VI. Qualitative Observations

A. Visual Observations of Exhaust Plume

As discussed previously, a 2.88-in.-diameter circular exhaust duct (Fig. 1) was used to carry the flow from the square channel to the vacuum tank. Flow was discharged from the exhaust duct into the vacuum tank through a 5.0-in.-diameter circular port and entered the vacuum tank at an axial distance of approximately 13 channel heights (26 in.) from the end of the square test section. The exhaust plume was observed through large view ports just downstream of that location; effects of the magnetic field were easily observed. Since the magnetic field strength was negligibly small in the region of the exhaust plume, the changes observed there were probably a consequence of more pronounced changes that occurred much further upstream in the region of strong magnetic field and persisted downstream.

Without magnetic field, the color of the exhaust plume during subsonic tests, at pressures of the order of one psia and above, ranged from lavender to violet as is typical of low speed, slightly ionized argon flows. The plumes

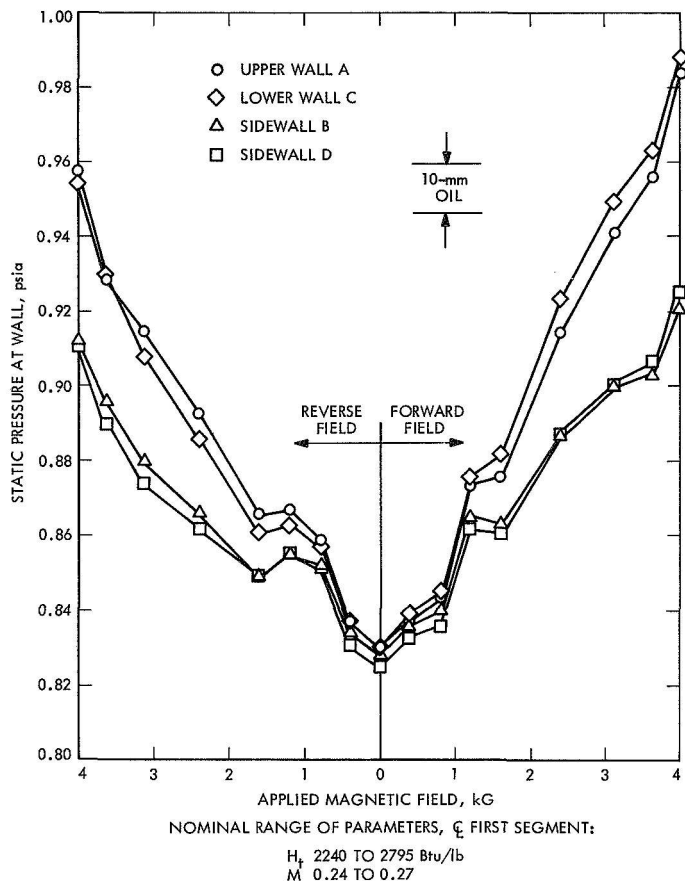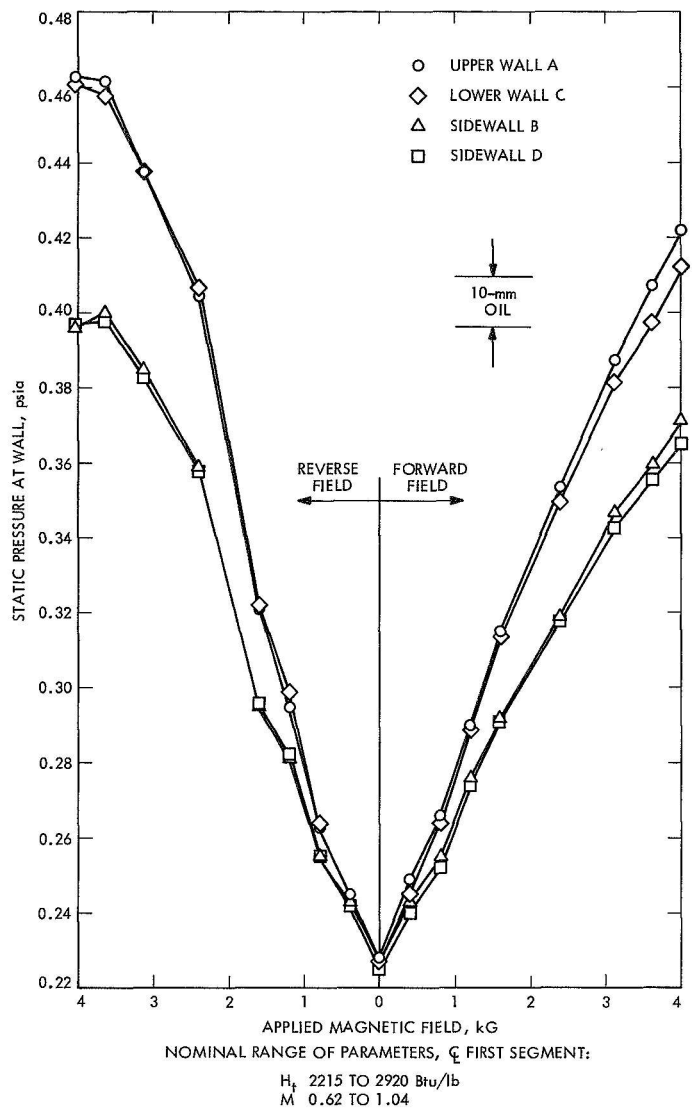**Fig. 26. Static pressure in inlet section at an axial location one channel-height upstream of test section, Test Series 26-H**

were blunt and relatively short, perhaps 6 in. long. At lower pressures, higher values of ionization fraction and higher velocities, the plumes became more brilliant, more devoid of color approaching white, and were generally longer and thinner than the plumes seen at higher pressures. No evidence of shock waves was seen for tests in which the Mach number in the test section exceeded unity.

Even small magnetic fields, applied upstream, had noticeable visible effects on the plumes; both color and shape of the plumes changed. Generally, the plumes became dimmer and blunter, and shortened increasingly with increasing magnetic field. The boundaries of the

plume became diffuse with poor definition, but sometimes the plume appeared to expand radially as it contracted in length. Radial expansion was usually more pronounced in the direction perpendicular to the direction of the magnetic field. As the magnetic field was increased, the core of the plume would take on a pale violet color and, at very large magnetic fields, appeared to be surrounded by a hazy blue fringe. Very often at high magnetic fields, the plume would be seen to split into two or more separate plumes. For tests that were initially supersonic at zero magnetic field, large magnetic fields tended to generate plumes of complex structure with zones of varying color; and splitting of the plume into three or more parts was evident. These plumes appeared to have a violet-to-lavender core with a reddish fringe. Multiple splitting of the plume could be evidence of Hall-induced cross-flows (e.g., Ref. 16).

A typical result for subsonic flow is shown by the series of photographs in Fig. 27. These are side views, i.e., the direction of view is perpendicular to the direction of the magnetic field. Values of magnetic field listed are for values occurring far upstream, at the end of the test section; only results for forward field are shown. Test conditions for this series of photographs were not greatly different from those of Test Series 18-H. The diameter of the exhaust port was 5 in.

Lateral motion of the plume was easily observed in top views, for which the direction of view was parallel to the direction of the magnetic field. Lateral motions were most easily seen, and appeared to be the most pronounced, at relatively low values of magnetic field. The power supply for the magnet could be prearranged to give a near-linear transient buildup of magnetic field to its maximum value in time spanning approximately 30 s. In such an experiment, the lateral motion of the plume was easily observed; and, of course, it reversed in direction when the field was reversed. These lateral deflections were believed to have been the result of Hall effects, even though the observed direction of deflection sometimes was opposite to that which would be expected theoretically. Lateral deflections were more pronounced in some tests than in others, and were not observed consistently when no swirl was present in the flow.

A series of photographs showing lateral deflections is given in Fig. 28. Test conditions were similar to those of Test Series 26-H, for which flow upstream was initially supersonic at zero magnetic field. Both side views (viewed perpendicular to magnetic field direction) and top views

SIDE VIEW
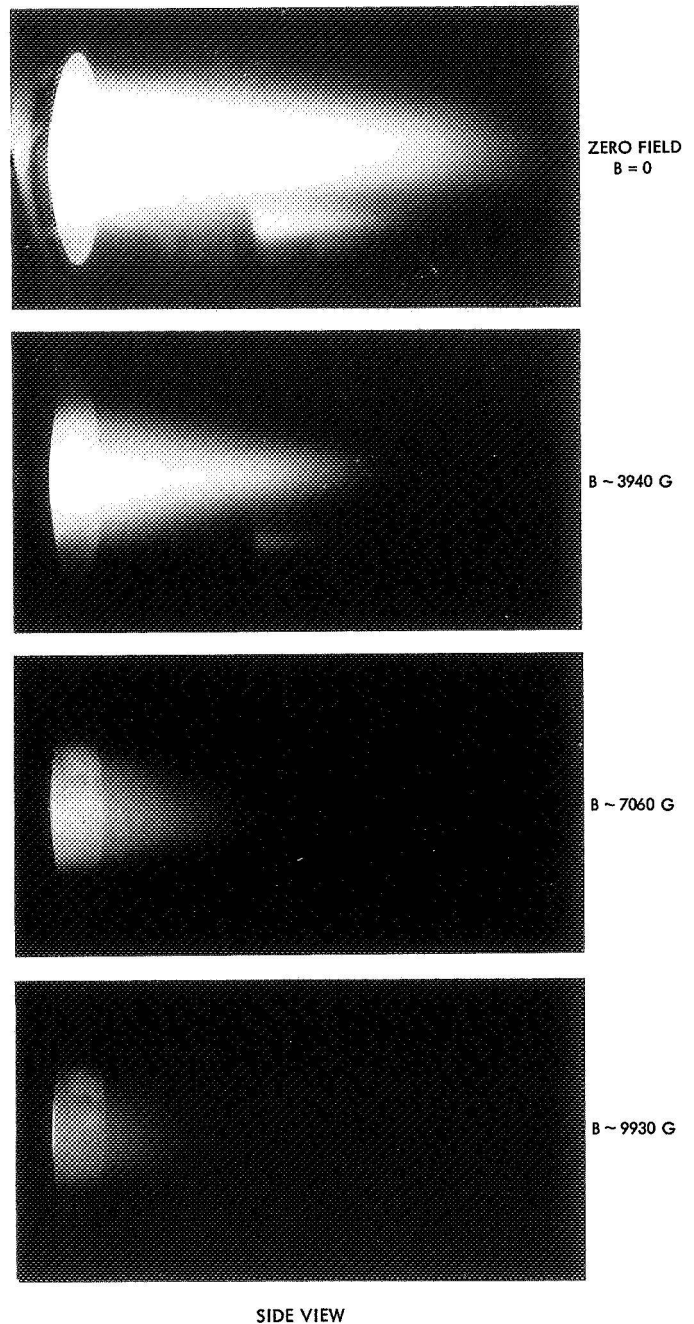
Fig. 27. Appearance of exhaust plume when forward magnetic field applied upstream in 2 × 2-in.-square test section, approximate conditions in test section: 0.006 lb/s mass flow rate, 1.0 psia

(viewed parallel to magnetic field direction) are shown; centerlines of the flow are indicated by the straight lines superimposed on the photographs. The lengths of the plumes appear shorter in the photographs than they actually were to the eye, especially at zero magnetic

3940 G FORWARD
FIELD

1970 G FORWARD
FIELD

ZERO FIELD

1970 G REVERSE
FIELD

3940 G REVERSE
FIELD

SIDE VIEW

TOP VIEW

Fig. 28. Effect of magnetic field on exhaust plume test conditions comparable to Test Series 26-H

field, because the camera had to be stopped down considerably on account of the brilliance of the plume. Because of this, the downstream portion was not wholly recorded on the film. At zero field the plume was very long and thin, and almost white. The plume broadened in both side and top views as the field increased for both forward and reverse directions. Again, values of the magnetic field refer to values far upstream at the end of the test section.

Side views in Fig. 28 indicate a nearly symmetric plume, with some asymmetry below the centerline towards wall C for zero and forward field. The plume appears symmetric in the top view at zero field. For increasing forward field, the plume was deflected left, toward wall D; for increasing reverse field the plume was deflected right, toward wall B. These results agree with the relative change in magnitude of the sidewall heat transfer seen in Fig. 20 for Test Series 26-H. However, these directions of deflection are opposite those expected from an axial, Hall component of current in the direction of flow. Although it may not be readily apparent from Fig. 28, the sharpness of the boundaries of the plume decreased with increasing field and were more diffuse in top views than in side views.

B. Post-Experiment Examination of Apparatus

After all the tests had been completed, the apparatus was disassembled and internal walls of the various parts were examined for evidence of (1) high local heat transfer as indicated by discoloration or burning, (2) erosion of metal or insulator surfaces, and (3) possible current flow into walls as indicated by etching or pitting of surface.

The most obvious feature noted was the deposition of a thin, granular, gray coating of material on all interior surfaces. This coating was hard to the touch and did not scrape or flake off easily. Most likely, this was a deposition of tungsten vaporized from the cathode surface although the cathode did not appear to be severely eroded. Walls of the inlet section appeared to be more or less evenly coated except in the corners immediately downstream of the anode orifice and for several uncoated, irregular patches of bare, parent metal surrounding pressure taps. There was a decided difference in the degree of deposition on the walls of the copper segments forming the test section, but the surface of the coating was finer than that in the inlet section. Wall C clearly received the greatest deposition of material, as might be expected, because the heavy tungsten particles would be deflected towards the lower wall by gravity. If that were

true, upper wall A would have had the least deposition of material; however, wall A had a greater deposition than either of the sidewalls B or D. Since there was no ferrous material present in the apparatus except for the stainless steel inlet section, which showed no evidence of erosion, the magnetic field could have had no influence on particle trajectories of the material before deposition. It is not known whether the preferential plating on the copper walls was related to the surface temperature of the metal or if it were related to, or were a consequence of, the heat transfer differences between the walls. Recall, that walls A and C invariably received the highest heat transfer in the presence of the magnetic field.

If current flow into or out of the copper walls was a result of an electron flow, the mechanism for that electron flow requires explanation. An electron flow into one part of the wall is not difficult to imagine, but an electron flow out of another part of the wall requires explanation in terms of a physical emission mechanism. Thermionic emission requires surface metal temperatures far exceeding those encountered in these experiments. If current flow into the wall was, rather, by ions flowing to the wall and recombining with e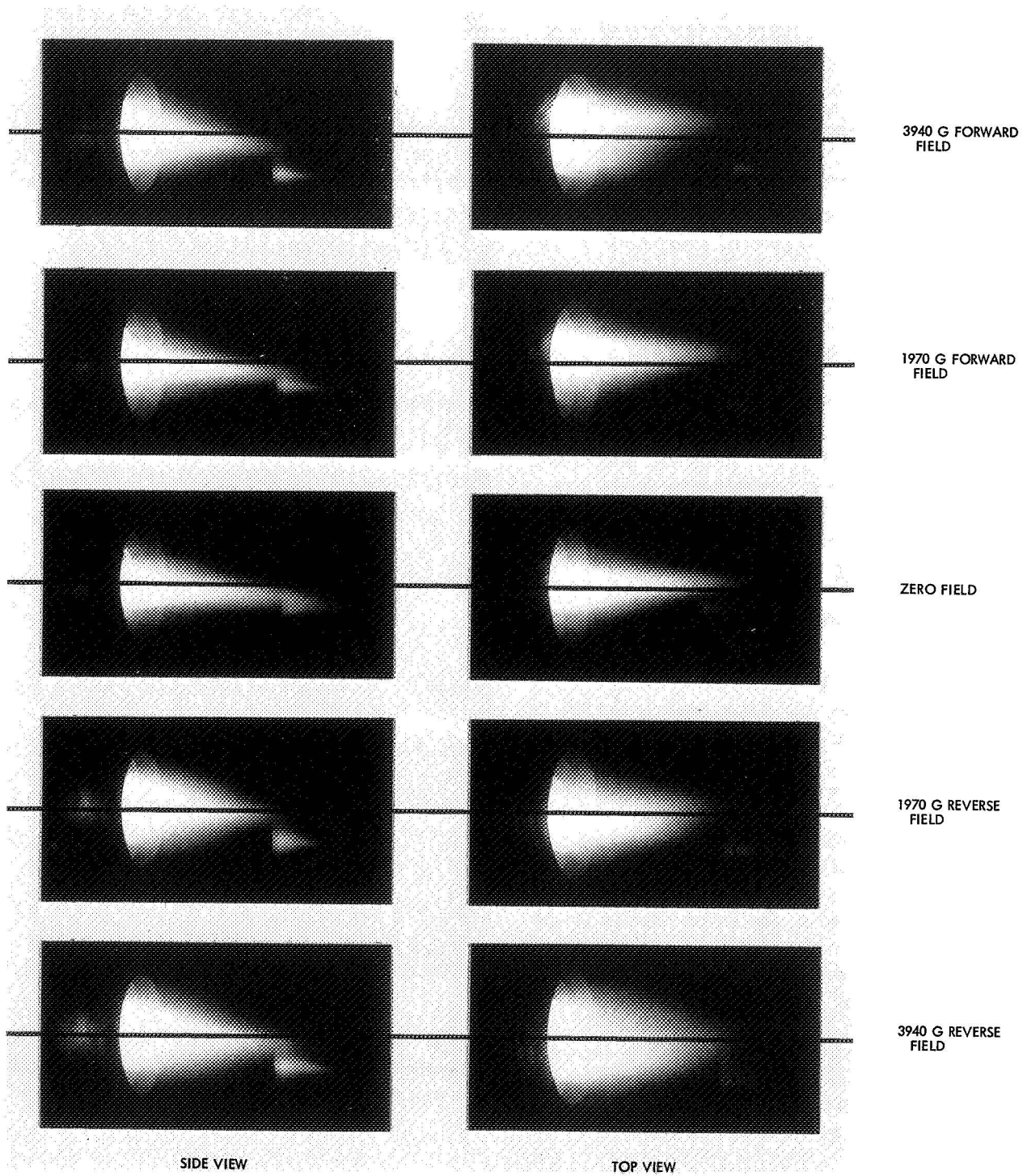lectrons at the surface, some pitting of the surface might be expected because of a sputtering effect. Not only was very little pitting of the copper surfaces evident, but there was no evidence of erosion. Thus, there was no obvious physical evidence that an electrical current had flowed into or out of any of the walls of the channel. However, this evidence cannot be considered as conclusive.

An examination of the uncooled flange of the exhaust duct, used to mate the square channel to the exhaust duct, revealed obvious discolorations at walls A and C. These discolorations were taken as supporting evidence for the high heat transfer to walls A and C with applied magnetic field.

VII. Discussion of Results

Several factors that could have influenced the heat transfer results were discussed in Section IV. In this coming section, factors related to magnetic field effects will be emphasized and will be discussed with respect to the experimental data.

A. Nonequilibrium Ionization and Effects on Electrical Conductivity

A discussion of the various mechanisms that can lead to an elevated electron temperature $T_e > T_h$ has been

given by Rosa (Ref. 22). The effect of a strong magnetic field in producing an induced electric field by the motion of a conducting fluid is an important factor leading to nonequilibrium. If the Hall parameter $\omega_e \tau_e > 1$, ionization instability can exist so that fluctuations in electron density occur (Refs. 22, 68). Magnetically induced ionization has been demonstrated experimentally by Zauderer (Refs. 23, 24) for pure argon as well as various mixtures of noble gases. He obtained values of T_e/T_h exceeding two and values of the Hall parameter approaching 20; electron number densities were increased by as much as a factor of 10^3 when the initial upstream electron density exceeded a threshold value of approximately $10^{11}/cm^3$. In Ref. 23 the magnetic field was 15 kG and a stable, nonequilibrium plasma was produced by the magnetic field for pure argon.

An analysis by Sherman (Ref. 20) for laminar, nonequilibrium plasma flows was facilitated by assuming an electrical conductivity that was a linear function of the current density. This assumption reduced his problem to one involving a single fluid, but a limitation on the enhanced electrical conductivity was a consequence of the mathematics; it was found that $\sigma/\sigma_0 < 2$ for the short-circuit case. Sherman's results are interesting because they indicate that the velocity profiles become appreciably flattened in the presence of nonequilibrium for the short-circuit case, even for rather low values of Hartmann number. But Hall effects were found to produce an opposite result in that large values of the Hall coefficient $\omega_e \tau_e \sim 10$ caused the velocity profiles to become more rounded, even in the presence of nonequilibrium.

Both Sherman (Ref. 20) and Maksimov (Ref. 21) evaluated the Saha equation at the electron temperature to obtain the ionization fraction α. Sherman derived an alternate form for Ohm's law for the case in which the electrical conductivity was a power-law function of current density. On the other hand, Louis (Ref. 68) postulated a modified Ohm's law to account for the Hall effect by introducing a mean-square deviation in the electron-density fluctuation.

However, Monti and Napolitano (Ref. 69) have shown that evaluation of the Saha equation at the electron temperature can lead to a large over-estimation of both ionization fraction and electrical conductivity for nonequilibrium conditions. They derived a generalized Saha equation and compared the ionization fraction α obtained from that to the ionization fraction α_e obtained from the usual form of Saha equation evaluated at the electron temperature. At the same plasma pressure, heavy-particle temperature, and electron temperature, an expression relating the actual ionization fraction α to the ionization fraction based on electron temperature α_e was derived in terms of the degree of nonequilibrium T_e/T_h. For argon, $\alpha > \alpha_e$ for $\alpha_e > 6/7$, $\alpha = \alpha_e$ for $\alpha_e = 6/7$, and $\alpha < \alpha_e$ for $\alpha_e < 6/7$. The result for argon is shown in Fig. 29 for various values of T_e/T_h. The disparity between α and α_e increases with increasing T_e/T_h and becomes increasingly large as α_e decreases.

As an example, consider an argon plasma at 0.1 atm pressure, a heavy-particle temperature $T_h = 6000°K$ and $T_e/T_h = 1.5$. For this case, $\alpha_e \sim 0.02$ based on T_e, whereas $\alpha_a = \alpha_h \sim 0.75 \times 10^{-4}$ based on T_a; $\alpha_e/\alpha_h \sim 270$. From Fig. 29, the actual ionization fraction is $\alpha \sim 0.0065$ so that $\alpha_e/\alpha \sim 3$, an overestimation by a factor of three. Still, the actual ionization fraction is roughly 90 times larger than the value based on heavy-particle temperature. The effects on electrical conductivity would be correspondingly large because for low α_e, $\sigma/\sigma_e = \alpha/\alpha_e$, and $\sigma_e/\sigma_h = \alpha_e/\alpha_h$. The foregoing results do not account for Hall effect. If, in addition, $\omega_e \tau_e \simeq 5$, then the final electrical conductivity in this example could be approximately three to four times larger than a value based on heavy-particle temperature.

In the present experiments there was no way to establish clearly the existence of magnetically induced, nonequilibrium ionization, or what the degree of nonequilibrium might have been. Perhaps the change of color observed sometimes in the exhaust plume at large values of applied magnetic field (in contrast to just a change in luminosity) is some evidence that nonequilibrium may have occurred in the presence of the magnetic field. Since the magnetic field could not have added energy to the gas, an increase in ionization corresponding to a new state of magnetically induced nonequilibrium could have occurred only at the expense of a decreased heavy particle temperature (Part IV-E). That effect alone would have tended to reduce the heat transfer with magnetic field. However, a greatly enhanced ionization fraction would have had the effects of increasing the relative amount of heat transfer caused by ionization (Fig. 8) and increasing the electrical and thermal conductivities of the gas. Figure 8 must be used with caution because both q_{dw} and q_{Tw} would undoubtedly be altered by the presence of nonequilibrium, i.e., Ref. 44 does not consider nonequilibrium. Thus, the net effect of magnetically induced nonequilibrium on heat transfer is very difficult to estimate. This would be true even if T_e and T_a could have been determined experimentally in
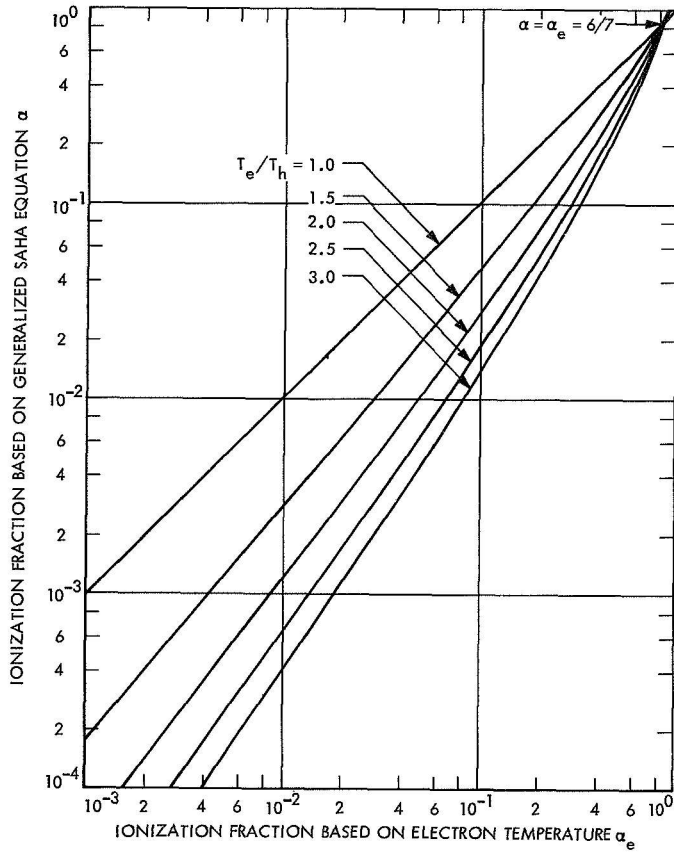
Fig. 29. Ionization fraction for argon in nonequilibrium. A comparison of values based on a generalized Saha equation (Ref. 69) to values based on electron temperature

the presence of the magnetic field, since the effect on transport properties would still have been largely unknown. However, taking into account the differences in enthalpy and heat flux that occurred from zero to maximum applied magnetic field, and then using Fig. 8, it is estimated that nonequilibrium ionization could have accounted for a maximum of approximately 30% of the rise in heat transfer produced by the magnetic field.

B. Hall and Ion Slip Coefficients and Effects on Joule Heating

Hall and ion slip coefficients have been computed (Ref. 70) according to the methods of Cann, et al. (Ref. 71). The expressions for $\beta_e = \omega_e \tau_e$ and $\beta_i = \omega_i \tau_i$ are

$$\frac{\omega_e \tau_e}{B} \simeq \frac{3}{4} e \left(\frac{\pi}{8 \, m_e \, k \, T_e} \right)^{1/2} \left(\frac{n_e \, q_{ei}}{2} + n_a \, q_{ea} \right)^{-1} \tag{32}$$

$$\frac{\omega_i \tau_i}{B} \simeq \frac{3}{4} e \left(\frac{\pi}{8 \, m_i \, k \, T_i} \right)^{1/2} \frac{n_a}{(n_a + n_e)^2 \, q_{ia}} \tag{33}$$

Calculations for argon in the pressure range of interest are presented in Fig. 30 for the equilibrium condition $T_e = T_i = T_a = T_h$. Except for an empirical relation that was used for q_{ia} (Ref. 70), all collision cross sections were taken directly from Ref. 71. Since $\beta_e \geq 10^2 \, \beta_i$, it does not appear that ion slip could be significant for the equilibrium condition. However, for $\beta_e > 1$, it is possible that $T_e > T_i$ so that β_i could be somewhat larger relative to β_e than indicated, but not sufficiently increased to warrant further consideration.

In the presence of Hall and ion slip effects the Joule heating term in the energy equation is not simply j^2/σ but includes an additional term arising from those effects (e.g., Ref. 34, p. 121). For present purposes the first order correction to Joule heating due to Hall and ion slip effects, neglecting this additional term, would yield (Ref. 70)

$$S' = \frac{S}{(1 + \beta_e \, \beta_i)^2 + \beta_e^2} \tag{34}$$

where S' represents a modified (corrected) value of the Joule heating parameter. In view of Fig. 30, it is possible to ignore ion slip; hence

$$S' = \frac{S}{1 + \beta_e^2} \tag{35}$$

The corrective term may be viewed as a reduction factor for electrical conductivity (Ref. 34, p. 394).

It is obvious that values of β_e need not be very large to drastically reduce Joule heating. In the present experiments, the theoretical values of β_e were so large that values of S' were not sufficient to explain the increases in heat transfer experienced at high values of applied magnetic field. It is probable that the effective values of β_e were much smaller than the theoretical values. This possibility is examined in the following paragraphs.

Since S or S' involves the square of the current density, the direction of current flow appears to be unimportant. Thus, the effect of a magnetic field on the heat transfer in a channel with walls electrically insulated would appear to produce a uniform rise in heat flux at all walls, i.e., around the perimeter. This was not so in these experiments. However, transverse Lorentz forces arising from axial current flow would alter that situation.
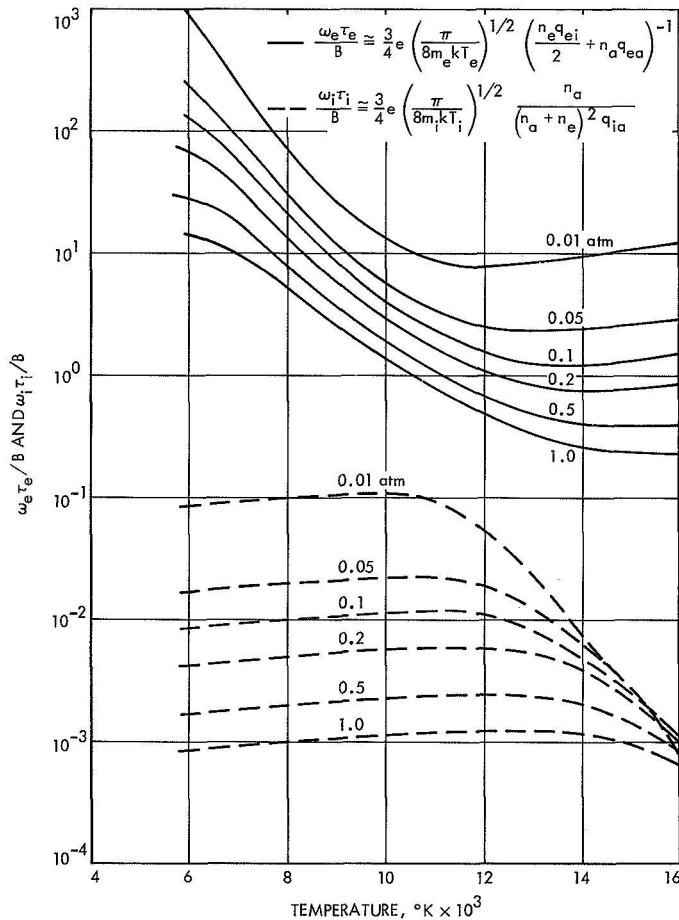
Fig. 30. Hall and ion slip coefficients for singly ionized equilibrium argon

C. An Assessment of Joule Heating in the Experiments

The constant property, slug-flow theory (Ref. 10) predicts only modest increases in heat transfer for $S \leq 5$ above the value for $S = 0$ except when $\bar{x}$ is very large (Fig. 11, and Ref. 10). It is expected that the slug-flow theory tends to over-predict the actual heat flux in the absence of applied electric or magnetic fields (Ref. 58). In fact, the present experimental data at zero applied field (Fig. 12) indicates that result in both trend and magnitude. At high magnetic fields ($Ha > 5$) the velocity profile becomes theoretically so flat that the slug-flow approximation should be a very good one in that case. Thus, for high magnetic fields, the results depicted in the upper set of curves (Fig. 11) are too conservative because Q_0^* has been over-predicted by approximately 70%.

To compare theoretical Joule heating with experimental results, a chart similar to the upper part of Fig. 11 was prepared except that the levels of the S-curves were all increased by a factor of 1.7 in view of the arguments just presented. Data for the selected Test Series of 18-H, 25-H, 26-H, and 30-H were plotted on this chart to estimate the effective values of Joule heating parameter S_{eff}. Only the data for high applied magnetic fields were used, i.e., only data for $B > 5$ kG. Values of $\bar{x}$ were estimated using flow attachment results for zero-field conditions modified slightly to account for upstream movement of the attachment point at high magnetic fields. Values of $\bar{x}$ ranged from 0.0075 to 0.009 for Test Series 18-H and from 0.036 to 0.042 for Test Series 26-H. Only heat transfer data for walls A and C were used, and the results for those two walls were averaged before plotting.

The effective values of the Joule heating parameter determined by the method just described are plotted in Fig. 31 against the theoretical values based on scalar electrical conductivity. Values of S_{eff} are very small compared with theoretical values, but a general trend is evident. Effective values of the Hall coefficient $(\beta_e)_{eff}$ were next computed from Eq. (35) by setting $S' = S_{eff}$ and solving for $(\beta_e)_{eff}$. The results are shown in Fig. 32. Theoretical values of the Hall coefficient were calculated from the simple relation $\beta_e = \sigma_0 B/en_e$ with σ_0 taken from Ref. 36. These values tend to be somewhat lower than values obtained either from Eq. (32) or Fig. 30. Note that the effective values scatter in the range $4.5 < (\beta_e)_{eff} < 7.5$ and show little trend with increasing β_e (theoretical). This flat trend with increasing magnetic field was also obtained by Louis (Ref. 68); however, his values for $(\beta_e)_{eff}$ (a compilation of the works of several authors) were approximately half the values obtained here.

Effective Hartmann numbers were next calculated from the simple relation $(Ha)_{eff} = Ha/[1 + (\beta_e)_{eff}^2]^{1/2}$. Significantly, all values of effective Hartmann number exceeded five, strengthening the slug-flow assumption for high magnetic field.

The situation is less clear in regard to changes in static, bulk temperature of the gas as a consequence of Joule heating. Thus, the lower set of curves in Fig. 11 indicates that the relative effect of an applied magnetic field (Joule heating) on the static bulk temperature is such that T_b increases with increasing S and $\bar{x}$. However, the same line of argument that was used to increase the levels of S-curves in the Q^*/Q_0^* plot of Fig. 11 by a factor of 1.7 would result in the S-curves for θ/θ_0 to be decreased by a factor of 1.7. Thus, for small S,

EFFECTIVE JOULE HEATING PARAMETER S_{eff}

O TEST SERIES 18-H
△ TEST SERIES 25-H } WITH SWIRL
◇ TEST SERIES 26-H
□ TEST SERIES 30-H, WITHOUT SWIRL
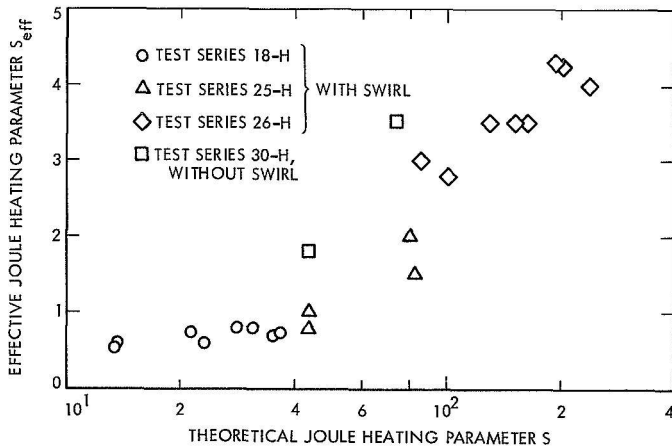
THEORETICAL JOULE HEATING PARAMETER S

Fig. 31. Comparison of effective Joule heating parameter with theoretical values. Values of S_{eff} obtained from forced correlation between experiment and modified slug-flow theory, Ref. 10
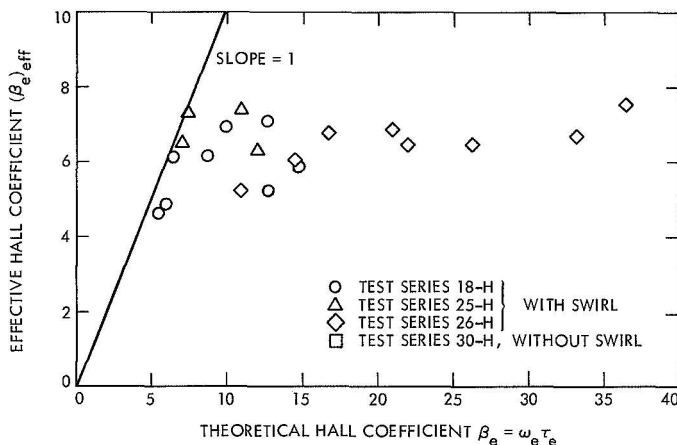
EFFECTIVE HALL COEFFICIENT $(\beta_e)_{eff}$

SLOPE = 1

O TEST SERIES 18-H
△ TEST SERIES 25-H } WITH SWIRL
◇ TEST SERIES 26-H
□ TEST SERIES 30-H, WITHOUT SWIRL

THEORETICAL HALL COEFFICIENT $\beta_e = \omega_e \tau_e$

Fig. 32. Comparison of effective Hall coefficient with theoretical values. $(\beta_e)_{eff}$ obtained from results of Fig. 31

$\theta/\theta_0 = (T_b - T_w)/(T_b - T_w)_0 < 1.0$ provided $\bar{x}$ is not too large. Yet, for constant $RePr$, $d(\theta/\theta_0)/dx > 1.0$ for all $S \geq 0$. It was always true in the experiments that $\theta < 1.0$ and $d\theta/dx < 1.0$ (Fig. 17) with or without a magnetic field.

In view of the preceding argument, it was possible to reconcile the magnitudes of the experimental axial temperature distributions of θ/θ_0 with the results of Fig. 31 for Test Series 18-H and 25-H. Comparisons for Test Series 26-H and 30-H were marginal at best. However, the trend of θ/θ_0 with $\bar{x}$ for high magnetic fields was never completely resolved with the theoretical results. Another factor enters in when magnetically induced nonequilibrium is considered. Then, the heavy particle

temperature would have to decrease to accommodate an elevated electron temperature and an increased ionization fraction, because the magnetic field does not increase the energy of the gas. Hence, even in the presence of substantial Joule heating, the magnetic field could have the effect of reducing the static temperature as a consequence of (1) increased heat transfer, and (2) nonequilibrium effects.

If ionization and electron heating effects were excluded, local heat transfer to a wall could increase owing to (1) an increased temperature gradient at the wall, (2) an increased thermal conductivity of the gas at, or near, the wall, or (3) a combination of (1) and (2). In the present experiments, the applied magnetic field brought about large increases in heat transfer to the walls at a given axial location, despite the fact that the local bulk temperature and enthalpy of the gas decreased as compared with the case of zero magnetic field. At walls perpendicular to the direction of the applied field, it is expected that the thickness of both the velocity and thermal boundary layers would be decreased by the action of the magnetic field. This would cause higher velocity and temperature gradients at the wall than with zero field conditions. However the thermal conductivity of the gas would not have been greatly altered at those walls, and could have been enhanced in the presence of nonequilibrium ionization. Thus, the temperature profile across the channel must have been altered in such a way as to yield increased gradients at the wall consistent with an overall reduction in gas energy, as would be obtained from an integral or average value across the channel.

At walls parallel to the direction of the applied magnetic field, the sidewalls in the present experiments, the boundary layers would not have been severely retarded and could even have become thickened by the magnetic field. Furthermore, because of the anisotropic effects of a strong magnetic field on gas transport properties, the thermal conductivity could have been substantially less than its value at the other walls. Hence, heat transfer to walls parallel to the direction of the applied magnetic field would not be as great as at walls perpendicular to the direction of the field.

Therefore, for a partially ionized gas subject to a transverse magnetic field, it appears that the natural consequences of a small amount of Joule heating (1) would lead to heat transfer variations on walls that have different orientation with respect to the direction of the field, and (2) would produce results which were qualitatively the same as those that were actually observed.

D. Estimates of Current Flow in the Gas

No experimental measurements were made for electric current flow either within the channel walls or within the gas. An axial momentum balance was used to estimate the transverse current density j_z which, when compared with the theoretical transverse current density, also yielded an estimate of $(\beta_e)_{eff}$. This was done to see if results for $(\beta_e)_{eff}$ were reasonable and compatible with the estimates previously made with heat transfer (Fig. 32). Acceleration (actually deceleration, in this case) and wall friction terms were retained in the axial momentum equation, which was used in the form

$$-\frac{dp}{dx} - (\bar{\rho}\bar{u})\frac{d\bar{u}}{dx} = j_z B + \tau_w \left(\frac{\mathscr{P}}{A}\right) \qquad (36)$$

where τ_w is the shear stress at the wall, $\mathscr{P}$ is the perimeter of the channel, and A is the cross-sectional area. Within the test section of the channel both dp/dx and $d\bar{u}/dx$ were negative.

Skin friction is rather complicated to evaluate in hydromagnetic channel flows because it not only differs in magnitude for walls perpendicular to the magnetic field from walls parallel to the magnetic field, but also varies along the walls themselves (Ref. 72). In fact, the wall shear-stress decreases with increasing Hartmann number for walls parallel to the magnetic field and increases with increasing Hartmann number for walls perpendicular to the magnetic field. These phenomena occur, of course, because the character of the boundary layers on the different walls depends on the local direction of the magnetic field.

A much less sophisticated approach was adopted here because the friction-force term in Eq. (36) was small compared with the other terms, except at low values of magnetic field. It was assumed that wall-shear on vertical walls B and D was not influenced by the magnetic field and the usual parallel-plate skin-friction coefficient for laminar flow was applied to those walls. The simple Hartmann result (e.g., Ref. 73) was used for horizontal walls A and C. It was further assumed that horizontal and vertical walls did not influence one another and that there were no corner effects. The last term in Eq. (36) was estimated by the relations

$$\tau_w \left(\frac{\mathscr{P}}{A}\right) \sim \left(\frac{\mathscr{P}}{A}\right)\left(\frac{1}{2}\bar{\rho}\bar{u}^2\right)\left(\frac{C_{fo}}{2} + \frac{C_f}{2}\right) \qquad (37)$$

where

$$C_{fo} = \frac{12}{Re} \qquad (38)$$

and

$$C_f = \frac{4\,Ha^2}{Re}\left[\frac{\tanh(Ha)}{Ha - \tanh(Ha)}\right] \qquad (39)$$

For a single segment of the test section $\mathscr{P} = 8a$ and $A = 4a^2$ so that Eq. (37) can be written as

$$\tau_w\left(\frac{\mathscr{P}}{A}\right) = \left(\frac{\dot{m}}{A}\right)^2\left(\frac{1}{\rho a}\right)\left(\frac{6}{Re}\right)\left[1 + \frac{Ha^2}{3}\frac{\tanh(Ha)}{Ha - \tanh(Ha)}\right] \qquad (40)$$

In Eq. (40), Ha was taken to be the effective Hartmann number in the presence of Hall effect.

The list of relations used to perform the axial momentum balance and to calculate the components of electric current density were:

$$-\left(\frac{\Delta p}{\Delta x}\right) - \left(\frac{\dot{m}}{A}\right)\left(\frac{\Delta\bar{u}}{\Delta x}\right) = (j_z)\,B_{eff} + \left(\frac{\dot{m}}{A}\right)^2\left(\frac{1}{\rho a}\right)\left(\frac{6}{Re}\right)\left[1 + \frac{(Ha)_{eff}}{3}\frac{\tanh(Ha)_{eff}}{(Ha)_{eff} - \tanh(Ha)_{eff}}\right] \qquad (41)$$

$$(Ha)_{eff} = \frac{Ha}{\left[1 + (\beta_e)^2_{eff}\right]^{1/2}} \qquad (42)$$

$$Ha = Ba\left(\frac{\sigma_0}{\mu}\right)^{1/2} \qquad (43)$$

$$(j_x)_{eff} = \frac{(\beta_e)_{eff}\,\sigma_0\,\bar{u}\,B}{\left[1 + (\beta_e)^2_{eff}\right]} \qquad (44)$$

$$(j_z)_{eff} = \frac{\sigma_0\,\bar{u}\,B}{\left[1 + (\beta_e)^2_{eff}\right]} \qquad (45)$$

$$(j)^2_{eff} = (j_x)^2_{eff} + (j_z)^2_{eff} \qquad (46)$$

All items in Eqs. (41) to (46) were known or estimated from experimental data except the effective Hall coefficient. These equations were iterated until a balance was achieved for Eq. (41). At high values of magnetic field the pressure-gradient term and the Lorentz-force term were dominant. At low values of magnetic field all terms were small and comparable in magnitude, so that accuracy in those cases was poor. Test Series 18-H was examined by this method.

Values of the effective total current density established by iterating Eqs. (41) to (46) are shown in Fig. 33 for Test Series 18-H. Values of j_{eff} were of the order of one-eighth the values of $j_z = \sigma_0\,\bar{u}B$. Corresponding values of $(\beta_e)_{eff}$ are compared with theoretical values in Fig. 34; shaded points from Fig. 32 are included for further comparison. It is first noted that values of $(\beta_e)_{eff}$ determined by the momentum-balance technique tend to be higher than those determined by the heat transfer method in which S′ or S_{eff} was used to estimate $(\beta_e)_{eff}$. Also, values of $(\beta_e)_{eff}$ from the momentum-balance technique exceed theoretical values for $\beta_e < 7$. It was previously stated that the accuracy of the momentum-balance technique was judged to be poor at low values of magnetic field because all terms in Eq. (41) were small and similar in magnitude; this was not so at high values of the magnetic field. The agreement between the two techniques (Fig. 34) is considered surprisingly good but testifies more to the consistency of the experimental measurements than to the accuracy of the predictions of j_{eff} and $(\beta_e)_{eff}$ by the momentum-balance technique. Of the two methods of prediction, the one used to obtain Figs. 31 and 32 is probably the most reliable.

The path of current flow in the present experiments is of much interest because this, in part, determines the magnitude of the current that is probably the most important variable controlling the physical processes in these experiments. It is to be recalled that the walls of the channel formed a continuous hollow metallic conductor through which the gas flowed. If the fluid were a liquid metal, flow of electric current into and out of
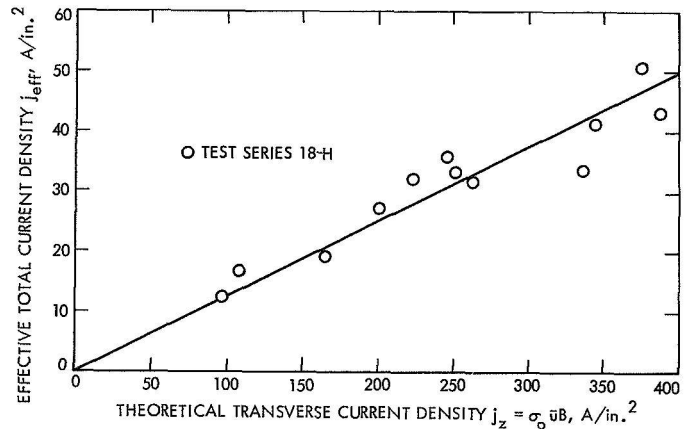
Fig. 33. Comparison of effective current density with theoretical values determined without Hall effect. Value of j_{eff} obtained for Test Series 18-H from an axial momentum balance
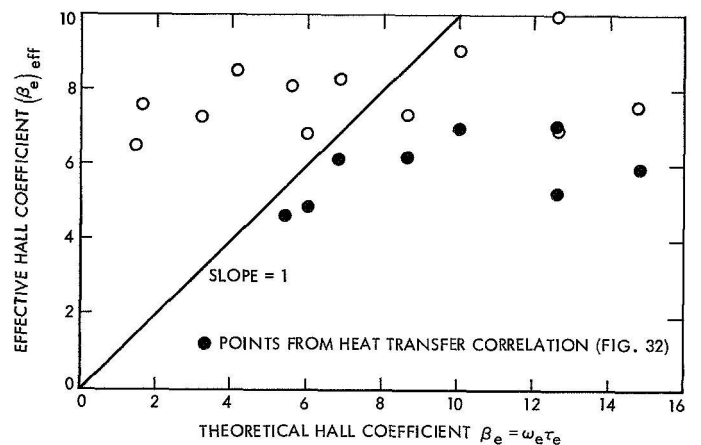
Fig. 34. Effective Hall coefficient for Test Series 18-H as obtained from an axial momentum balance

the walls would be likely. For a partially ionized gas with highly cooled walls, however, this possibility appears much reduced because of the insulating qualities of the cold boundary layers immediately adjacent to the walls.

Several possibilities for flow of the transverse component of current are shown schematically in Fig. 35, in cross sections of the square channel. The first drawing indicates current flow completely confined to the gas, a return circuit for the current being provided by the outer parts of the boundary layers. This is the situation considered by Dukowicz (Ref. 32) except that his square shock-tube had insulating walls. Dukowicz argues that

the current flow in the boundary layers is higher than in the core flow (despite the fact that the current density is less in the boundary layer owing to lower gas velocities) because the cross-sectional flow area occupied by the boundary layers is small compared with that occupied by the core flow. Current rather than current density is shown in Fig. 35. This may not be true for highly cooled walls as used here, because of reduced electrical conductivity in the boundary layers immediately adjacent to the walls, unless those regions were in nonequilibrium.

The second and third diagrams (Fig. 35) show current passing through upper and lower walls and through all walls, respectively. Case (2) is considered more likely than case (3) because of the anisotropic effects of the magnetic field on both boundary layer thickness and electrical conductivity. On a relative basis, walls parallel to the magnetic field would have boundary layers of greater thickness and much lower electrical conductivity than would walls perpendicular to the magnetic field.

Case (1) is considered the most likely of the three cases because of the difficulty to explain the physical mechanism that could account for current flow into the walls (or electron flow out of the walls). Thermionic or field emission of electrons from the walls was highly unlikely in these experiments; walls were cold (highly cooled) and no electric fields were applied in the test section. Current flow by flow of ions to the walls, or electron

emission by positive-ion bombardment, is usually accompanied by sputtering (Ref. 74), and is not an efficient process. No physical evidence of sputtering was seen on the walls of the test section. It is well known that current will flow between cold electrodes immersed in a hot plasma; the physics of this situation has been studied both theoretically and experimentally by Distefano and Pain (Ref. 75). However, for argon, current flow between cold electrodes requires much higher values of electron density, electrical conductivity, and gas temperature than were obtained in the present experiments and, further, large voltage gradients sufficient to cause field emission are necessary.

Case (2) should be considered further because it suggests the possibility of electron heating as a mechanism contributing to increased heat transfer for walls perpendicular to the magnetic field, a mechanism that has not yet been examined in this report. If case (2) were the situation in the present experiments, a basis for explaining the reasons for walls A and C undergoing relatively higher heat transfer than walls B and D would be available. However, it is more plausible to argue that these relative differences in heat transfer were instead caused by differences in temperature profile in the two directions, as well as large differences in thermal and electrical conductivities at walls differing in orientation with respect to the magnetic field. Finally, it should be considered that the presence of an axial component of current flow (not illustrated in Fig. 35) would lead to axial

MAGNETIC FIELD DIRECTED VERTICALLY AND UPWARDS
FLOW VELOCITY DIRECTED NORMALLY AND INTO PLANE OF DIAGRAMS

(1) CURRENT FLOW CONFINED TO GAS
(2) PART OF CURRENT FLOWS IN UPPER AND LOWER WALLS
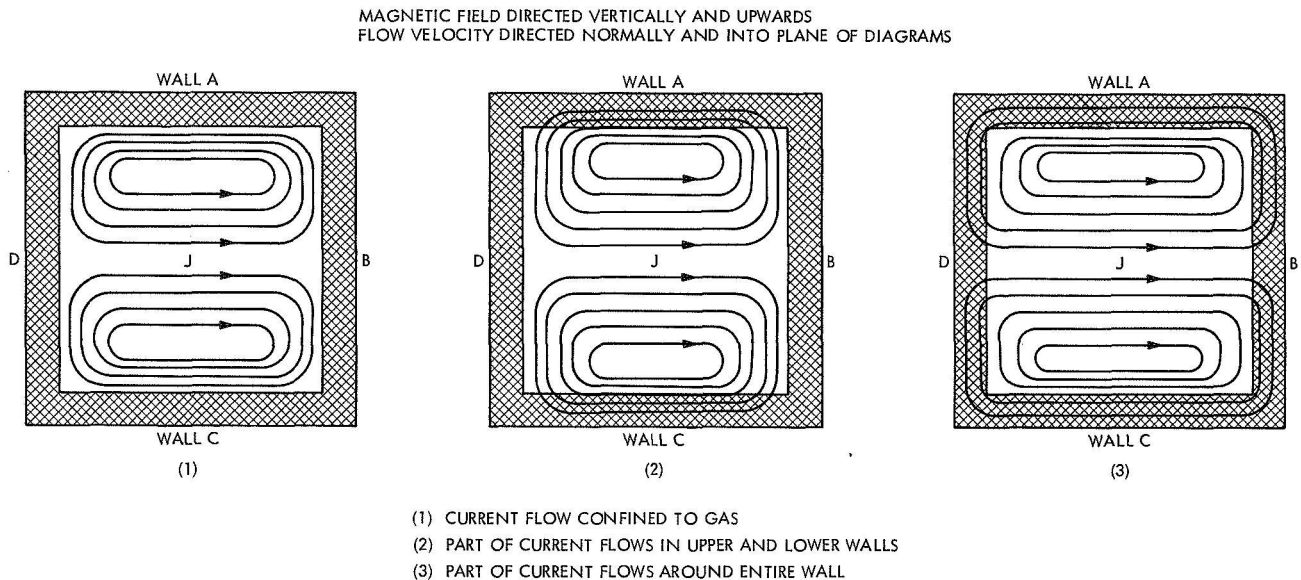(3) PART OF CURRENT FLOWS AROUND ENTIRE WALL

Fig. 35. Cross section of square conducting channel indicating several possibilities for flow of transverse component of electrical current

current loops as well, with return loops through the boundary layers in the axial direction.

E. Power Dissipation in the Walls

Current flow into the walls, either case (2) or case (3) of Fig. 35, would have been accompanied by power dissipation within the wall material. It is useful to clarify that the change in coolant water temperature in these experiments was a measure of the total heat transfer to the wall because of all contributing mechanisms, none of which could be isolated and identified in relation to the others. Power dissipation in the walls, had that occurred, would have been included in the overall, or total, measurement. It is important to estimate the relative effect of power dissipation on the heat transfer measurements but this is difficult to accomplish because current flow in the copper walls was not measured and, therefore, was not known.

However, the results of approximate calculations indicate that currents of the order of 1000 A would have been required to produce power dissipation in the walls of the same order of magnitude as the heat flux measured with magnetic field; such large values of wall current were unlikely to have occurred. Wall currents of the order of 100 A would have contributed only 10% of the measured wall heat flux. By assuming that all the current induced in the gas passed into the walls, and then by applying the effective current density values given for the gas in Fig. 33, it is clear that a current flow of 100 A in the walls was just within the limit of possibility.

F. Velocity and Thermal Entrance Lengths

A summary of some estimates available for velocity and thermal entrance lengths in various cases of channel flows with and without a transverse magnetic field is presented in Table 4 (from Refs. 10, 19, and 76). For the purpose of comparison in the present experiments, it is sufficient to take a range of values of Re and $RePr$ consistent with those given in Table 1; values of $(Ha)_{eff}$ ranged as high as 10 or 12 at maximum magnetic field. Heat transfer measurements were made in a region $4.5 < x/2a < 6.5$ as measured from the anode outlet which, however, cannot be considered as the starting point of the flow because the flow was not yet attached to the walls at that location.

With zero applied magnetic field, Table 4 indicates that the flow could not have been considered fully developed, either thermally or in velocity, within the test

Table 4. Velocity and thermal entrance lengths in channels, from the literature[a]

Case	Range[b]
Laminar flow, parallel plates	$(\ell_V/2_a) = 0.04\ Re$ [76] $(\ell_V/2_a) = 0.05\ Re$ [10] $(\ell_T/2_a) > RePr,\ S = 0$ [10]
Laminar flow, circular pipe	$(\ell_V/D) = 0.03\ Re$ [76]
Turbulent flow, circular pipe	$25 < (\ell_V/D) < 40$ [76]
Laminar flow with magnetic field, parallel plates	$(\ell_V/2_a) = Re/4Ha^2$ [10] $(\ell_T/2_a) \sim 0.5\ RePr,$ $S > 1$ [10]
Turbulent flow with magnetic field, parallel plates, measured from edge of magnet pole-piece	$(\ell_V/2_a) = (Re/Ha^2)^{1/2}$ [19]

[a]Re based on channel height or pipe diameter.
  Ha based on channel half-height.

[b]Numbers in brackets are References.

section. This situation would be true even if the flow could have been considered as originating at the anode outlet (Fig. 1). With applied magnetic field, the situation was somewhat improved but, considering the flow as originating at the edge of the magnet pole-piece, the flow still could not have been fully developed within the length of the test section.

G. Summary of Discussion

Strong magnetic fields can induce thermal nonequilibrium and produce an enhanced ionization fraction due to an elevated electron temperature. This thermal nonequilibrium has been demonstrated in the past by Zauderer (Refs. 23, 24). Even though the common practice of determining ionization fraction from the usual Saha equation evaluated at the electron temperature has been shown to be in error (Ref. 69), the related electrical conductivity is still much enhanced by thermal nonequilibrium. The effects of these phenomena on heat transfer in an ionized gas are difficult to estimate. However, in the present experiments, it was estimated that nonequilibrium ionization could have accounted for approximately 30% of the relative change in heat transfer owing to the applied magnetic field. The actual effect was unknown.

Theoretical values of the Hall coefficient were large for the conditions of these experiments, and were shown to be large compared with the ion-slip coefficient. However, theoretical values of the Hall coefficient were so large that Joule heating became insignificant as a factor

for promoting increased heat transfer. Estimates of an effective Joule heating parameter were made from heat transfer data; these effective values were only 2 to 5% of the theoretical values. Corresponding values of the effective Hall parameter were 4.5 to 7.5 and values of the effective Hartmann number were greater than 5.

Taking into account the various factors that could occur in the presence of strong magnetic fields, such as Hall effects, directional effects that can produce anisotropy in boundary layer thicknesses and gas transport properties in different directions, and thermal nonequilibrium, it was shown that the effects of Joule heating could be consistent qualitatively with several experimental observations. These observations included (1) variation in heat transfer between walls having different orientation with respect to the applied magnetic field, and (2) increased heat transfer at the walls caused by the applied magnetic field, despite a reduction in energy content of the gas as compared with zero field conditions.

An independent analysis based on the axial momentum equation was used to estimate the total current density within the gas. The effective current density, which included a Hall component, was approximately one-eighth of the theoretical transverse current based on scalar electrical conductivity and no Hall effect. In the present experiments it was considered unlikely that electric current induced by the magnetic field penetrated the conducting walls, which were highly cooled, because (1) the boundary layers immediately adjacent to the walls would have had low electrical conductivity, and (2) there were no applied electric fields. Without current flow in the walls there would have been no contribution to heat transfer arising from electron bombardment of the walls or electric power dissipation within the walls. An examination of thermal and velocity entrance lengths indicated that the flow in the test section in these experiments could never have become fully developed.

Several factors that could have influenced the heat transfer results have been discussed in this section and also in Section IV. A summary of these factors, and estimates of their relative influence on the experimental heat transfer results, are given in Table 5.

VIII. Summary

The practical design of magnetogasdynamic devices includes an engineering assessment of cooling requirements for the walls, especially electrode surfaces. Up to the present time, however, very few experimental results

Table 5. Estimates of modifying effects on convective heat transfer

Effect	Contribution to convective heat transfer	
	Without magnetic field[a]	With magnetic field
Axial heat conduction	Negligible, [10]	Negligible
Thermal radiation	Negligible, 2% at most [39]	Negligible
Ionization	Small except near arc conservatively, less than 10% [44]	Unknown (See Nonequilibrium)
Free convection	Negligible [45,46,47]	Negligible
Swirl velocity component	Negligible [48]	Unknown; probably negligible
Nonequilibrium	Unknown, probably negligible; in core but present in boundary layers [53,54,55]	Unknown; could be 30% of relative increase (enhanced ionization)
Electron heating at walls	Zero	Unknown; zero if current confined to gas
Electrical power dissipation within walls	Zero	Unknown, zero if current confined to gas; maximum of 10% of measured heat flux

[a]Numbers in brackets are References.

were available for estimating the effects of electric or magnetic fields on heat transfer from partially ionized gases in steady-state internal flows.

In this investigation, experimental heat transfer measurements were obtained for partially ionized argon flowing in a square channel with and without an applied, transverse magnetic field; the results have been presented and discussed. The channel formed a continuous, hollow, metallic conductor insulated at both ends from the remainder of the apparatus. Experiments were performed at an equivalent short-circuit condition; there were no applied electric fields. Reynolds numbers were well within the laminar regime.

A. Results for Zero Applied Magnetic Field

With zero applied magnetic field it was found that the experimental heat flux measurements, averaged over the four walls of the channel, could be correlated in terms of a nondimensional heat flux and a nondimensional axial distance parameter. This correlation yielded

results that were approximately 70% less than a theoretical prediction for laminar, constant property, slug-flow. The effects of thermal radiation, ionization, and swirl were not considered significant for zero magnetic field. It was estimated that the combined effect of those factors could have accounted for a maximum of 20% of the total heat transfer, but was probably much less than that.

B. Results With an Applied Magnetic Field

Large increases in heat transfer to the walls were experienced with the application of magnetic field strengths ranging up to nearly 10 kG. The relative increases in heat transfer owing to the magnetic field became larger as the pressure in the test section was decreased. Measurements were obtained with both forward and reversed (reversed polarity) directions of the magnetic field to assess the effects of a small amount of swirl present in some of the experiments. Heat transfer data for individual walls was presented in terms of the Stanton number normalized to its value at zero magnetic field. In general, walls perpendicular to the direction of the applied magnetic field underwent the largest changes in heat transfer; increases in Stanton number of as much as a factor of six were observed. The changes in heat transfer experienced by the sidewalls, which were parallel to the direction of the applied magnetic field, were dependent on the pressure level and the direction of the field.

The effects of small amounts of swirl present in the flow were not significant, since the experimental heat transfer results did not depend on the direction of the applied magnetic field. Furthermore, the results obtained without swirl were qualitatively the same as when swirl was present. The differences that did occur were probably associated with the influence of the swirl on the location of flow attachment upstream of the test section (which was influenced further by the magnetic field) and not with the swirl component itself. Again, the effects of thermal radiation were negligible since the gas temperatures were even lower with a field than without a field. The occurrence of magnetically induced, non-equilibrium ionization in these experiments was considered possible, but there was no way to determine the presence or extent of this phenomenon nor its actual effect on heat transfer. If thermal nonequilibrium did indeed occur in the presence of the magnetic field, it is estimated that this could have accounted for approximately 30% of the large increases in heat transfer that were obtained above values obtained at zero magnetic field.

Since an applied magnetic field alone cannot increase the total energy content of a conducting fluid, the large increases in heat transfer observed experimentally must have been due to a greatly increased temperature gradient of the fluid at the wall. For reasons discussed in the text, it is believed that the electric current induced within the gas by the magnetic field did not actually penetrate the walls of the channel so that no heating of the walls occurred by electron impingement or by electric power dissipation within the walls.

On the one hand, theoretical values of the Hall coefficient were so large that the corrected values of the Joule heating parameter were insignificant, hence could not be used to explain the experimental results. On the other hand, theoretical values of the Joule heating parameter that were obtained ignoring Hall effects were approximately 20 to 50 times larger than the effective values that were estimated from the heat transfer data. Effective values of the Hall coefficient were also estimated and appeared to be of reasonable magnitude, i.e., $4.5 < (\omega_e \tau_e)_{eff} < 7.5$. The latter values agreed approximately with those that were obtained independently from an axial momentum balance. Effective values of the total current density were of the order of one-eighth of the theoretical values computed for the transverse current density. Effective values of the Hartmann number were $7 < (Ha)_{eff} < 13$.

It is believed that the increases in heat transfer due to the presence of the applied magnetic field were caused by a small but sufficient amount of Joule heating augmented or accompanied by magnetically induced nonequilibrium ionization. Compared with the case of zero magnetic field, large magnetic fields produced large increases in heat transfer despite a reduction in the total energy content and heavy-particle temperature of the gas caused by the increased heat transfer. This suggests that the magnetic field greatly altered the temperature profile of the gas, causing much steeper temperature gradients at the wall and, possibly, enhancing the gas transport properties. However, the presence of large Hall effects greatly reduced the increases of heat transfer as compared with values that would have occurred, theoretically, had no Hall effects existed.

IX. Conclusions

The results of this experimental investigation have demonstrated clearly that an applied, transverse magnetic field can produce large increases in heat transfer

from a partially ionized, laminar gas flow to the walls of a confining channel. These large increases in heat transfer were not the result of an energy increase in gas since an applied magnetic field alone cannot change the total energy content of a gas. However, a magnetic field can produce a spatial redistribution of energy, can alter the relative magnitudes of the various components of the total energy, and can produce changes in the transport properties of the gas. In these experiments, increases in heat transfer were obtained even though the bulk stagnation enthalpy of the gas was less than the value for zero magnetic field. Thus the temperature gradients at the wall and, possibly, the transport properties, must have been greatly increased by the magnetic field.

It is likely that the influence of the magnetic field becomes evident as a direct consequence of the local magnitude and direction of the induced current flow within the gas. Electric currents within the gas are believed to have been confined to the gas, not penetrating through the boundary layers to the conducting walls of the channel. Thus the heat transfer increases produced by the magnetic field could not be explained by electron impingement on the walls.

It is concluded that the mechanisms most likely to account for the increases in heat transfer observed with an applied magnetic field were (1) a small, but sufficient, amount of Joule heating augmented or accompanied by (2) magnetically induced thermal nonequilibrium and nonequilibrium ionization. The term *Joule heating* here means a nonzero value of the Joule heating parameter and is not meant to indicate that the gas was "heated" by the magnetic field.

The differences in heat transfer observed for walls perpendicular to the applied magnetic field as compared with walls parallel to the applied field are believed to have been associated with (1) differences in the velocity and thermal boundary layers on these two walls, which depended on the local direction of the field, and (2) the anisotropic effects on transport properties produced by the magnetic field.

Because of the large increases in heat transfer that were observed experimentally with large, applied magnetic fields, especially at low pressures and high gas velocities, these results merit consideration for the practical design of magnetogasdynamic generators and accelerators.

Nomenclature

A, B, C, D   walls of channel (Fig. 1)

A   cross-sectional area of square channel; $A = 4a^2$

a   channel half-height; $2a = 2$ in.

B   applied magnetic field strength

B_c field strength at center of magnet pole-pieces

C_f skin friction coefficient

c   specific heat, incompressible fluid

c_p specific heat at constant pressure; $c_p = 0.1243$ Btu/lb, °R, for argon

D   diameter of a circular pipe

E   applied electric field strength; $E = 0$ in experiment

Ec   Eckert number; $Ec = \bar{u}^2/c_p \, (T_i - T_w)$

e   charge on electron

H   enthalpy per unit mass

Ha   Hartmann number; $Ha = Ba \, (\sigma_0/\mu)^{1/2}$

h   local heat transfer coefficient based on temperature difference; $h = q_w/(T_b - T_w)$

h'   local heat transfer coefficient based on enthalpy difference; $h' = q_w/(H_b - H_w)$

I   ionizational potential, equivalent to 16,386 Btu/lb for Argon I

J   electric current, induced

j   electric current density, current per unit area, induced

K   load factor, ratio of applied-to-induced electric fields; $K = E/\bar{u}B = 0$ in experiment

k   thermal conductivity, except in Eq. (32), (33), and Fig. 30, where k is the Boltzmann constant

Le   Lewis number (see Ref. 44)

ℓ_T thermal entrance length

ℓ_V velocity entrance length

M   mach number

m   particle mass

$\dot{m}$ mass rate of flow

Nu   local Nusselt number; $Nu = (2a)h/k$ or $Nu = (2a)c_p h'/k$

n   particle number density, per unit volume

Pr   Prandtl number; $Pr = \mu c_p/k$

$\mathscr{P}$ perimeter of channel; $\mathscr{P} = 8a$

p   static pressure at wall

Q*   nondimensional local wall heat flux; $Q^* = 2aq_w/k_i \, (T_i - T_w)$ in theory $Q^* = 2ac_p q_w/k_i \, (H_{t,i} - H_w)$ in experiment

q_{dw} diffusive component of total wall heat flux from ionization effects (Fig. 8)

q_{Tw} total wall heat flux, sum of diffusive and conductive components (Fig. 8)

q_{exp} experimental local wall heat flux

q_w local wall heat flux

q   collision cross section

R   gas constant; $R = 38.7$ ft–lb/lb, °R, for argon

Re   Reynolds number; $Re = \dot{m}/(2a)\mu$

Re_m magnetic Reynolds number; $Re_m = \mu_0\sigma_0\bar{u}(2a)$ where μ_0 = magnetic permeability

RePr   Peclet number, product of Reynolds number and Prandtl number

S   Joule heating parameter; $S = Ha^2 Ec \, (1 - K)^2 Pr$

S'   Joule heating parameter corrected for Hall and ion-slip effects; $S' = S/[(1 + \beta_e\beta_i)^2 + \beta_e^2]$

St   Stanton number; $St = h/\bar{\rho u}c$ (incompressible), or $St = h'/\bar{\rho u}$

T   absolute temperature

$\bar{u}$ bulk gas velocity in axial direction

X, Y, Z   coordinates measured from center of magnet pole-pieces

x   axial coordinate, positive in direction of flow

Nomenclature (contd)

$\bar{x}$ nondimensional axial coordinate; $\mathbf{x} = x/(2a)$

y transverse coordinate parallel to direction of applied magnetic field

z transverse coordinate perpendicular to x and y

α ionization fraction; $\alpha = n_e/(n_e + n_a)$

β_e, β_i Hall and ion-slip coefficients, respectively; $\beta_e = \omega_e \tau_e, \beta_i = \omega_i \tau_i$

Δ indicates an increment of a quantity

μ viscosity

θ temperature difference ratio; $\theta = (T_b - T_w)/(T_i - T_w)$

ρ density

$\overline{\rho u}$ bulk or average mass flux; $\overline{\rho u} = \dot{m}/A$

σ electrical conductivity

σ_0 scalar electrical conductivity, zero magnetic field

τ_e, τ_i particle collision times

τ shear stress in fluid

Φ_a fraction of total energy bound in ionization; $\Phi_a = \alpha I/H_t$ (Fig. 8)

χ Lewis number function; $\chi \simeq (Le^{0.63} - 1)$

Ω Lewis number function; $\chi + \Omega = (Le)^{2/3}$

ω_e, ω_i particle collision frequencies

Subscripts

a, e, i atom, electron, and ion, respectively

b bulk value

exp experimental

eff effective

h heavy particle or atom

i inlet condition

0 condition at zero, applied magnetic field

t total or stagnation condition

w wall

References

1. Romig, M. F., "The Influence of Electric and Magnetic Fields on Heat Transfer to Electrically Conducting Fluids," in *Advances In Heat Transfer*, Vol. 1, pp. 268–352. Edited by T. F. Irvine and J. P. Hartnett. Academic Press, Inc., New York, 1964.

2. Viskanta, R., "Effect of Transverse Magnetic Field on Heat Transfer to an Electrically Conducting and Thermally Radiating Fluid Flowing in a Parallel-Plate Channel," *Z. Angew. Math. Phys.*, Vol. 14, pp. 353–368, 1963.

3. Michiyoshi, I., and Matsumoto, R., "Heat Transfer by Hartmann's Flow in Thermal Entrance Region," *Int. J. Heat Mass Transfer*, Vol. 7, pp. 101–112, 1964.

4. Erickson, L. E., Wang, C. S., Hwang, C. L., and Fan, L. T., "Heat Transfer to Magnetohydrodynamic Flow in a Flat Duct," *Z. Angew. Math. Phys.*, Vol. 15, pp. 408–418, 1964.

5. Dhanak, A. M., "Heat Transfer in Magnetohydrodynamic Flow in an Entrance Section," *ASME J. Heat Transfer, Series C*, Vol. 87, pp. 231–236, 1965.

6. Hwang, C. L., Knieper, P. J., and Fan, L. T., "Heat Transfer to MHD Flow in the Thermal Entrance Region of a Flat Duct," *Int. J. Heat Mass Transfer*, Vol. 9, pp. 773–789, 1966.

7. Yen, J. T., "Effect of Wall Electrical Conductance on Magnetohydrodynamic Heat Transfer in a Channel," *ASME J. Heat Transfer, Series C*, Vol. 85, pp. 371–377, 1963.

8. Snyder, W. T., "The Influence of Wall Conductance on Magnetohydrodynamic Channel-Flow Heat Transfer," *ASME J. Heat Transfer, Series C*, Vol. 86, pp. 552–558, 1964.

9. Hwang, U. P., Fan, L. T., and Hwang, C. L., "Compressible Laminar MHD Flow Inside a Flat Duct with Heat Transfer," *AIAA J.*, Vol. 5, pp. 2113–2121, 1967.

10. Back, L. H., "Laminar Heat Transfer in Electrically Conducting Fluids Flowing in Parallel-Plate Channels," *Int. J. Heat Mass Transfer*, Vol. 11, pp. 1621–1636, 1968.

11. Eraslan, A. H., and Eraslan, N. F., "Heat Transfer in Magnetohydrodynamic Channel Flow," *Phys. Fluids*, Vol. 12, pp. 120–128, 1969.

12. Back, L. H., "Effects of Surface Cooling and Heating on Structure of Low-Speed, Laminar Boundary-Layer Gas Flows With Constant Free-Stream Velocity," Technical Report 32-1301, Jet Propulsion Laboratory, Pasadena, Calif., 1968.

13. Apollonskii, S. M., and Koskin, Y. P., "Need for Taking into Account the Variable Electrical Conductivity of Plasma when Calculating Overflow Currents on Insulator Walls in MHD-Channels," *High Temperature*, Vol. 5, pp. 464–466, May-June, 1967 (translation from Russian).

14. Iotkovskii, B. G., and Kirillov, V. V., "Effect of Boundary Layers on the Electrical Characteristics of MHD Generators," *High Temperature*, Vol. 6, pp. 566–573, July-August, 1968 (translation from Russian).

References (contd)

15. Reilly, J. P., and Oates, G. C., "Insulator Boundary Layers in a Supersonic Magnetogasdynamic Channel," Paper 67-717, *AIAA Electric Propulsion and Plasmadynamics Conference*, Colorado Springs, Colo., September 1967.

16. Tani, I., "Steady Flow of Conducting Fluids in Channels under Transverse Magnetic Fields, with Consideration of Hall Effect," *J. Aerospace Sci.*, Vol. 29, pp. 297–305, 1962.

17. Sakao, F., "Some Physical Interpretations of Magnetohydrodynamic Duct Flows," *AIAA J.*, Vol. 1, pp. 915–916, 1963.

18. Witalis, E. A., "MHD Flow Distortion Caused by Strong Hall Effect," *Plasma Physics*, Vol. 10, pp. 109–116, 1968.

19. Khozhainov, A. I., "Experimental Study of the Initial Region of a Square Magnetohydrodynamic Channel Taking Account of the Inhomogeneity of the Magnetic Field in the Longitudinal Direction," *Soviet Phys.-Tech. Phys.*, Vol. 10, pp. 1213–1218, 1966.

20. Sherman, A., "Magnetohydrodynamic Flows of Non-Equilibrium Plasmas," *J. Fluid Mech.*, Vol. 25, Part 3, pp. 621–637, 1966.

21. Maksimov, A. M., "Calculation of Non-Equilibrium Plasma Ionization Induced by a Magnetic Field," *High Temperature*, Vol. 6, pp. 610–612, 1968 (translation from Russian).

22. Rosa, R. J., "Nonequilibrium Ionization," in *Magnetohydrodynamic Energy Conversion*, Chap. 5, McGraw-Hill Book Co., Inc., New York, 1968.

23. Zauderer, B., "Experimental Study of Nonequilibrium Ionization in a Linear MHD Generator," *AIAA J.*, Vol. 6, pp. 701–707, 1968.

24. Zauderer, B., and Tate, E., "Electrical Characteristics of a Linear, Nonequilibrium MHD Generator," *AIAA J.*, Vol. 6, pp. 1685–1694, 1968.

25. Chmieleski, R. M., and Ferziger, J. H., "Transport Properties of a Nonequilibrium Partially Ionized Gas in a Magnetic Field," *Phys. of Fluids*, Vol. 10, pp. 2520–2530, 1967.

26. Schweitzer, S., and Mitchner, M., "Electrical Conductivity of a Partially Ionized Gas in a Magnetic Field," *Phys. of Fluids*, Vol. 10, pp. 799–806, 1967.

27. Lykoudis, P. S., "Experimental Studies for the Determination of Transport Properties in the Presence of a Magnetic Field for a Conducting Medium Flowing Turbulently," International Symposium on Properties and Applications of Low-Temperature Plasma, held in Moscow, USSR, July 1965.

28. Blum, E. Y., "Effect of a Magnetic Field on Heat Transfer in the Turbulent Flow of Conducting Liquid," *High Temperature*, Vol. 5, pp. 68–74, January-February, 1967 (translation from Russian).

29. Kovner, D. S., Krasilnikov, E. Y., Nikolaenko, V. S., and Panevin, I. G., "Experimental Study of the Effect of a Transverse Magnetic Field in the Turbulent Flow of an Electrically Conducting Fluid in a Channel," *Akad. Nauk SSSR, Izvestiia, Mekhanika Zhid. Gaza*, pp. 91–94, March-April, 1968 (in Russian).

References (cont'd)

30. Krasilnikov, E. Y., "The Effect of a Transverse Magnetic Field upon Convective Heat Transfer in Magnetohydrodynamic Channel Flows," *Magnetohydrodynamics*, Vol. 1, pp. 26–28, July-September, 1965 (translation from Russian).

31. Olin, J. G., and Kruger, C. H., "Turbulence Suppression in Magnetohydrodynamic Flows," Eighth Symposium on Engineering Aspects of Magnetohydrodynamics, p. 69, held at Stanford University, March 1967 (Abstr.).

32. Dukowicz, J. K., *A Magnetohydrodynamic Flow in the Shock Tube Boundary Layer with Transverse Magnetic Field*, UTIAS Rept. No. 115, Institute for Aerospace Studies, University of Toronto, Canada, July 1966.

33. Selamoglu, S., "Experiments on Joule Heating of Shock-Ionized Air," *AIAA J.*, Vol. 5, pp. 847–852, 1967.

34. Sutton, G. W., and Sherman, A., "Engineering Magnetohydrodynamics," Chap. 4, pp. 120–123. McGraw-Hill Book Co., Inc., New York, 1965.

35. Witte, A. B., *Analysis of One-Dimensional Isentropic Flow With Tables for Partially Ionized Argon*, Technical Report 32-661, Jet Propulsion Laboratory, Pasadena, Calif., Sept. 30, 1964.

36. deVoto, R. S., *Argon Plasma Transport Properties*, SUDAER Report No. 217, Stanford University, Department of Aeronautics and Astronautics, Stanford, Calif., February 1965. Also *Phys. Fluids*, Vol. 10, pp. 354–364, February 1967.

37. deVoto, R. S., *Tables of the Composition and Transport Coefficients of Partially Ionized Argon*, unpublished tables that replace SUDAER No. 217, available upon request to author, Stanford University, Department of Aeronautics and Astronautics, Stanford, Calif.

38. Hanks, R. W., and Song, D. S., "Experimental Investigation of the Laminar-Turbulent Transition for Newtonian Flow in Rectangular Ducts," *Ind. Eng. Chem. Fundamentals*, Vol. 6, August 1967.

39. Roschke, E. J., "Thermal Radiation From Ionized Argon: Results Obtained With an Annular Hohlraum," in *Supporting Research and Advanced Development*, Space Programs Summary 37-43, Vol. IV, pp. 206–216. Jet Propulsion Laboratory, Pasadena, Calif., Feb. 28, 1967.

40. Barzelay, M. E., "Continuum Radiation from Partially Ionized Argon," *AIAA J.*, Vol. 4, pp. 815–822, 1966.

41. Tankin, R. S., and Berry, J. M., "Experimental Investigation of Radiation from an Argon Plasma," *Phys. Fluids*, Vol. 7, pp. 1620–1624, 1964.

42. Incropera, F. P., and Leppert, G., "Laminar Flow Heat Transfer from an Argon Plasma in a Circular Tube," *Int. J. Heat Mass Transfer*, Vol. 10, pp. 1861–1873, 1967.

43. Emmons, H. W., "Arc Measurement of High-Temperature Gas Transport Properties," *Phys. Fluids*, Vol. 10, pp. 1125–1136, 1967.

44. Back, L. H., "Laminar Boundary-Layer Heat Transfer from a Partially Ionized Monatomic Gas," *Phys. Fluids*, Vol. 10, pp. 807–819, 1967.

References (contd)

45. Mori, Y., and Futagami, K., "Forced Convective Heat Transfer in Uniformly Heated Horizontal Tubes," (2nd Report, Theoretical Study), *Int. J. Heat Mass Transfer*, Vol. 10, pp. 1801–1813, 1967.

46. Cheng, K. C., and Hwang, G. J., "Numerical Solution for Combined Free and Forced Laminar Convection in Horizontal Rectangular Channels," *ASME J. Heat Transfer, Series C*, Vol. 91, pp. 59–66, 1969.

47. Shannon, R. L., and Depew, C. A., "Forced Laminar Flow Convection in a Horizontal Tube with Variable Viscosity and Free-Convection Effects," *ASME J. Heat Transfer, Series C*, Vol. 91, pp. 251–258, 1969.

48. Back, L. H., "Flow and Heat Transfer in Laminar Boundary Layers with Swirl," *AIAA J.*, Vol. 7, pp. 1781–1789, 1969.

49. Montgomery, S. R., and Wibulswas, P., "Laminar Flow Heat Transfer in Ducts of Rectangular Cross-Section," in *Proceedings of the Third International Heat Transfer Conference*, Vol. 1, pp. 104–112, Chicago, Ill., August 1966.

50. Boedker, L. R., and Covert, E. E., *Measurements of Helical Flow of a Strong Electrolyte With and Without a Transverse Magnetic Field*, Technical Report 23. Massachusetts Institute of Technology, Aerophysics Laboratory, April 1962.

51. Prandtl, L., *Essentials of Fluid Dynamics* (Authorized Translation), Hafner Publishing Co., pp. 145–149, New York, 1952.

52. Griem, H. R., "Validity of Local Thermal Equilibrium in Plasma Spectroscopy," *Phys. Rev.*, Vol. 131, pp. 1170–1176, 1963.

53. Eckert, E. R. G., and Pfender, E., "Plasma Heat Transfer," in *Advances in Heat Transfer: Vol. 4*, pp. 229–316. Edited by J. P. Hartnett and T. F. Irvine. Academic Press, Inc., New York, 1967.

54. Olsen, H. N., Bedjai, G., and Martindill, R. E., "Determination of Departures from Local Thermodynamic Equilibrium in Arc Plasmas," ARL Report 67-0060, Aerospace Research Laboratories, Wright-Patterson Air Force Base, Ohio, March 1967.

55. Jacobs, P. F., and Grey, J., "Criterion for Electron-Heavy Particle Nonequilibrium in a Partially Ionized Gas," Paper 66-192, presented at the AIAA Plasmadynamics Conference, Monterey, Calif., March 1966. Also, ARL Report 66-0143, Aerospace Research Laboratories, Wright-Patterson Air Force Base, Ohio, July 1966.

56. Roschke, E. J., "Laminar Heat Transfer in a Square Channel," in *Supporting Research and Advanced Development*, Space Programs Summary 37-55, Vol. III, pp. 213–217. Jet Propulsion Laboratory, Pasadena, Calif., Feb. 28, 1969.

57. Roschke, E. J., "Observations on Flow Attachment in a Square Channel," in *Supporting Research and Advanced Development*, Space Programs Summary 37-55, Vol. III, pp. 217–220. Jet Propulsion Laboratory, Pasadena, Calif., Feb. 28, 1969.

References (cont'd)

58. Back, L. H., and Witte, A. B., "Prediction of Heat Transfer from Laminar Boundary Layers, With Emphasis on Large Free-Stream Velocity Gradients and Highly Cooled Walls," *ASME J. Heat Transfer, Series C,* Vol. 88, pp. 249–256, 1966.

59. Montgomery, S. R., and Wibulswas, P., "Laminar Flow Heat Transfer for Simultaneously Developing Velocity and Temperature Profiles in Ducts of Rectangular Cross Section," *Appl. Sci. Res.,* Vol. 18, No. 4, pp. 247–259, 1967.

60. Schmidt, P. S., "Heat Transfer from a Plasma in Tube Flow," Technical Report SU 247-14. Stanford University, Thermosciences Division, Department of Mechanical Engineering, Stanford, Calif., September 1968.

61. Wethern, R. J., and Brodkey, R. S., "Heat and Momentum Transfer in Laminar Flow: Helium Initially at Plasma Temperatures," *AIChE J.,* Vol. 9, pp. 49–54, 1963.

62. Johnson, J. R., Choksi, N. M., and Eubank, P. T., "Entrance Heat Transfer from a Plasma Stream in a Circular Tube," *Ind. Eng. Chem.,* Process Design and Development, Vol. 7, pp. 34–41, 1968.

63. Kays, W. M., "Numerical Solutions for Laminar-Flow Heat Transfer in Circular Tubes," *ASME Trans.,* Vol. 77, pp. 1265–1294, 1955.

64. Roschke, E. J., "Further Heat Transfer Results for Partially Ionized Argon Flowing in a Square Channel Under the Influence of an Applied Transverse Magnetic Field," in *Supporting Research and Advanced Development,* Space Programs Summary 37-49, Vol. III, pp. 199–201. Jet Propulsion Laboratory, Pasadena, Calif., Feb. 29, 1968.

65. Branover, G. G., Tsinober, A. B., and Shcherbinin, E. V., "Effect of a Transverse Magnetic Field on the Structure of a Turbulent Flow of Mercury Behind a Sudden Expansion," *J. Eng. Physics,* Vol. 8, p. 83, Letter to Editor, January 1965 (translation from Russian).

66. Branover, G. G., Vasilev, A. S., and Gelfgat, Y. M., "Effect of a Transverse Magnetic Field on the Flow in a Duct at a Sudden Cross Section Enlargement," *Magnetohydrodynamics,* Vol. 3, No. 3, pp. 61–65, Fall 1967 (translation from Russian).

67. Branover, G. G., et al., "Numerical Calculation of a Conducting Fluid Between Rough Surfaces in a Transverse Magnetic Field," *Magnetohydrodynamics,* Vol. 3, No. 3, pp. 61–70, Fall 1967 (translation from Russian).

68. Louis, J. F., "Effective Ohm's Law in a Partially Ionized Plasma with Electron Density Fluctuations," *Phys. Fluids,* Vol. 10, pp. 2062–2064, 1967.

69. Monti, R., and Napolitano, L. G., "Generalized Saha Equation for Non-Equilibrium Two-Temperature Plasmas," in *Energy Sources and Energy Conversion,* proceedings of the 6th AGARD Combustion and Propulsion Colloquium, held in Cannes, France, March 1964. Edited by H. M. DeGroff, R. F. Hoglund, J. Fabri, T. F. Nagey, and M. E. Rumbaugh, Jr. Gordon and Breach Science Publ., New York, London, 1967, pp. 517–534.

References (cont'd)

70. Roschke, E. J., "Hall and Ion-Slip Effects in Channel Flow," in *Supporting Research and Advanced Development*, Space Programs Summary 37-52, Vol. III, pp. 109–112. Jet Propulsion Laboratory, Pasadena, Calif., Aug. 31, 1968.

71. Cann, G. L., Ziemer, R. W., and Marlotte, G. L., "The Hall Current Plasma Accelerator," Paper 63-011, presented at the AIAA Electric Propulsion Conference, Colorado Springs, Colo., March 1963.

72. Drake, D. G., and Abu-Sitta, A. M., "Magnetohydrodynamic Flow in a Rectangular Channel at High Hartmann Number," *Z. Angew. Math. Phys.*, Vol. 17, pp. 519–527, 1966.

73. Harris, L. P., *Hydromagnetic Channel Flows*, Chap. 5, p. 32. John Wiley & Sons, Inc., New York, 1960.

74. Cobine, J. D., *Gaseous Conductors*, pp. 113–115. Dover Publications, Inc., New York, 1958.

75. Distefano, E., and Pain, H. J., "Electrical Current in a Moving Plasma Between Cold Electrodes," *Brit. J. Appl. Phys.*, Vol. 18, pp. 1085–1093, 1967.

76. Schlichting, H., *Boundary Layer Theory*, pp. 146–149 and p. 400. Pergamon Press, Inc., New York, 1955.

Appendix

Comparative Results

Since the completion of this study, the author has received a personal communication from Dr. Gustav A. Carlson of the Lawrence Radiation Laboratory, University of California. Dr. Carlson has also obtained data on the effect of a transverse magnetic field upon heat transfer from unseeded ionized argon.* His experiments were performed in an accelerator operating at open circuit conditions, in a device that was remarkably similar to the author's apparatus in terms of dimensions. The flow entering Carlson's accelerator was heated by means of a supersonic constricted-arc jet. The inlet of the accelerator was a square 5- × 5-cm duct, but a divergence half-angle of 2 deg was incorporated in the walls perpendicular to the direction of the applied magnetic field, which was variable from 0 to 5 kG. All walls were water-cooled; however, the insulator walls (perpendicular to the direction of the applied magnetic field) were nonconductors fabricated from anodized aluminum and were insulated from the electrode walls.

Qualitatively, Carlson's results were similar to those presented in this report. He found that heat transfer to walls perpendicular to the direction of the applied magnetic field increased appreciably with increasing field strength. In contrast, he obtained very little change in heat transfer on walls parallel to the direction of the applied magnetic field. Carlson concludes that the heat-transfer increases incurred by the action of the magnetic field were due to ohmic (Joule) heating and viscous dissipation, and were in reasonable agreement with his theoretical analysis. However, his results do not include the Hall effect and he has not attempted to correct his results (particularly, the Hartmann number) for the Hall effect.

Direct comparison of the results in this report with Carlson's results is not straightforward, because he presents his data in terms of different parameters and had somewhat different experimental conditions than the present experiments entail. His nondimensional heat-transfer parameter is defined by

$$\widetilde{Q} = \frac{\widetilde{q}}{4\bar{u}^2\mu l} \qquad (A\text{-}1)$$

*Carlson, G. A., *Circulating Currents in Linear Crossed-Field Generators and Accelerators*, NASA TN D-5244. National Aeronautics and Space Administration, Washington, May 1969.

where $\widetilde{q}$ is the rate of heat transfer to the wall (not heat flux), l is the length of the accelerator test section in the direction of flow, and the other symbols are the same as defined in this report. His definition of the Hartmann number was identical to that used in this report and was based on scalar electrical conductivity and the channel half-height, i.e., $(Ha) = Ba\,(\sigma_0\mu)^{1/2}$. His data are presented in terms of $\widetilde{Q} - \widetilde{Q}_0$, where $\widetilde{Q}_0$ is the value of $\widetilde{Q}$ for zero magnetic field. Carlson's results for supersonic flow were based on transport properties taken from deVoto at 10-mm Hg pressure assuming equilibrium; his accelerator exhausted into a vacuum tank maintained at 2.5-mm Hg pressure. His heat-transfer results were given for the total accelerator length of 22 cm, in terms of the Hartmann number.
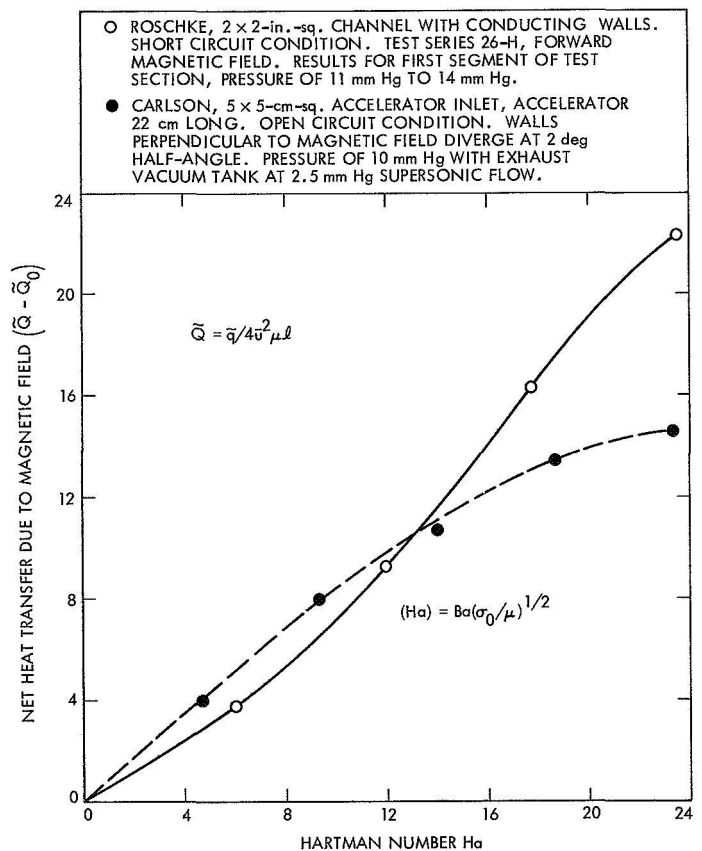

Fig. A-1. Comparison of experimental heat transfer data for unseeded argon subject to an applied transverse magnetic field. Results are for total heat transfer to all four walls of confining channel. Equilibrium assumed, Hartmann number based on scalar electrical conductivity

In this report, the test condition that best matches Carlson's test condition is Test Series 26H, which had a nominal pressure of 11-mm Hg pressure in the first segment of the test section before applying the magnetic field. Test Series 26H was conducted at slightly supersonic conditions before applying the magnetic field; however, the flow became subsonic when the magnetic field was applied.

A comparison of the heat-transfer results for Test Series 26H and Carlson's results are shown in Fig. A-1 and are given in terms of Carlson's variables. Both experimental results shown are for total heat transfer to all four walls of the channel. Hartmann number has been based on scalar electrical conductivity and has not been corrected for Hall effect. The present results agree well with Carlson's at low Hartmann number but diverge upwards at higher Hartmann number. The agreement is fair considering that there were differences in dimensions and flow regime. It is significant that the author's results and Carlson's results are in qualitative agreement, and that both results display prominent effects of an applied magnetic field on heat transfer from partially ionized argon to walls perpendicular to the direction of the magnetic field. It is also interesting that Carlson's concept of circulating currents within the gas is identical to that shown by case (1) of Fig. 35, which was considered the most likely circumstance by the author.

N71-18680

TECHNICAL REPORT STANDARD TITLE PAGE

1. Report No. 32-1510	2. Government Accession No.	3. Recipient's Catalog No.

4. Title and Subtitle	5. Report Date December 15, 1970
HEAT TRANSFER FROM PARTIALLY IONIZED ARGON FLOWING IN A CONDUCTING CHANNEL WITH AN APPLIED, TRANSVERSE MAGNETIC FIELD	6. Performing Organization Code

7. Author(s) E. J. Roschke	8. Performing Organization Report No.

9. Performing Organization Name and Address	10. Work Unit No.
JET PROPULSION LABORATORY California Institute of Technology 4800 Oak Grove Drive Pasadena, California 91103	11. Contract or Grant No. NAS 7-100
	13. Type of Report and Period Covered Technical Report

12. Sponsoring Agency Name and Address	
NATIONAL AERONAUTICS AND SPACE ADMINISTRATION Washington, D.C. 20546	14. Sponsoring Agency Code

15. Supplementary Notes

16. Abstract

Wall heat transfer measurements were obtained for laminar flow of partially ionized argon flowing in a square channel with and without an applied, transverse magnetic field. Tests were conducted for subsonic flows and for flows that were supersonic before a magnetic field was applied. Principal results are presented in terms of the Stanton number. The Stanton number increased by a factor of as much as six at the highest magnetic field strengths available (nearly 10 kG) over results observed at zero field. Heat transfer and flow data were used to estimate the effective values of the Joule heating parameter, the Hall coefficient, the Hartmann number, and the current density; these values appeared to be physically realistic. It is believed that the large increases in heat transfer observed with an applied magnetic field were due to (1) a small but sufficient amount of Joule heating, which caused significant changes in the temperature distribution, augmented or accompanied by (2) magnetically induced nonequilibrium ionization. These results represent the only known experimental measurements obtained thus far for heat transfer from a partially ionized gas in steady internal flow with an applied, transverse magnetic field.

17. Key Words (Selected by Author(s))	18. Distribution Statement
Fluid Mechanics Heat Transfer Plasma Physics Propulsion, Nuclear—Electric	Unclassified — Unlimited

19. Security Classif. (of this report)	20. Security Classif. (of this page)	21. No. of Pages	22. Price
Unclassified	Unclassified	54	

HOW TO FILL OUT THE TECHNICAL REPORT STANDARD TITLE PAGE

Make items 1, 4, 5, 9, 12, and 13 agree with the corresponding information on the report cover. Use all capital letters for title (item 4). Leave items 2, 6, and 14 blank. Complete the remaining items as follows:

3. Recipient's Catalog No. Reserved for use by report recipients.

7. Author(s). Include corresponding information from the report cover. In addition, list the affiliation of an author if it differs from that of the performing organization.

8. Performing Organization Report No. Insert if performing organization wishes to assign this number.

10. Work Unit No. Use the agency-wide code (for example, 923-50-10-06-72), which uniquely identifies the work unit under which the work was authorized. Non-NASA performing organizations will leave this blank.

11. Insert the number of the contract or grant under which the report was prepared.

15. Supplementary Notes. Enter information not included elsewhere but useful, such as: Prepared in cooperation with... Translation of (or by)... Presented at conference of... To be published in...

16. Abstract. Include a brief (not to exceed 200 words) factual summary of the most significant information contained in the report. If possible, the abstract of a classified report should be unclassified. If the report contains a significant bibliography or literature survey, mention it here.

17. Key Words. Insert terms or short phrases selected by the author that identify the principal subjects covered in the report, and that are sufficiently specific and precise to be used for cataloging.

18. Distribution Statement. Enter one of the authorized statements used to denote releasability to the public or a limitation on dissemination for reasons other than security of defense information. Authorized statements are "Unclassified—Unlimited," "U. S. Government and Contractors only," "U. S. Government Agencies only," and "NASA and NASA Contractors only."

19. Security Classification (of report). NOTE: Reports carrying a security classification will require additional markings giving security and down-grading information as specified by the Security Requirements Checklist and the DoD Industrial Security Manual (DoD 5220.22-M).

20. Security Classification (of this page). NOTE: Because this page may be used in preparing announcements, bibliographies, and data banks, it should be unclassified if possible. If a classification is required, indicate separately the classification of the title and the abstract by following these items with either "(U)" for unclassified, or "(C)" or "(S)" as applicable for classified items.

21. No. of Pages. Insert the number of pages.

22. Price. Insert the price set by the Clearinghouse for Federal Scientific and Technical Information or the Government Printing Office, if known.